AD NUMBER

AD886916

NEW LIMITATION CHANGE

TO

Approved for public release, distribution unlimited

FROM

Distribution authorized to U.S. Gov't. agencies only; Test and Evaluation; AUG 1971. Other requests shall be referred to Air Force Avionics Laboratory, Attn: RSA, Wright-Patterson AFB, Oh 45433.

AUTHORITY

AFWAL ltr, 29 Jul 1981

AFAL-TR-71-199

SPECTRAL AND POLARIZATION CHARACTERISTICS OF SELECTED TARGETS AND BACKGROUNDS: INSTRUMENTATION AND MEASURED RESULTS (3.3 - 14.0 μm)

Informal Technical Report

D. Faulkner
R. Horvath
J. P Ulrich
E. Work

Infrared and Optics Laboratory
Willow Run Laboratories
Institute of Science and Technology
The University of Michigan
Ann Arbor, Michigan

TECHNICAL REPORT AFAL-TR-71-199

August 1971

Air Force Avionics Laboratory
Air Force Systems Command
Wright-Patterson Air Force Base, Ohio

NOTICE

When Government drawings, specifications, or other data are used for any purpose other than in connection with a definitely related Government procurement operation, the United States Government thereby incurs no responsibility nor any obligation whatsoever; and the fact that the government may have formulated, furnished, or in any way supplied the said drawings, specifications, or other data, is not to be regarded by implication or otherwise as in any manner licensing the holder or any other person or corporation, or conveying any rights or permission to manufacture, use, or sell any patented invention that may in any way be related thereto.

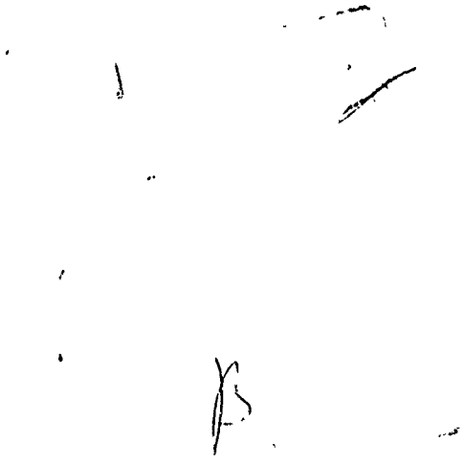

Copies of this report should not be returned unless return is required by security considerations, contractual obligations, or notice on a specific document.

UNCLASSIFIED
Security Classification

DOCUMENT CONTROL DATA - R & D

(Security classification of title, body of abstract and indexing annotation must be entered when the overall report is classified)

1 ORIGINATING ACTIVITY *(Corporate author)*
Willow Run Laboratories, Institute of Science and Technology, The University of Michigan, Ann Arbor

2a. REPORT SECURITY CLASSIFICATION
UNCLASSIFIED

2b GROUP

3 REPORT TITLE
SPECTRAL AND POLARIZATION CHARACTERISTICS OF SELECTED TARGETS AND BACKGROUNDS: INSTRUMENTATION AND MEASURED RESULTS (3.3-14.0μm)

4 DESCRIPTIVE NOTES *(Type of report and inclusive dates)*
Theory, instrumentation, and data analysis. January 1968 to May 1971

5 AUTHOR(S) *(First name, middle initial, last name)*
D. Faulkner J. P. Ulrich
R. Horvath E. Work

6 REPORT DATE	7a. TOTAL NO. OF PAGES	7b. NO. OF REFS
August 1971	xii + 107	13

8a CONTRACT OR GRANT NO
F33615-68-C-1281 and F33615-70-C-1698

b. PROJECT NO
4414 26 and 6239 10

c.

d.

9a. ORIGINATOR'S REPORT NUMBER(S)
036920-23-T

9b. OTHER REPORT NO(S) *(Any other numbers that may be assigned this report)*
AFAL-TR-71-199

10 DISTRIBUTION STATEMENT
Distribution limited to U.S. Gov't. agencies only; Test and Evaluation; other requests for this document must be referred to AFAL (26 AUG 1971)
~~"This document is subject to special export controls and each transmittal to foreign governments or foreign nationals may be made only with prior approval of AFAL/RSA, WPAFB, Ohio."~~

11 SUPPLEMENTARY NOTES

12. SPONSORING MILITARY ACTIVITY
Air Force Avionics Laboratory
Air Force Systems Command
Wright-Patterson Air Force Base, Ohio

13 ABSTRACT

Spectral, polarization, and view-angle dependent characteristics of 3.3-14.0 μm radiance have been measured for a number of target and background materials. Emittances have been measured in the laboratory and radiances measured in the field. Significant characteristics have been found to exist in these data which allow for improved target/background discrimination for reconnaissance and weapon delivery. The instrumentation built to collect these data and its principles of operation are described, and collected data are presented. The angular-dependent spectral and polarized emittance type data measured in the laboratory were unavailable prior to this measurement program. The data are used to show how spectral and polarization characteristics in the infrared provide a substantially improved capability of discriminating targets from backgrounds in real environments.

DD FORM 1 NOV 65 1473

UNCLASSIFIED
Security Classification

14 KEY WORDS	LINK A		LINK B		LINK C	
	ROLE	WT	ROLE	WT	ROLE	WT
Infrared spectra						
Spectral radiance						
Spectral normal emittance						
Polarized apparent temperature						
Instrumentation						
Data						

SPECTRAL AND POLARIZATION CHARACTERISTICS OF SELECTED TARGETS AND BACKGROUNDS: INSTRUMENTATION AND MEASURED RESULTS (3.3 - 14.0μm)

Informal Technical Report

D. Faulkner
R. Horvath
J. P. Ulrich
E. Work

FOREWORD

This work reported herein, covering the period from January 1968 to May 1971, was carried out by the Infrared and Optics Laboratory of the Willow Run Laboratories, a unit of the University of Michigan's Institute of Science and Technology, Ann Arbor, Michigan. The work was performed under U.S. Air Force Contracts F33615-68-C-1281, Project 4144 26, and F33615-70-C-1698, Project 6239 10, for the Air Force Avionics Laboratory, (AFAL), Air Force Systems Command, Wright-Patterson Air Force Base, Ohio; Capt Kenneth Trumble (AFAL/RSA) is project monitor for the work.

The target-signature program is part of a comprehensive program at the University of Michigan devoted to the improvement of remote-sensing capabilities; this comprehensive program has been guided by Richard L. Legault, Associate Director of the Infrared and Optics Laboratory of Willow Run Laboratories.

The work reported herein had as Principal Investigator Dr. J. R. Maxwell, with Mr. Max E. Bair serving as Project Leader. One of the authors (D. Faulkner) served in the capacity of Visiting Scientist from Weapons Research Establishment, Department of Supply, Australia.

This report was submitted by the authors June 1971.

This technical report has been reviewed and is approved.

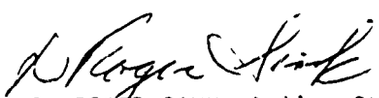

D. ROGER SINK, Acting Chief
Reconnaissance Applications Branch
Reconnaissance Division
Air Force Avionics Laboratory

ABSTRACT

Spectral, polarization, and view-angle dependent characteristics of 3.5-14.0 μm radiance have been measured for a number of target and background materials. Emittances have been measured in the laboratory and radiances measured in the field. Significant characteristics have been found to exist in these data which allow for improved target/background discrimination for reconnaissance and weapon delivery. The instrumentation built to collect these data and its principles of operation are described, and collected data are presented. The angular-dependent spectral and polarized emittance type data measured in the laboratory were unavailable prior to this measurement program. The data are used to show how spectral and polarization characteristics in the infrared provide a substantially improved capability of discriminating targets from backgrounds in real environments.

TABLE OF CONTENTS

TABLE OF CONTENTS (Cont)

LIST OF FIGURES

LIST OF FIGURES (Cont)

LIST OF FIGURES (Cont)

LIST OF TABLES

NOTATIONAL CONVENTIONS

In order to describe the operation and underlying principles of the instrumentation to be discussed in this Report, it is necessary to introduce a considerable amount of mathematical notation. Since much of this notation has not yet attained any standard worldwide representation, a rather complete list of the conventions used in this Report is given here for clarity and convenience. Further, each symbol is defined where it first appears in the text.

FUNCTIONS AND ARGUMENTS

SYMBOL	MEANING
a	Absorptance
E_λ	Spectral irradiance
L_λ	Spectral radiance
M_λ	Spectral exittance
T	Temperature
V	Voltage
ε	Emittance
θ	Polar angle
λ	Electromagnetic wavelength
ρ	Directional reflectance
ρ'	Bidirectional reflectance distribution function
ϕ	Azimuth angle
Ω	Solid angle

INDICES

SYMBOL	MEANING
b	Refers to a blackbody
c	Refers to a reference cavity
e	Means emitted
i	Means incident
p	Represents arbitrary polarization state
r	Means scattered ("reflected")
t	Refers to target material
sky	Refers to sky
app	Means apparent
λ	(Subscript only) Indicates a spectral quantity
$\parallel$	Represents the parallel polarization state
$\perp$	Represents the perpendicular polarization state

EXAMPLES

SYMBOL	MEANING
$L^{e}_{\lambda,\perp}(T^{t};\theta_{e},\phi_{e})$	Emitted spectral radiance in the direction (θ_{e},ϕ_{e}) from a target material at temperature T^{t} having the perpendicular polarization state.
$\rho'_{\parallel,\parallel}(\lambda,T^{t};\theta_{i},\phi_{i},\theta_{r},\phi_{r})$	Bidirectional reflectance distribution function for both source and receiver having parallel polarization states, the incident direction being (θ_{i},ϕ_{i}) and the scattered direction being (θ_{r},ϕ_{r}).

Units and dimensions are indicated within brackets: [ ].

1

INTRODUCTION

When the program to be discussed in the present report was initiated, there was no significant data base of the spectral and polarization distributions of radiance in the 4.4 - 5.5 μm and 7.0 - 14.0 μm spectral windows which might be encountered in the field. Since spectral analysis (usually referred to as "multispectral sensing") had already produced such spectacular results in the visible and very-near-IR spectral regions, there was reason to believe that the extension of the multispectral techniques into the thermal-IR could do likewise. After all, even broadband radiometry was not without its successes. Conceivably, some very significant target signature characteristics could exist in the thermal-IR spectral region. There were already some independent broadband data which indicated that polarization signatures existed there.

Thus, the Infrared and Optics Laboratory of The University of Michigan initiated a program under which an instrument would be developed and subsequently used to obtain the data base necessary for the successful spectral analysis of the thermal-IR region.* This data base was to consist of spectral radiance taken in the field on many target and background materials together with sky spectral radiance. The field data were to be taken under a variety of environmental conditions and parameters. In addition, it would be necessary to obtain laboratory data on the spectral emittance of various materials. The polarization content of the measured spectral radiance (both for field radiance and laboratory emittance data) would also need to be recorded.

*This was begun under Air Force Contract No. F33615-68-C-1281 and continued under Contract No. F33615-70-C-1698.

The instrumentation required to execute the task was designed, built, and calibrated and has already been used to obtain a substantial portion of the necessary data. The basic instrument is a Field Infrared Spectro-Radiometer and it is hereinafter referred to as the FISR. The instrument is basically a double-beam differencing device which can be used to measure the spectral radiance difference in two optical beams, the spectral radiance in one of which is known. The spectral radiance in the other beam (the target beam) can then be determined. From this, either target radiance or emittance can be deduced. The details of the theory are given in Section 3.

Some interpretation and application of the data already collected are presented in Section 8. The value of FISR-type data for predictive purposes is evident from the material in that Section.

2
RADIATION-THEORETIC PRINCIPLES

The following discussion provides the basis for the methodology presented in this report and defines the terminology used. It is not intended to be an exhaustive presentation of radiation theory. The principles presented are straightforward and they are valid within the limitations cited. The terminology and notation used are largely accepted in the scientific community, but they do contain some local provincialisms. This is defended by the observation that no satisfactory, complete, and universally-accepted notational system yet exists.

2.1. EXITTANCE, EMITTANCE AND REFLECTANCE

Any object having a finite absolute temperature emits radiation from its surface because of internal atomic and molecular motions. The detailed nature of this radiative process depends on material properties. A perfect emitter, called a blackbody*, emits the maximum possible radiant power at any given temperature. Planck's law gives a description of blackbody radiation as a function of wavelength, λ[m], and absolute temperature, T[°K]. The quantity treated here is called spectral exittance and is denoted by $M_\lambda^b(T)$. The Planck law for a spectral exittance is**

$$M_\lambda^b(T) = c_1 \lambda^{-5} \left[\exp\left(\frac{c_2}{\lambda T}\right) - 1 \right]^{-1} \quad \text{[power/area-wavelength]} \qquad (2.1)$$

*Throughout this report, the term blackbody is used exclusively for describing a perfect emitter. Actual materials and/or devices at best only approach having this property, the better ones being referred to as radiation references or standards.

**The subscript λ is used to indicate that the symbol bearing it has dimensions of "per unit wavelength." Otherwise, spectral dependence is indicated by treating λ as a function argument; e.g., $f(\lambda)$. See reference 1, page 9, item 2. Examination of Paragraph 45-05-215 is also strongly urged.

where c_1 and c_2 are universal radiation constants defined in terms of basic physical constants. They are, specifically [1],

$$c_1 = 2\pi hc^2 = (3.74150 \pm 0.0003) \times 10^{-16} [\text{watts-m}^2]$$

$$c_2 = hc/k = (1.43879 \pm 0.00019) \times 10^{-2} [\text{m-}^{\circ}\text{K}]$$

A real material emits less radiant power than a blackbody at the same temperature. A quantity, $\varepsilon(\lambda,T)$, defined by

$$\varepsilon(\lambda,T) = \frac{M_\lambda^e(T)}{M_\lambda^b(T)} < 1 \qquad (2.2)$$

where $M_\lambda^e(T)$ is the actual spectral exittance of the real material at temperature T and $M_\lambda^b(T)$ is the (calculable) spectral exittance of a blackbody at the same temperature is used to describe this effect. This quantity is called the hemispherical spectral emittance*. It defines the relative emitting efficiency of a surface for radiating into the entire hemisphere above the surface.

The directional distribution of the radiation composing the spectral exittance of a blackbody is described by Lambert's law which states that the spectral intensity [power/wavelength-solid angle] emitted by a unit area of a blackbody in the direction normal to its surface is equal numerically to the spectral exittance divided by π,** that this intensity decreases as

*The term emittance is used through this report in describing the emitting efficiency of an arbitrary surface. At the Willow Run Laboratories, the term "emissivity" is reserved specifically for describing the efficiency of a pure substance with a perfectly flat surface and of sufficient thickness to be completely opaque, conditions not applicable to all objects considered in this Report. This convention is contrary to the one adopted in reference 1, Paragraph 45-05-170, Notes 1 and 2 and Paragraph 45-05-175.

**Reference 1, Paragraph 45-05-170, Note 3.

$\cos\theta_e$ at polar emission angles θ_e away from the surface normal, and that it is independent of the azimuth angle ϕ_e (see Figure 1). Thus, the spectral radiance $L_\lambda^b(T;\theta_e,\phi_e)$ [power/area-wavelength-solid angle], which is the spectral intensity per projected area at polar angle θ_e and azimuth angle ϕ_e, is invariant with angle for a blackbody since the $\cos\theta_e$ intensity dependence is exactly compensated by a $\frac{1}{\cos\theta_e}$ projected area dependence:

$$L_\lambda^b(T) = \frac{M_\lambda^b(T)}{\pi} \quad \text{for all } \theta_e,\phi_e$$

The use of projected area in L_λ^b and actual area in M_λ^b requires a factor of $\cos\theta_e$ if radiance is integrated over the hemisphere to obtain exittance. That is,

$$M_\lambda^b(T) = \int_{\theta_e=0}^{\pi/2} \int_{\phi_e=0}^{2\pi} L_\lambda^b(T)\cos\theta_e\, d\omega_e \tag{2.3}$$

in which $d\omega_e = \sin\theta_e d\theta_e d\phi_e$ is the elemental solid angle.

A blackbody surface emits with unit efficiency not only into a hemisphere, but also into every direction in that hemisphere. Real materials do not have this property, so an angularly-variable spectral directional emittance, $\varepsilon(\lambda,T;\theta_e,\phi_e)$, is defined for them:

$$\varepsilon(\lambda,T;\theta_e,\phi_e) = \frac{L_\lambda^e(T;\theta_e,\phi_e)}{L_\lambda^b(T)} \tag{2.4}$$

where $L_\lambda^e(T;\theta_e,\phi_e)$ is the radiance of wavelength λ emitted from the material surface of temperature T in the direction (θ_e,ϕ_e).

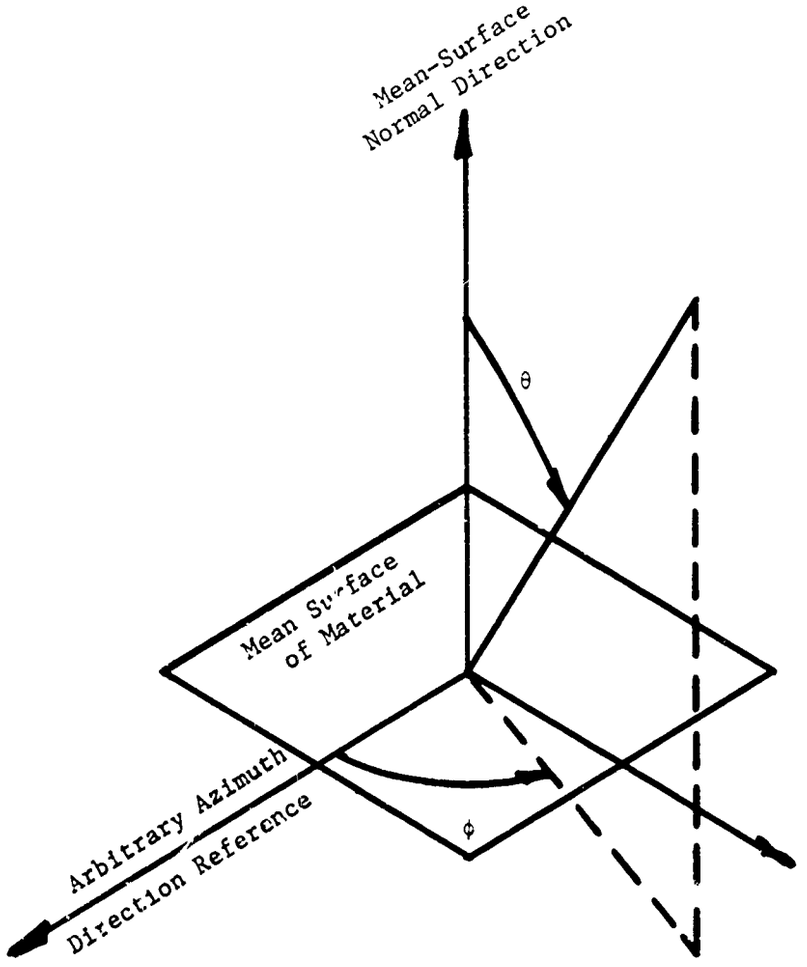

FIGURE 1. AN ILLUSTRATION OF THE POLAR ANGLE, θ, AND AZIMUTH ANGLE, ϕ. THESE CAN REPRESENT INCIDENCE ANGLES, (θ_i,ϕ_i), REFLECTION ANGLES, (θ_r,ϕ_r), OR EMISSION ANGLES, (θ_e,ϕ_e).

The radiation emanating from a blackbody is completely unpolarized and incoherent. Consequently, if such radiation is analyzed with a perfect linear polarizer, exactly one half of it will get through. This characteristic is independent of the polarization axis of the polarizer. Thus, any linearly-polarized component of blackbody radiance is equal to one-half of the total (unpolarized) radiance:

$$L^b_{\lambda,p}(T) = \frac{1}{2} L^b_\lambda(T) \tag{2.5}$$

where the subscript p indicates that the symbol bearing it denotes some particular linearly-polarized component. A linearly-polarized spectral directional emittance, $\varepsilon_p(\lambda,T;\theta_e,\phi_e)$, can then be defined for any material by

$$\varepsilon_p(\lambda,T;\theta_e,\phi_e) = \frac{L^e_{\lambda,p}(T;\theta_e,\phi_e)}{L^b_{\lambda,p}(T)} = \frac{L^e_{\lambda,p}(T;\theta_e,\phi_e)}{\frac{1}{2} L^b_\lambda(T)} \tag{2.6}$$

where $L^e_{\lambda,p}(T;\theta_e,\phi_e)$ is the component of emitted radiance transmitted by a perfect linear polarizer which passes the polarization state represented by p.

Commonly, two specific linear components are defined with reference to the plane of emission (the plane defined by the surface normal and the θ_e-direction). These are the perpendicular component ($p = \perp$) for which the electric vector is perpendicular to the plane of emission and the parallel component ($p = \parallel$) for which the electric vector is in the plane of emission. The plane of emission can be seen in Figure 1. These polarization components of the spectral emittance are thus

$$\varepsilon_{\perp}(\lambda,T;\theta_e,\phi_e) = \frac{L^e_{\lambda,\perp}(T;\theta_e,\phi_e)}{\frac{1}{2} L^b_\lambda(T)} \tag{2.7a}$$

$$\varepsilon_{\parallel}(\lambda,T;\theta_e,\phi_e) = \frac{L^e_{\lambda,\parallel}(T;\theta_e,\phi_e)}{\frac{1}{2} L^b_\lambda(T)} \tag{2.7b}$$

Since

$$L^e_\lambda(T;\theta_e,\phi_e) = L^e_{\lambda,\perp}(T;\theta_e,\phi_e) + L^e_{\lambda,\parallel}(T;\theta_e,\phi_e) \tag{2.8}$$

the relationship between the unpolarized spectral directional emittance and its polarized components is

$$\varepsilon(\lambda,T;\theta_e,\phi_e) = \frac{L^e_\lambda(T;\theta_e,\phi_e)}{L^b_\lambda(T)} = \frac{L^e_{\lambda,\perp}(T;\theta_e,\phi_e) + L^e_{\lambda,\parallel}(T;\theta_e,\phi_e)}{L^b_\lambda(T)}$$

$$= \frac{1}{2} [\varepsilon_{\perp}(\lambda,T;\theta_e,\phi_e) + \varepsilon_{\parallel}(\lambda,T;\theta_e,\phi_e)] \tag{2.9}$$

so the unpolarized emittance is simply the mean of the two orthogonally-polarized components.

The emittance of a material surface can be related to other optical properties of that surface. Kirchhoff's law, based upon conservation of energy considerations, states the equality of the emittance and absorptance of an opaque material in equilibrium with its environment. This law holds both for total hemispherical quantities and for spectral directional quantities [2]. For the latter,

$$\varepsilon(\lambda,T;\theta_e,\phi_e) = a(\lambda,T;\theta_i=\theta_e,\phi_i=\phi_e) \tag{2.10}$$

where $a(\lambda,T;\theta_i,\phi_i)$ is the absorptance* for radiation of wavelength λ incident on the surface of temperature T at polar angle θ_i and azimuth angle ϕ_i. For an opaque material, conservation of energy requires that the absorptance and reflectance sum to unity if both quantities are evaluated at the same wavelength, temperature, angles, and polarization. Thus, it follows that

$$\rho(\lambda,T;\theta_e,\phi_e) = 1 - \rho(\lambda,T;\theta_i=\theta_e,\phi_i=\phi_e) \tag{2.11}$$

where $\rho(\lambda,T;\theta_i,\phi_i)$ is the spectral directional hemispherical reflectance** of the material surface of temperature T, for radiation of wavelength λ incident at polar angle θ_i and azimuth angle ϕ_i. This relationship applies not only to the unpolarized functions as shown, but also to each polarization component individually. It is independent of surface character, layering of different materials, etc., as long as the total ensemble of materials forming the target is opaque and in strict thermal equilibrium with its environment. The directional reflectance of a surface can be regarded as the integral of the spectral reflectance distribution function,*** $\rho'(\lambda,T;\theta_i,\phi_i,\theta_r,\phi_r)$ [ster^{-1}] over all reflectance angles (θ_r,ϕ_r) so

---

*The temperature dependence of absorptance and reflectance is often ignored in the literature. Generally, it should not be.

**This is simply the fraction of the radiant power incident on a surface from the direction (θ_i,ϕ_i) which is reflected (into all directions) by the surface.

***See reference 3 for a full discussion of this quantity. The terminologies, notations, and mathematics used to describe it in the literature are very diverse, equally naive, and subject to frequent change, even in the hands of the largely acknowledged experts who call the tune in such matters. For example, see references 4-6. No claim of perfection is made for the notation used in the present Report either.

$$\varepsilon(\lambda,T;\theta_e,\phi_e) = 1 - \rho(\lambda,T;\theta_i=\theta_e,\phi_i=\phi_e)$$

$$= 1 - \int_{\theta_r=0}^{\pi/2} \int_{\phi_r=0}^{2\pi} \rho'(\lambda,T;\theta_i=\theta_e,\phi_i=\phi_e,\theta_r,\phi_r)\cos\theta_r d\Omega_r \qquad (2.12)$$

2.1.1. SPECIAL CASES

2.1.1.1. The Diffuse Reflector. The directional hemispherical reflectance of a diffuse (Lambertian) reflector is independent of the incident angles. Therefore, its directional emittance is also independent of angle.

2.1.1.2. The Specular Reflector. A specular reflector has the property that $\rho'(\lambda,T;\theta_i,\phi_i,\theta_r,\phi_r)$ is zero everywhere except at $\theta_r=\theta_i, \phi_r=\phi_i + \pi$, for which $\rho(\lambda,T;\theta_i,\phi_i) = \pi\,\rho'(\lambda,T;\theta_i,\phi_i,\theta_r,\phi_r)$. For this case, the directional hemispherical reflectance is usually called the specular reflectance and is completely described by the Fresnel equations. The polarized directional emittance components can also be determined from these. The results are especially simple for the case of any opaque specular dielectric material. For this case, the Fresnel equations give [7]

$$\varepsilon_{\perp}(\lambda,T;\theta_e,\phi_e) = 1 - \rho_{\perp}(\lambda,T;\theta_i=\theta_e,\phi_i=\phi_e) = 1 - \frac{\sin^2(\theta_e - \theta_n)}{\sin^2(\theta_e + \theta_n)} \qquad (2.13a)$$

$$\varepsilon_{\parallel}(\lambda,T;\theta_e,\phi_e) = 1 - \rho_{\parallel}(\lambda,T;\theta_i=\theta_e,\phi_i=\phi_e) = 1 - \frac{\tan^2(\theta_e - \theta_n)}{\tan^2(\theta_e + \theta_n)} \qquad (2.13b)$$

where $\theta_n = \sin^{-1}[\sin\theta_e/n(\lambda)]$ and $n(\lambda)$ is the spectral index of refraction of the dielectric material. For specular metals or stacks of partially-transparent specular layers, analogous (though more complex) relations can be written to analytically define the polarized spectral directional emittance. It is equal numerically to one minus the equivalent polarized spectral directional reflectance component in all cases where the total target system is opaque and in thermal equilibrium with its environment. For example, a semitransparent layer of paint deposited upon steel is an opaque target system for which the emittance equals one minus the reflectance, even though the paint layer itself may not be opaque.

2.2. TOTAL RADIANCE

The total spectral radiance of an object is the quantity usually measured by a spectral radiometer. This quantity is the sum of both an emitted and a reflected component,

$$L_\lambda(T;\theta_e,\phi_e) = L_\lambda^e(T;\theta_e,\phi_e) + L_\lambda^r(T;\theta_r=\theta_e,\phi_r=\phi_e) \qquad (2.14)$$

where $L_\lambda(T;\theta_e,\phi_e)$ is the total spectral radiance of wavelength λ leaving the object of temperature T in direction (θ_e,ϕ_e) and $L_\lambda^e(T;\theta_e,\phi_e)$ and $L_\lambda^r(T;\theta_r=\theta_e,\phi_r=\phi_e)$ are, respectively, the emitted and reflected components making up that total spectral radiance. The quantity $L_\lambda(T;\theta_e,\phi_e)$ is composed of linearly-polarized components each of which is a sum of the particular polarization components of the emitted and reflected spectral radiances:

$$L_{\lambda,\perp}(T;\theta_e,\phi_e) = L^e_{\lambda,\perp}(T;\theta_e,\phi_e) + L^r_{\lambda,\perp}(T;\theta_r=\theta_e,\phi_r=\phi_e) \tag{2.15a}$$

$$L_{\lambda,\parallel}(T;\theta_e,\phi_e) = L^e_{\lambda,\parallel}(T;\theta_e,\phi_e) + L^r_{\lambda,\parallel}(T;\theta_r=\theta_e,\phi_r=\phi_e) \tag{2.15b}$$

The emitted components of polarized spectral radiance follow immediately from the emittance definitions,

$$L^e_{\lambda,\perp}(T;\theta_e,\phi_e) = \frac{1}{2}\,\varepsilon_{\perp}(\lambda,T;\theta_e,\phi_e)L^b_\lambda(T) \tag{2.16a}$$

$$L^e_{\lambda,\parallel}(T;\theta_e,\phi_e) = \frac{1}{2}\,\varepsilon_{\parallel}(\lambda,T;\theta_e,\phi_e)L^b_\lambda(T) \tag{2.16b}$$

The reflected components of the polarized spectral radiance are determined by an integration over all incidence angles of the product of the polarized reflectance distribution function and the environmental irradiance available for reflection. But before the results can be given, some digression regarding definitions must be made. Specifically, for any two polarizations, pi and pr, of incident and scattered radiation, respectively, the polarization-dependent spectral reflectance distribution function for a material surface at temperature T is defined by

$$\rho'_{pr,pi}(\lambda,T;\theta_i,\phi_i,\theta_r,\phi_r) \equiv \frac{L^r_{\lambda,pr}(T;\theta_r,\phi_r)}{E^i_{\lambda,pi}(\theta_i,\phi_i)} \tag{2.17}$$

where $L^r_{\lambda,pr}(T;\theta_r,\phi_r)$ is the polarized spectral radiance scattered in the direction (θ_r,ϕ_r) by the surface in question due to the incident polarized spectral irradiance $E^i_{\lambda,pi}(\theta_i,\phi_i)$ coming from the direction (θ_i,ϕ_i). Then

$$L^r_{\lambda,\perp}(T;\theta_r,\phi_r) = \int_{\theta_i=0}^{\pi/2}\int_{\phi_i=0}^{2\pi} [\rho'_{\perp,\perp}(\lambda,T;\theta_i,\phi_i,\theta_r,\phi_r)L^i_{\lambda,\perp}(\theta_i,\phi_i)$$

$$+ \rho'_{\perp,\parallel}(\lambda,T;\theta_i,\phi_i,\theta_r,\phi_r)L^i_{\lambda,\parallel}(\theta_i,\phi_i)]\cos\theta_i d\Omega_i \qquad (2.18a)$$

$$L^r_{\lambda,\parallel}(T;\theta_r,\phi_r) = \int_{\theta_i=0}^{\pi/2}\int_{\phi_i=0}^{2\pi} [\rho'_{\parallel,\perp}(\lambda,T;\theta_i,\phi_i,\theta_r,\phi_r)L^i_{\lambda,\perp}(\theta_i,\phi_i)$$

$$+ \rho'_{\parallel,\parallel}(\lambda,T;\theta_i,\phi_i,\theta_r,\phi_r)L^i_{\lambda,\parallel}(\theta_i,\phi_i)]\cos\theta_i d\Omega_i \qquad (2.18b)$$

where $L^i_{\lambda,p}(T;\theta_i,\phi_i)$ is the spectral radiance of polarization p incident from the direction (θ_i,ϕ_i) due to the environment.

2.2.1. SPECIAL CASES

2.2.1.1. Diffuse Surface. The rather complex radiance equations 2.18 become much simpler for the case of a perfectly diffuse (Lambertian) surface. The concept of perfect diffuseness requires that there be no polarization preference for the emittance and reflectance terms in equations 2.18. Thus, there is no polarization in either the emitted or reflected radiance or in their sum, the total radiance. Hence,

$$L^e_{\lambda,\perp}(T;\theta_e,\phi_e) = L^e_{\lambda,\parallel}(T;\theta_e,\phi_e) = \frac{1}{2}\,\varepsilon(\lambda,T)L^b_\lambda(T) \qquad (2.19)$$

where $\varepsilon(\lambda,T)$ is independent of both θ_e and ϕ_e. In addition, all $\rho'_{p1,p2}$ are equal (at any given wavelength and temperature), independent of the polarizations p1 and p2, and independent of angles. Thus

$$L^r_{\lambda,\perp}(T;\theta_r,\phi_r) = L^r_{\lambda,\parallel}(T;\theta_r,\phi_r) = \frac{1}{2}\frac{\rho(\lambda,T)}{\pi}\int_{\theta_i=0}^{\pi/2}\int_{\phi_i=0}^{2\pi} L^i_\lambda(\theta_i,\phi_i)\cos\theta_i\, d\Omega_i$$

$$= \frac{1}{2}\rho(\lambda,T)\frac{E^i_\lambda}{\pi} = \frac{1}{2}[1 - \varepsilon(\lambda,T)]\frac{E^i_\lambda}{\pi} \qquad (2.20)$$

where E^i_λ is the total irradiance [power/area-wavelength] incident on the surface from the environment. Thus, the total spectral radiance from a diffuse material is both unpolarized and independent of angle, whatever the angular distribution of environmental irradiance:

$$L_\lambda(T) = \varepsilon(\lambda,T)L^b_\lambda(T) + [1 - \varepsilon(\lambda,T)]\frac{E^i_\lambda}{\pi} \qquad (2.21)$$

and

$$L_{\lambda,\perp}(T) = L_{\lambda,\parallel}(T) = \frac{1}{2}L_\lambda(T) \qquad (2.22)$$

2.2.1.2. Isotropic Environment. If the irradiance on the material from the environment is unpolarized and isotropically distributed [i.e., independent of (θ_i,ϕ_i)], then another simplified description of the reflected radiance is possible:

$$L^r_{\lambda,\perp}(T;\theta_r=\theta_e,\phi_r=\phi_e) = \frac{1}{2}L^i_\lambda\int_{\theta_i=0}^{\pi/2}\int_{\phi_i=0}^{2\pi}[\rho'_{\perp,\perp}(\lambda,T;\theta_i,\phi_i,\theta_r,\phi_r)$$

$$+ \rho'_{\perp,\parallel}(\lambda,T;\theta_i,\phi_i,\theta_r,\phi_r)]\cos\theta_i\, d\Omega_i$$

$$= \frac{1}{2}\rho_\perp(\lambda,T;\theta_r=\theta_e,\phi_r=\phi_e)L^i_\lambda = \frac{1}{2}[1 - c_\perp(\lambda,T;\theta_e,\phi_e)]L^i_\lambda \qquad (2.23a)$$

and

$$L^r_{\lambda,\parallel}(T;\theta_r=\theta_e,\phi_r=\phi_e) = \frac{1}{2}\rho_{\parallel}(\lambda,T;\theta_r=\theta_e,\phi_r=\phi_e)L^i_\lambda = \frac{1}{2}[1-\varepsilon_{\parallel}(\lambda,T;\theta_e,\phi_e)]L^i_\lambda \quad (2.23b)$$

so that the total polarized spectral radiance components are

$$L_{\lambda,\perp}(T;\theta_e,\phi_e) = \frac{1}{2}\varepsilon_{\perp}(\lambda,T;\theta_e,\phi_e)L^b_\lambda(T) + \frac{1}{2}[1-\varepsilon_{\perp}(\lambda,T;\theta_e,\phi_e)]L^i_\lambda \quad (2.24a)$$

$$L_{\lambda,\parallel}(T;\theta_e,\phi_e) = \frac{1}{2}\varepsilon_{\parallel}(\lambda,T;\theta_e,\phi_e)L^b_\lambda(T) + \frac{1}{2}[1-\varepsilon_{\parallel}(\lambda,T;\theta_e,\phi_e)]L^i_\lambda \quad (2.24b)$$

2.2.1.3. Specular Surface. For a perfectly specular surface, the reflectance distribution functions are non-zero only if $\theta_r=\theta_i, \phi_r=\phi_i+\pi$. Additionally, the mixed-polarization terms $\rho'_{\perp,\parallel}$ and $\rho'_{\parallel,\perp}$ are zero everywhere since specular reflection does not change $\perp$ to $\parallel$ or vice versa. Thus,

$$\begin{aligned} L^r_{\lambda,\perp}(T;\theta_r,\phi_r) &= \pi\,\rho'_{\perp,\perp}(\lambda,T;\theta_i=\theta_r,\phi_i=\phi_r+\pi,\theta_r,\phi_r)L^i_{\lambda,\perp}(\theta_i=\theta_r,\phi_i=\phi_r+\pi) \\ &= \rho_{\perp}(\lambda,T;\theta_r,\phi_r)L^i_{\lambda,\perp}(\theta_r,\phi_r+\pi) \\ &= [1-\varepsilon_{\perp}(\lambda,T;\theta_r,\phi_r)]L^i_{\lambda,\perp}(\theta_r,\phi_r+\pi) \end{aligned} \quad (2.25a)$$

and

$$L^r_{\lambda,\parallel}(T;\theta_r,\phi_r) = [1-\varepsilon_{\parallel}(\lambda,T;\theta_r,\phi_r)]L^i_{\lambda,\parallel}(\theta_r,\phi_r+\pi) \quad (2.25b)$$

Therefore, the polarized components of the total spectral radiance are

$$L_{\lambda,\perp}(T;\theta_e,\phi_e) = \frac{1}{2}\varepsilon_{\perp}(\lambda,T;\theta_e,\phi_e)L^b_\lambda(T) + [1-\varepsilon_{\perp}(\lambda,T;\theta_e,\phi_e)]L^i_{\lambda,\perp}(\theta_e,\phi_e+\pi) \quad (2.26a)$$

$$L_{\lambda,\parallel}(T;\theta_e,\phi_e) = \frac{1}{2}\varepsilon_{\parallel}(\lambda,T;\theta_e,\phi_e)L^b_\lambda(T) + [1-\varepsilon_{\parallel}(\lambda,T;\theta_e,\phi_e)]L^i_{\lambda,\parallel}(\theta_e,\phi_e+\pi) \quad (2.26b)$$

The totality of results based on radiation-theoretic principles which will be of use at later points in this Report have now been enumerated. In fact, for the sake of internal consistency, more results have been included in this Section than will receive direct use in the sequel.

3

THEORY OF MEASUREMENT

3.1. GENERAL REMARKS

The signal (voltage), V, from a detector in a system, the entrance aperture of which is exposed in the spectral interval $\Delta\lambda$ to a spectral radiance L_λ, is

$$V = \bar{R}(\lambda)\ \bar{L}_\lambda \Delta\lambda \tag{3.1}$$

where $\bar{R}(\lambda)$ is the mean-spectral system responsivity and $\bar{L}_\lambda$ the mean-spectral radiance in $\Delta\lambda$. If equation 3.1 is to be an accurate result, it is necessary that the spectral interval $\Delta\lambda$ be so small that $R(\lambda)$ and L_λ do not vary substantially in that interval. The nature of $R(\lambda)$ is not examined in detail here since it plays no role in the final results. The bar over any symbol is used to indicate that the quantity represented by the symbol has been averaged over some spectral interval, $\Delta\lambda$. Notationally, then, for example, $\bar{R}(\lambda)$ and $R(\bar{\lambda})$ are equivalent and neither of these quantities depends on λ in the strictest sense, but only on the central spectral location of $\Delta\lambda$. If $\Delta\lambda$ is sufficiently small, this central-location dependence essentially becomes a functional spectral dependence. The assumption is here made that $\Delta\lambda$ is so small that the spectral averaging has no significant effect and the bar notation is thus dropped at this point.

In a double-beam differencing system, the signal produced is $V_{1,2} = V_1 - V_2$ where

$$V_1 - V_2 = R(\lambda)\{[L_\lambda]_1 - [L_\lambda]_2\}\Delta\lambda \tag{3.2}$$

and where $[L_\lambda]_1$ and $[L_\lambda]_2$ are the spectral radiances at the entrance apertures in beams 1 and 2, respectively. If $[L_\lambda]_1$ is produced by emission and reflection from a target (t1) of temperature T_1 being viewed (see Figure 1) from the direction (θ_e^1, ϕ_e^1), then

$$[L_\lambda]_1 = \tau_1(\lambda)[\varepsilon^{t1}(\lambda, T_1, \theta_e^1, \phi_e^1)\, L_\lambda^b(T_1) + \int_{\theta_i=0}^{\pi/2} \int_{\phi_i=0}^{2\pi} \rho^{t1}(\lambda, T_1; \theta_i, \phi_i, \theta_r=\theta_e^1, \phi_r=\phi_e^1) L_\lambda^i(\theta_i, \phi_i) \cos\theta_i \, d\Omega_i] \quad (3.3)$$

where $\tau_1(\lambda)$ is the spectral transmission of the optical path from the target to the fore-optics of the instrument containing the detector to which $R(\lambda)$ refers. The remainder of the notation has been defined in Section 2. An expression similar to equation 3.3 also holds for $[L_\lambda]_2$. Calibration of a double-beam differencing system is achieved by simultaneously letting each beam view a different reference source, the difference being one of temperature only. The signal produced under these circumstances, $V_{c1,c2}$, is

$$V_{c1,c2} = R(\lambda)\tau(\lambda)\varepsilon^c(\lambda, T^c)[L_\lambda^b(T_1^c) - L_\lambda^b(T_2^c)]\Delta\lambda \quad (3.4)$$

where ε^c is the (known) reference emittance, T_1^c and T_2^c are the temperatures of references 1 and 2, respectively, and T^c may be taken as T_1^c, T_2^c or any intermediate temperature.* In equation 3.4 , the reflected radiance terms are absent because the incident radiation environment is the same for

*The temperature dependence of the emittance of most materials is so weak that it can be ignored. However, for theoretical completeness, the notational indication of this weak dependence is retained.

both references and they thus cancel in the difference. Since the product $R(\lambda)\tau(\lambda)$ is the only unknown in equation 3.4 , this product is determined by that equation. The actual procedures used in making (apparent) radiance and emittance measurements do not involve direct determination of $R(\lambda)\tau(\lambda)$, though. As will be described shortly, the evaluation of (apparent) radiance or emittance involves ratios of voltages in which the $R(\lambda)\tau(\lambda)$ product is the same. This product cancels in the ratio so its actual value is unimportant.

3.2. PRINCIPLES OF RADIANCE MEASUREMENT

Spectral radiance measurements are made by spectrally sampling the difference in radiance from a target surface of temperature T^t and from a reference source of temperature T^c. This radiance difference produces a signal $V_{t,c}$:

$$V_{t,c} = R(\lambda)\tau(\lambda)[L_\lambda^t(T^t) - L_\lambda^b(T^c)]\Delta\lambda \tag{3.5}$$

where $L_\lambda^b(T^c)$ represents the <u>total</u> cavity radiance, including that reflected. When this result is divided by equation 3.4, after appropriate rearrangement the result is

$$L_\lambda^t(T^t) = L_\lambda^b(T^c) + \varepsilon^c(\lambda,T^c)\,\frac{V_{t,c}}{V_{c1,c2}}\,[L_\lambda^b(T_1^c) - L_\lambda^b(T_2^c)] \tag{3.6}$$

The tacit assumption has clearly been made that $\tau(\lambda)$ was the same for the measurement of both $V_{t,c}$ and $V_{c1,c2}$. This assumption is met when laboratory measurements are made, but it may not be met when field measurements are made. For the former, it is no problem to use the same optical path for

both the $V_{t,c}$ and $V_{c1,c2}$ measurements. In the field, this would present unreasonable difficulties because distances between the targets and the detecting instrument may be as large as several tens of feet. However, field data will be useful only in spectral regions where atmospheric transmission is appreciable over distances of several kilofeet. Thus, in such spectral regions, $\tau(\lambda)$ is essentially unity for the comparatively short ranges used for making field measurements and equation 3.6 is valid for such spectral regions. If there is doubt concerning the value of $\tau(\lambda)$, the left-hand side of equation 3.6 should be called "spectral apparent radiance." No angular dependence or polarization indication has been used in equations 3.5 and 3.6,but these can be routinely included as desired.

3.2.1. SPECTRAL APPARENT TEMPERATURE. This is the temperature which a blackbody would require in order to produce the observed spectral radiance at the wavelength in question. Spectral apparent temperature is denoted by $T^{app}(\lambda)$, and, from equation 2.1 and Lambert's law, it is implicitly defined by the equation

$$L_\lambda = \frac{c_1}{\pi\lambda^5}\left\{\exp\left[\frac{c_2}{\lambda T^{app}(\lambda)}\right] - 1\right\}^{-1} = L_\lambda^b(T^{app}) \qquad (3.7)$$

where L_λ is the spectral radiance from the object to which $T^{app}(\lambda)$ applies. It is evident that $T^{app}(\lambda)$ depends on the actual temperature of the object (since L_λ does) and the environmental spectral radiance scattered by the object. Spectral apparent temperature is a convenient quantity in terms

of which to present spectral data as compared to spectral apparent radiance. The reason is that the dynamic range of the former over the full spectral interval of interest is not large compared to the dynamic range of local-spectral variations. This is not true of spectral radiance. The original spectral radiance can be recovered via equation 3.7.

3.2.2. SPECTRAL APPARENT EMITTANCE. The spectral shape of $L_\lambda(T)$ from a given object describes the non-blackbody radiating characteristics of that object. An equivalent description of these characteristics can be given through the spectral apparent emittance, $\varepsilon^{app}(\lambda,T)$, defined implicitly by

$$L_\lambda(T) = \frac{c_1 \varepsilon^{app}(\lambda,T)}{\pi \lambda^5} \left[\exp\left(\frac{c_2}{\lambda T}\right) - 1\right]^{-1} = \varepsilon^{app} L_\lambda^b(T) \quad (3.8)$$

where T is the actual object temperature. Thus, apparent emittance can be gotten from field measurements. No angular dependence or polarization component designations are indicated in equation 3.8, but these can be included in each side of this equation as wanted.

3.3. PRINCIPLES OF EMITTANCE MEASUREMENT

The methodology of measuring apparent emittance in the field has just been presented. Some methodologies of measuring actual emittances in the laboratory are now given. A general presentation is given first and then some specializations are reported.

The basic technique used in an emittance measurement employing a double-beam differencing system is to view two samples of the material

in question which differ only in (known) temperature -- one sample occupying each beam of the instrument. The resulting voltage, $V_{t1,t2}$, is*

$$V_{t1,t2} = R(\lambda)\tau(\lambda)\ \varepsilon^{t}(\lambda,T;\theta_e,\phi_e)[L_\lambda^b(T_1^t) - L_\lambda^b(T_2^t)]\Delta\lambda \tag{3.9}$$

This result is divided by the result obtained when viewing two reference cavities (equation 3.4). After rearrangement, the result is

$$\varepsilon^{t}(\lambda,T;\theta_e,\phi_e) = \varepsilon^{c}(\lambda,T)\ \frac{V_{t1,t2}}{V_{c1,c2}}\left[\frac{L_\lambda^b(T_1^c) - L_\lambda^b(T_2^c)}{L_\lambda^b(T_1^t) - L_\lambda^b(T_2^t)}\right] \tag{3.10}$$

Strict cancellation of the $R(\lambda)\tau(\lambda)\Delta\lambda$ factor can be obtained for laboratory measurements because the same optical path from samples and cavities to the instrument can be realized. Equation 3.10 represents the basis for all laboratory emittance measurements (see Section 7).

The technique of measurement underlying the derivation of equation 3.10 was based on the assumption that two identical target samples were available. Actually, this assumption can be relaxed if appropriate precautions are taken. The total (emitted plus reflected) spectral radiance from any object contained in a black enclosure is independent of the material constituting that object, provided the temperatures of the enclosure walls and the object are the same. Thus, if $V_{t1,t2}$ were

*Strict cancellation of the reflected terms is ensured by placing the two samples in the same radiation environment.

measured with (say) $T_1^t = T^W$ where T^W is the wall temperature of a black enclosure around <u>both</u> target samples, precisely the same value would be obtained for $V_{\chi,t2}$ where "χ" represents any material -- provided $T^\chi = T^W$. Hence, if only one target sample is available, a "dummy" sample can be substituted for the second target sample; but the black enclosure and dummy-temperature control must be used. Such use is routine for all emittance measurements made with the FISR, independently of whether two samples of the target material are available.

4

INSTRUMENTATION: CONSTRUCTION, CHECK OUT, CALIBRATION, AND ERROR ANALYSIS

4.1. BASIC INSTRUMENTATION

As discussed in Section 3, a double-beam spectrophotometer, the output of which is proportional to the difference in the radiance from the objects in the two beams, can be used to provide absolute measurements of either emittance or radiance. Available commercial instruments are unsuited to the differencing technique. Therefore, such an instrument was custom designed and built under Air Force sponsorship by Willow Run Laboratories. For economic reasons, components from commercial instruments were used as practicality permitted.

The instrument consists of a monochromator with appropriate telescopic fore-optics ahead of the entrance slit. The radiometer system is shown schematically in Figure 2 and a photograph of it with the protective cover removed is presented in Figure 3. The fore-optics consist of two Herschelian-type reflecting telescopes, the primary mirrors of which are two symmetrically-placed 21°-off-axis paraboloids. Behind these, optical flats are used to fold the two convergent f/12 beams onto a common horizontally-oriented field stop which constitutes the entrance slit of the monochromator. An alternately transmitting and reflecting beam-chopper (chopping frequency of 390 Hertz) operates immediately ahead of the entrance slit to alternately sample the two beams and to direct the resulting samples to the detector via a common optical channel. The entrance slit (field stop) has fixed dimensions of 3mm by 12mm which define an angular field of view of 0.64° by 2.56°.

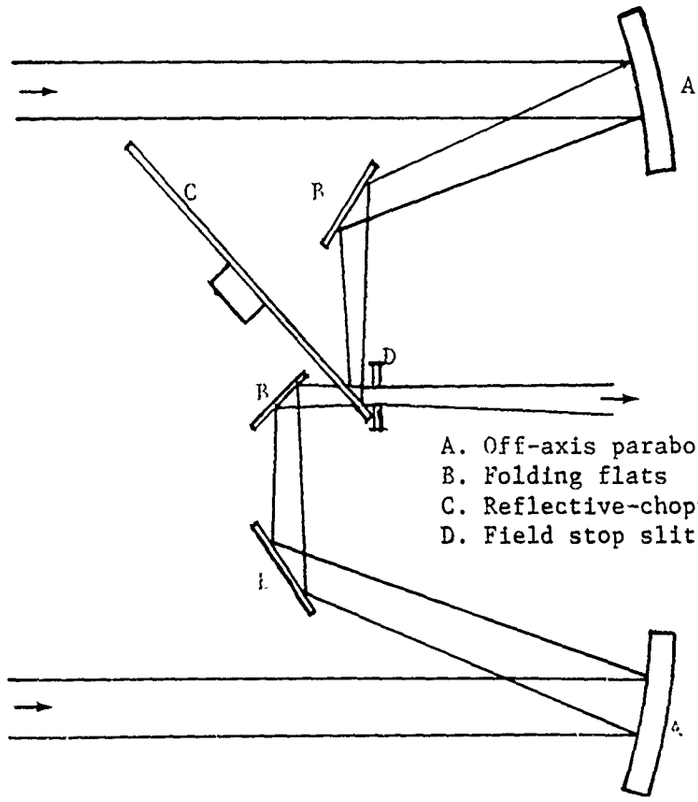

A. Off-axis paraboloid telescope objectives
B. Folding flats
C. Reflective-chopper beam switcher
D. Field stop slit

FIGURE 2. a) SCHEMATIC OF FISR FORE-OPTICS IN PLAN VIEW

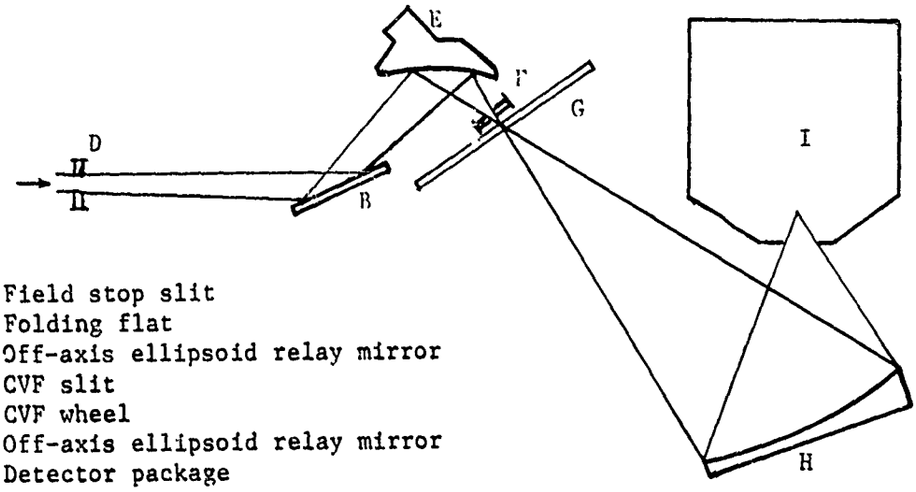

D. Field stop slit
B. Folding flat
E. Off-axis ellipsoid relay mirror
F. CVF slit
G. CVF wheel
H. Off-axis ellipsoid relay mirror
I. Detector package

FIGURE 2. b) SCHEMATIC OF FISR MONOCHROMATOR-DETECTOR OPTICS IN SIDE VIEW

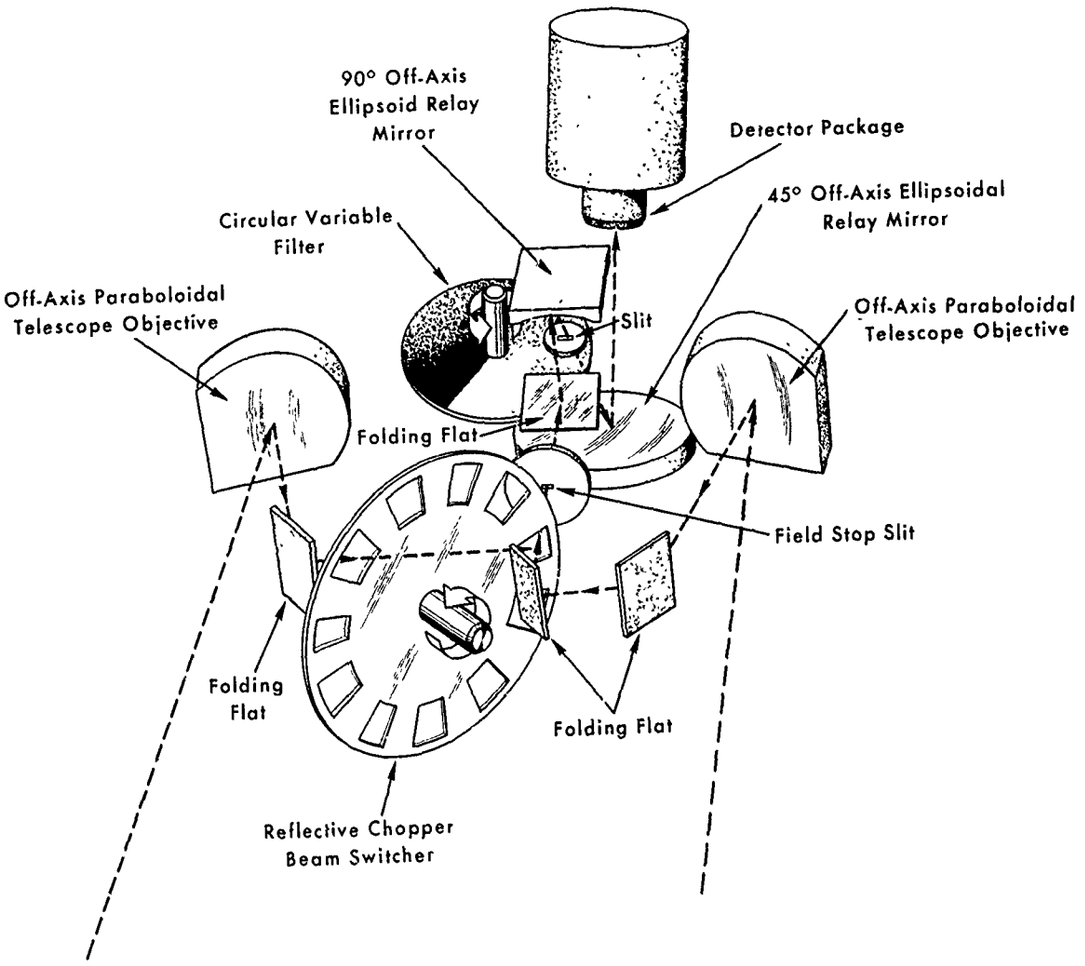

FIGURE 2. c) OVERALL PICTORIAL REPRESENTATION OF THE FISR FORE-OPTICS, MONOCHROMATOR, AND DETECTOR PACKAGE.

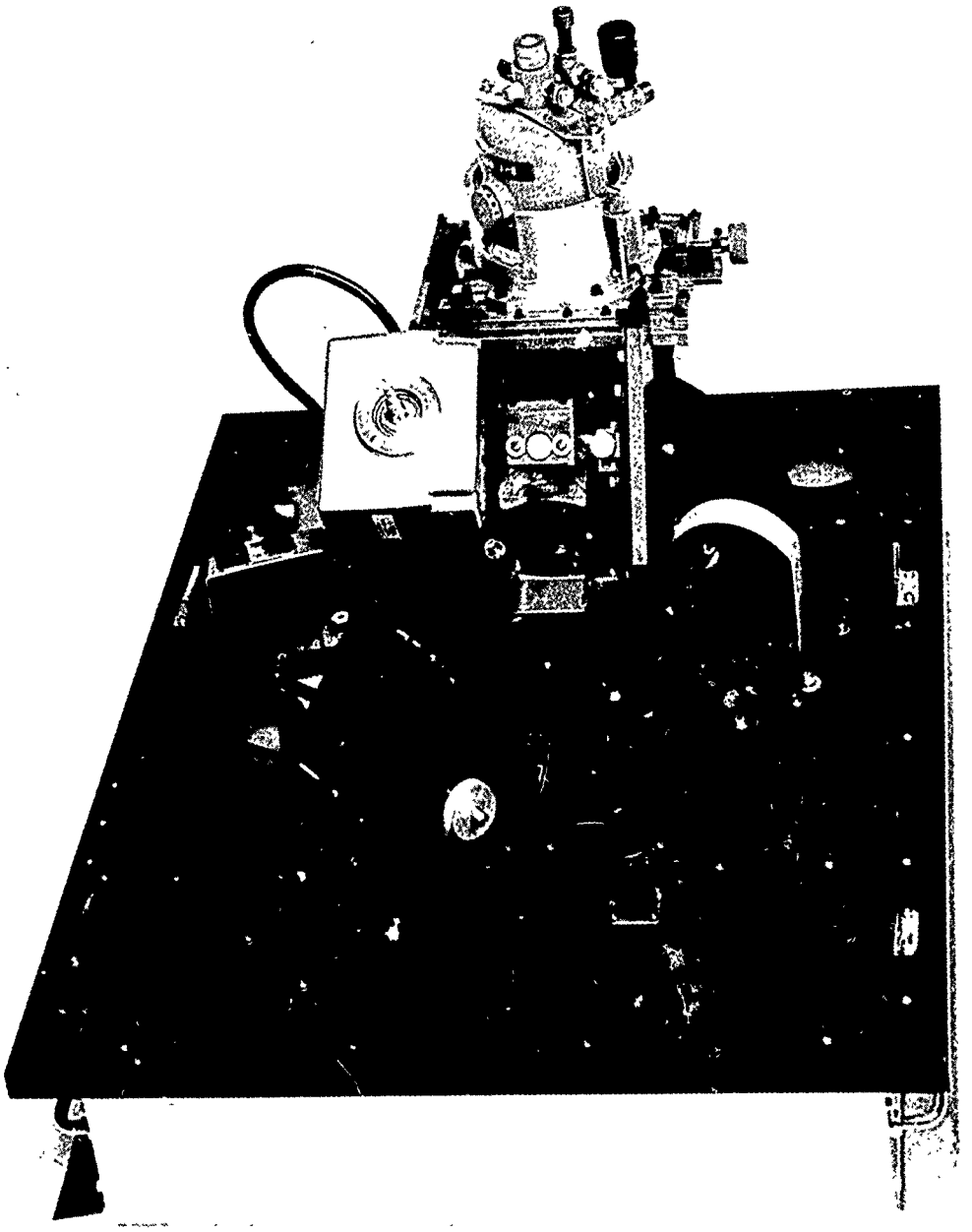

FIGURE 3. A PHOTOGRAPH OF THE FISR FORE-OPTICS, MONOCHROMATOR AND DETECTION PACKAGE WITH THE PROTECTIVE COVER REMOVED

From the entrance slit, the common beam is reimaged by use of a 90°-off-axis,ellipsoidal relay mirror with a demagnification ratio of 6:1. The demagnified image formed by this mirror is defined and sharpened by a second slit. Immediately behind this slit is a circular variable filter wheel (CVF) which passes only a narrow spectral band of energy, the wavelengths of which depend upon the rotation position of the filter wheel. The beam diverging from the filter is refocussed with a demagnification ratio of 2:1 by a 45°-off-axis,ellipsoidal relay mirror onto a cooled detector. This mirror represents the limiting aperture of the system. The CVF has been tilted slightly with respect to the optical axis in order to prevent the detector from being reflected back onto itself. Otherwise, noise could be produced by vibrations of the CVF which would give the detector a chopped version of its own radiation image.

In addition to the usual spectral analysis, a combination spectral and linear-polarization analysis may also be performed. This is done by inserting a gold-wire-grid polarizer element deposited on a silver bromide substrate* in the common beam immediately after the monochromator entrance slit. This location precludes the self-emission from the polarizer from being chopped and added to the difference signal.

Except for the reflecting portions of the chopper and 45°-off-axis ellipsoidal mirror, all reflective optics are stock components used in the Perkin-Elmer Model 99 Monochromator. The circular variable filter (see Figure 4) is a three piece segmented assembly manufactured by Optical Coating Laboratories. The filter spans the wavelength range of 2.5 to 14.5μm

*This is the Perkin-Elmer Model 186-0240.

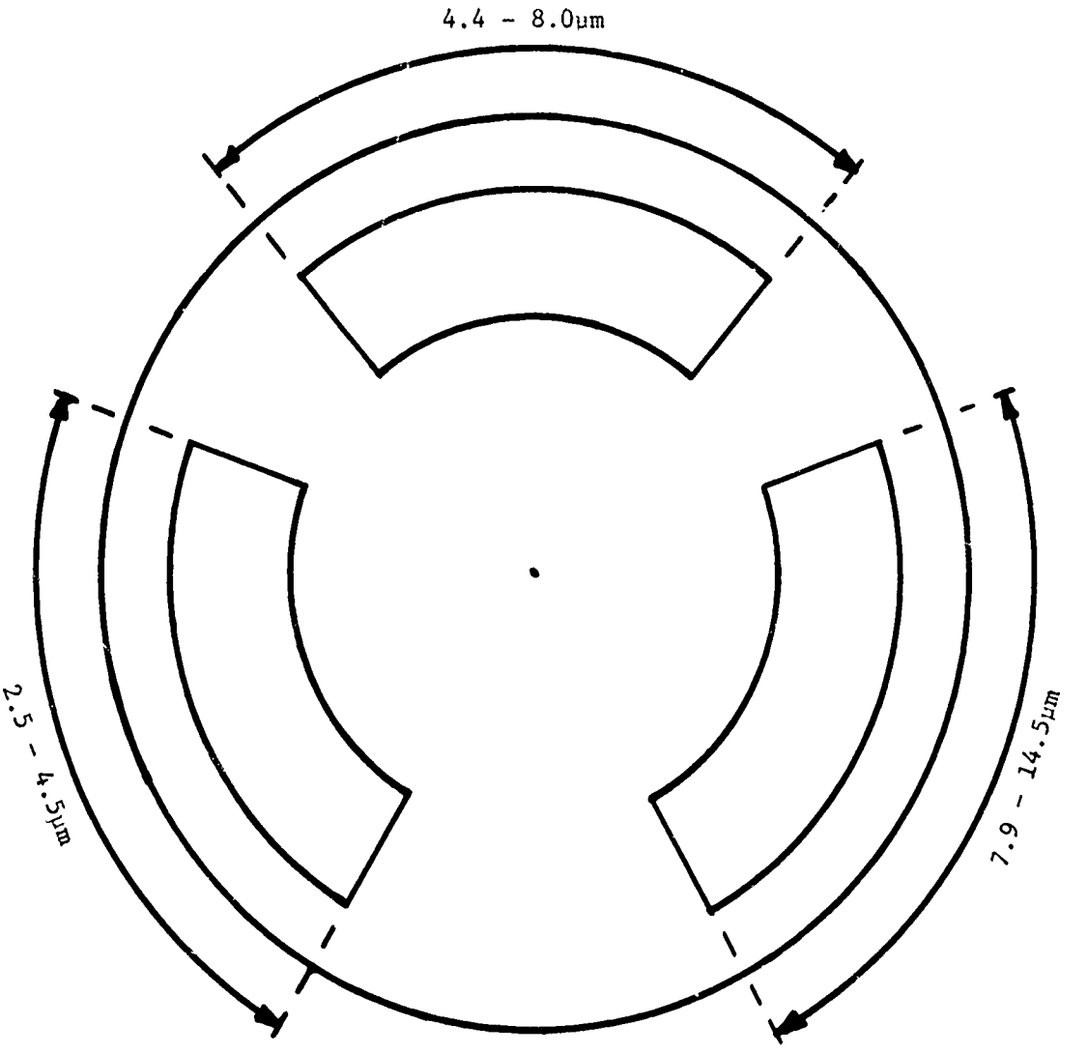

FIGURE 4. THE LAYOUT OF THE CIRCULAR VARIABLE FILTER WHEEL. ONLY THE THREE ANGULAR-SEGMENT WEDGE PORTIONS ARE TRANSPARENT: THE REMAINDER OF THE WHEEL IS PERFECTLY OPAQUE. AS THE FILTER WHEEL ROTATES, APPROXIMATELY 170 SPECTRAL SAMPLES ARE OBTAINED FROM EACH TRANSPARENT SEGMENT.

using three separated 80° annular segments with a 0.1μm spectral overlap between adjacent segments. The segments are separated by 30° opaque sectors. In the FISR, only the 3.3-14.0μm spectral range is utilized. The spectral resolution achieved with this filter wheel and slit-f/No. combination is 2 percent or less of the central wavelength ($\Delta\lambda/\lambda \leq 0.02$).

Because of the spectral region over which the instrument operates, two separate detectors are required. Below 5.6μm, an indium antimonide (InSb) detector cooled to 77°K is used. At the longer wavelengths, a mercury-doped germanium (Ge:Hg) detector cooled to 4°K is used. The total spectral scan time for the entire waveband of 3.3 to 14μm, including detector changing, is about 90 seconds.

The a-c signal from the detector is amplified and then synchronously demodulated. The synchronous demodulator transforms the signal component having the chopper-modulation frequency into a proportional d-c voltage while rejecting the remainder of the signal (i.e., noise). Thus, a voltage is produced by the demodulator with a d.c. value which is proportional to the radiance difference between the objects in the two optical beams at the wavelength being passed by the circular variable filter. This output voltage is recorded by using a digital voltmeter* as an analog-to-digital converter and recording the result on a digital paper-tape printer**. The wavelength is simultaneously recorded on the tape by reading a digital shift encoder mechanically linked to the circular variable filter. This encoder output also provides the trigger pulses for data recording to ensure that digitization always occurs at the same set of wavelengths. The digital

*Hewlett-Packard Model 3440A
**Hewlett-Packard Model 5960 562A

sampling rate is approximately twice the information rate imposed by the spectral resolution and CVF rotation rate, and only about half the limiting rate set by the electronics and recording system.*

Figure 5 is a photograph of the complete system as it is normally used for field measurements. It is often operated in the van used for transportation purposes,although this van is not included in the photograph. The spectroradiometer is shown mounted on a turntable with the digital voltmeter and recording rack mounted immediately below. If necessary, the spectroradiometer and the rack may be separated up to 140 feet, this distance being the length of the umbilical cord connecting the units.

The spectroradiometer as pictured has several ancillary units affixed to it. The two upright cylinders on the left are the reference cavities (to be described) which are used for calibration during emittance or radiance measurements. Immediately below each blackbody is a diagonal mirror which serves to fold the line of sight of each telescope by 90°. These removable mirrors are used only when making field measurements and may be independently rotated so that each of the two beams can contain either its respective reference cavity or targets of interest. A reflex sight, the eyepiece of which is visible above the spectroradiometer cover, is used to view the monochromater entrance slit. The operator may therefore view the scene upon which either of the fore-optic telescope systems is directed. The reflex sight is removed during measurement operations.

---

*The spectral "sampling rate" is $\Delta\lambda/\lambda = 0.00342$.

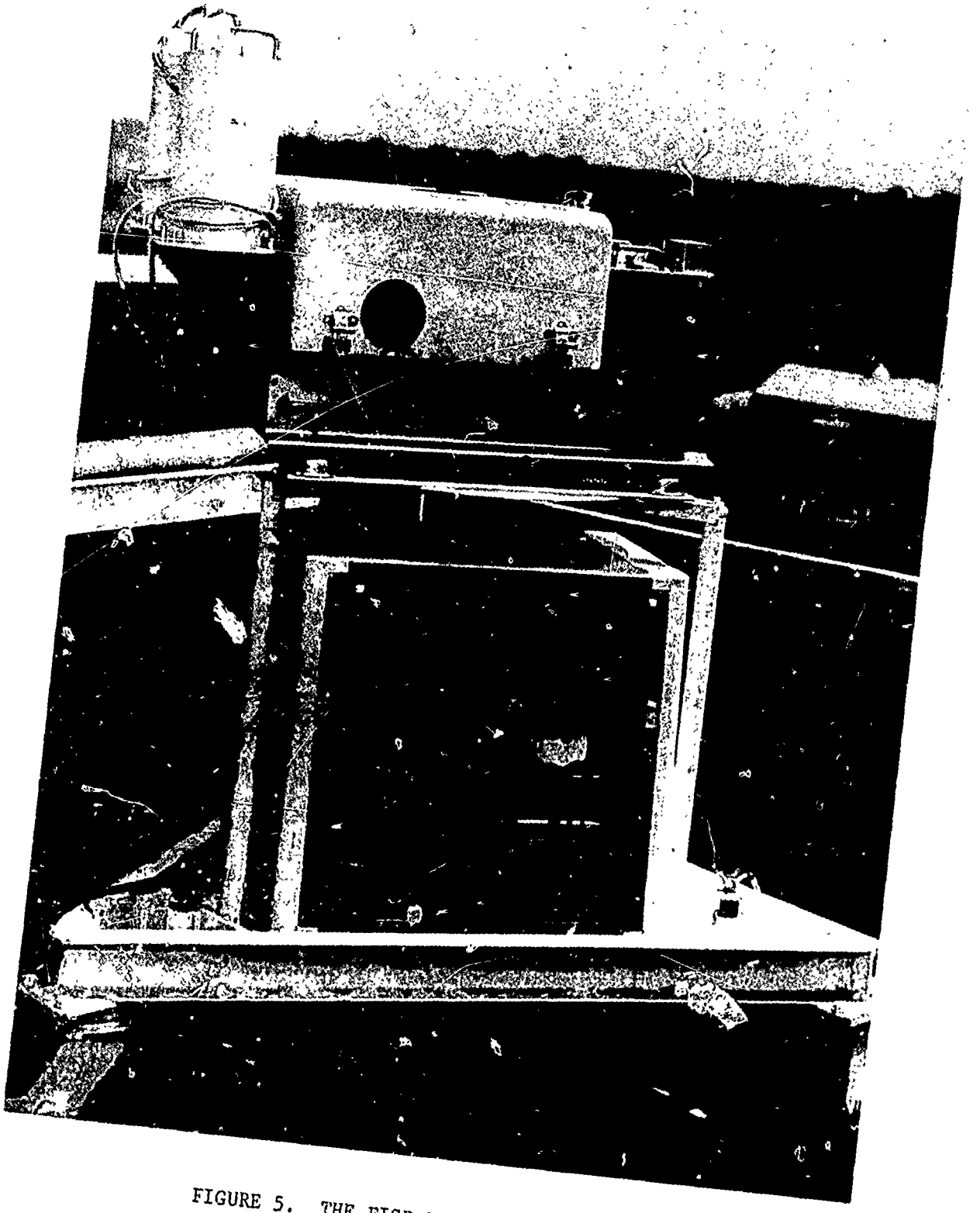

FIGURE 5. THE FISR READY FOR FIELD USE.

4.2. SPECIAL ASPECTS OF THE DESIGN AND FABRICATION

4.2.1. BEAM BALANCE. Because the FISR detects a difference between two optical beams, it is necessary to have equal optical throughputs for the beams. This equality was accomplished by defining the fields of view of both beams by use of the entrance slit, and by using the 45°-off-axis, ellipsoidal mirror as the limiting aperture of the monochrometer (no other optical elements are limiting). Obviously, these are both elements which are common to the two channels and which consistently and equally define their throughputs. Additionally, the coating of all reflecting surfaces was monitored and controlled to prevent differences in reflectivity. All optical surfaces were coated with a hard aluminum alloy designed to minimize unequal degradation of individual elements through normal handling and cleaning.

Beam unpolarized transmission balance has remained within $\pm 6\%$ since construction of the instrument. A correction for any imbalance is made during data reduction on every FISR run. These corrections are based on reference cavity data which are also taken on every run. Since the beam transmission balance is good and since the two beam geometries are essentially identical, the polarization balance is necessarily good. However, there is some polarization bias in the total instrument although it is about the same for each beam. For present purposes, $\tau_p(\lambda)$ is used to represent the spectral transmission of either FISR beam for the polarization state p. A spectral "degree of polarization" of the instrument is then

defined by $P(\lambda) = [\tau_{\perp}(\lambda) - \tau_{\parallel}(\lambda)]/[\tau_{\perp}(\lambda) + \tau_{\parallel}(\lambda)]$. The following measured values are typical

$$P(4.75\mu m) = 0.067$$

$$P(5.30\mu m) = 0.057$$

$$P(10.60\mu m) = 0.054$$

Here, the designation $\perp$ means the electric vector is perpendicular to the long axis of the entrance (field stop) slit.

The calculated angular field-of-view sensitivity is illustrated in Figure 6. The calculation was based on known properties of the optical components used.

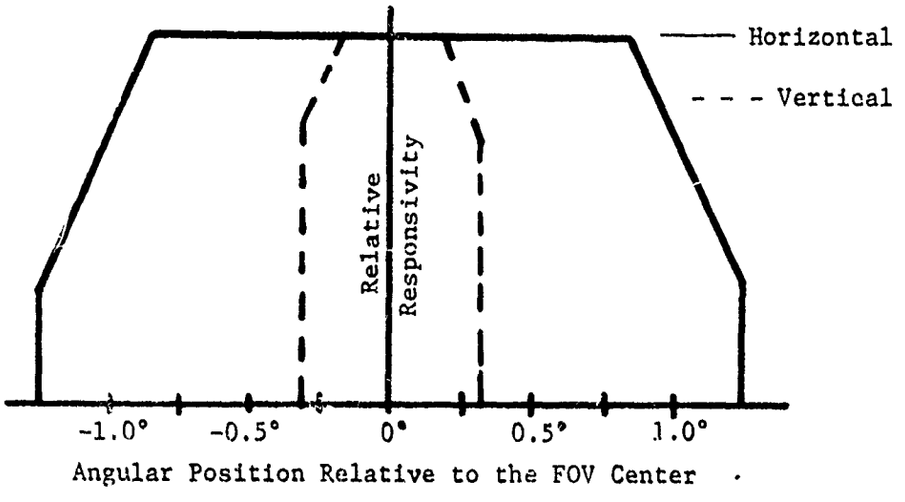

FIGURE 6. THE FISR SYSTEM RELATIVE ANGULAR RESPONSIVITY TO A POINT SOURCE

4.2.2. THE TRANSMITTING/REFLECTING BEAM CHOPPER. The chopper blank was manufactured by Corning Glass from a .060" thickness of their Fotoceram B ceramic using a photoetch process. Through careful preparation of the photo master, a transmitting slot width and reflecting-blade width constancy of $\pm$ 0.35% was achieved. This tolerance, in conjunction with electronic biasing, was deemed acceptable for the synchronous demodulation process. The chopper blank was ground and polished to optical flatness and was aluminized along with the remainder of the optics. The chopper is driven with a synchronous motor and chops at a frequency of 390 Hertz. This frequency was selected for three reasons: 1) it is high enough to avoid 1/f noise and 2) and 3) it is not significantly near 400 Hertz or any integer multiple of 60 Hertz.

4.2.3. REFERENCE CAVITIES. The use of reference cavities for calibration when making emittance and radiance measurements has been described in Section 3. A pair of identical cylindrical cavities was designed and built (one for each FISR channel), the cavity being about 7" deep with a conical termination and presenting a clear aperture of 2.3 inches diameter. This aperture is more than sufficient to fill the collecting aperture of either of the FISR telescopes. The cavities can be operated in the temperature range from ambient to 107°C by use of resistance wire windings. Active temperature control during a spectral scan has not proved to be necessary since the thermal capacity of the cavity walls, the low ratio of aperture area to internal surface area, and the appropriate use of radiation baffles and thermal insulation all tend to produce a uniform and

stable cavity temperature in the situations in which the FISR has been used. Even for windy field conditions, drift in cavity temperature during the time necessary for a spectral scan is not detectable. This temperature is monitored with thermistors mounted in the cavity walls.

The cavity inner surfaces are coated with 3M black paint. Theoretical calculation of the cavity emittance using the method of Gouffé [8, 9] and the known emittance of the paint [10, 11] indicated a value of not less than 0.996 throughout the 3.5 to 14.5μm region except around 9.0μm. See Figure 7. The calculated cavity emittance drops slightly below 0.992 at 9.0μm because the paint has a slightly lower emittance at this wavelength than in the remainder of the 3.5-14.5μm region.* Additionally, total goniometric reflectance measurements of the cavities at 0.633μm have indicated a normal emittance of 0.9985 $\pm$ 0.0005 in agreement with the calculated value for that wavelength using the known cavity geometry and the optical properties of the inner cavity material.

The temperature variation from point to point in the reference cavities is about $\pm$ 0.01°K which is much less than the accuracy with which this temperature can be measured, the latter being about $\pm$ 0.10°K.

4.2.4. THE DIGITAL VOLTMETER. Although this instrument is a commercial product, the results of an a-c-rejection check-out are given here for convenience. Figure 8 contains these results. They were obtained with a Wavetek III sine wave generator set for 0.3 volt peak-to-peak output, both

*This minute variation in reference cavity spectral emittance has no detectable effect on data measured using the FISR. In fact the FISR measurement accuracy makes the assumption of unit emittance (at all wavelengths) for the reference cavities perfectly reasonable, although this assumption has not been made for emittance calculations performed to date. Rather, the values represented in Figure 7 have been used.

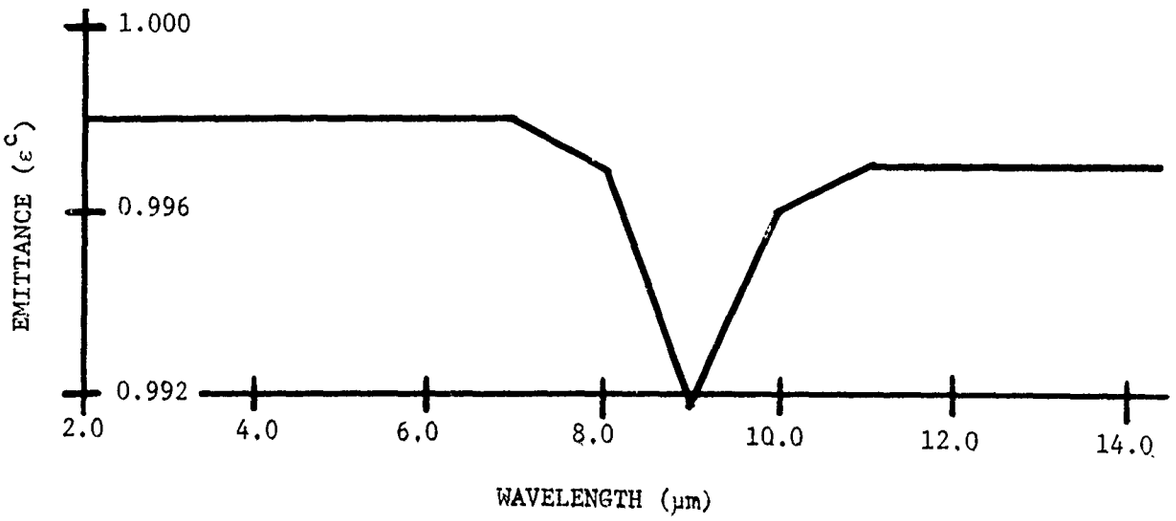

FIGURE 7. REFERENCE CAVITY SPECTRAL EMITTANCE
(FROM THE GOUFFÉ METHOD)

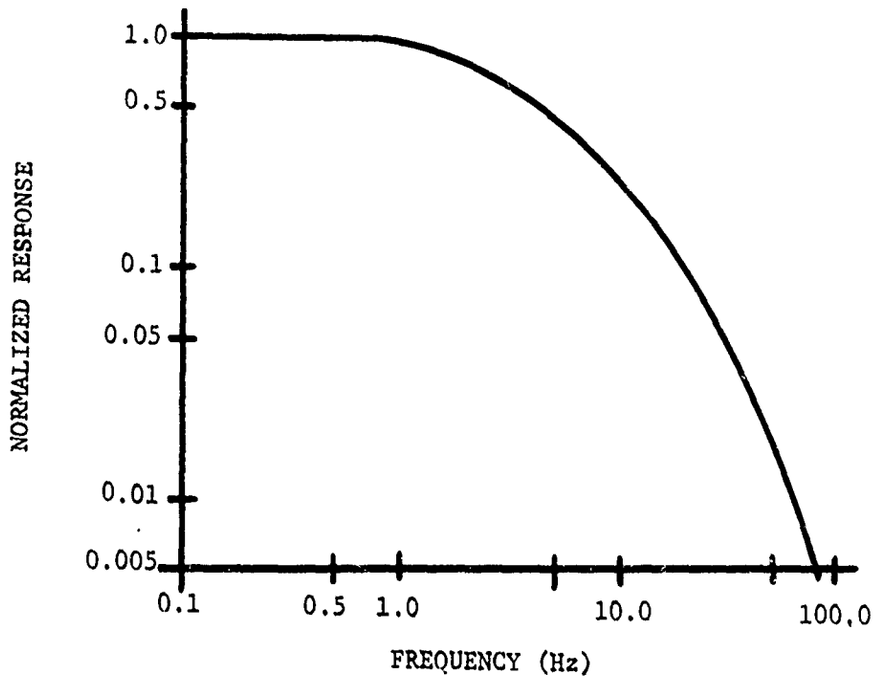

FIGURE 8. THE NORMALIZED FREQUENCY RESPONSE
OF THE DIGITAL VOLTMETER

with and without d.c. offset. The a.c. rejection was found to be independent of the d.c. offset.

4.3. CALIBRATION

There are two major aspects of the FISR operation which require calibration. These involve the determination of the reference cavity temperatures (thermistor calibration) and the determination of operating wavelength vs. filter-wheel orientation (spectral calibration). The results of the former have already been reported in Section 4.2.3.

Spectral calibration was achieved using 13 known transmission lines in Saran Wrap bounded by 2.72 and 13.38μm. These lines are roughly evenly-spaced and linear interpolation is used between them. Thus, the shaft encoder was spectrally calibrated in the wavelength vs. shaft-orientation sense. The wavelength accuracy is estimated to be 0.02μm.

4.4. PRECISION AND ACCURACY

4.4.1. PRECISION. The precision of emittance and radiance measurements is limited only by noise in the recorded voltage. This noise is automatically determined for each spectral scan of either target or reference. During rotation of the CVF, two opaque portions of the filter wheel occur which separate the three filter wheel segments (see Figure 4). One opaque section occurs within the spectrally-sensitive region of each detector. When these opaque sections are in the optical path, no chopped radiation reaches the detector; only noise and d.c. bias voltages are present. The data recording system continues to operate while the instrument scans through these opaque segments, producing approximately 30 samples

of the noise and d.c. offset from each opaque portion. During data reduction, these samples are averaged to determine the d.c. mean bias which is then subtracted from all measured voltages for the given spectral scan of the given detector. The 30 voltage samples are also analyzed to determine their standard deviation. Thus, an accurate one-sigma noise voltage, ΔV_n, is obtained for each detector on each spectral scan. This is one of the two primary noises. The other, ΔV_d, results from linearity and truncation errors in the digital voltmeter.* These two noise terms are added to produce a pessimistic estimate of the standard deviation of the detected voltage:

$\Delta V_n \tilde{=}$ FISR-system-voltage-output standard deviation

$\Delta V_d \tilde{=}$ voltage-recording-system "standard deviation"

$\Delta V = \Delta V_n + \Delta V_d \tilde{=}$ total recorded voltage standard deviation

The precision, ΔL_λ^t, of a spectral radiance measurement is here taken to be the difference, at each wavelength, between the radiance calculated from the recorded voltage, V, and the radiance calculated from $V \pm \Delta V$ where the $\pm$ signs are chosen so as to maximize this difference. That is, from equation 3.6,

$$\text{PRECISION:} \quad \Delta L_\lambda^t = \left[\frac{V_{t,c} + \Delta V}{V_{c1,c2} - \Delta V} - \frac{V_{t,c}}{V_{c1,c2}} \right] [L_\lambda^b(T_1^c) - L_\lambda^b(T_2^c)] \varepsilon^c(\lambda, T^c)$$

$$= \frac{\Delta V (V_{c1,c2} + V_{t,c})}{V_{c1,c2}(V_{c1,c2} - \Delta V)} [L_\lambda^b(T_1^c) - L_\lambda^b(T_2^c)] \varepsilon^c(\lambda, T^c) \qquad (4.1)$$

*Other sources of error, such as those resulting from temperature-measurement imprecision, are negligible.

Roughly, ΔL_λ^t represents the two-sigma precision since the actual noises in $V_{t,c}$ and $V_{c,c}$ are uncorrelated.

The two-sigma precision, $\Delta\varepsilon^t(\lambda)$, of an emittance measurement at any wavelength is calculated, using equation 3.10, from

$$\text{PRECISION:} \quad \Delta\varepsilon^t(\lambda) = \varepsilon^c(\lambda)\left[\frac{V_{t1,t2} + \Delta V}{V_{c1,c2} - \Delta V} - \frac{V_{t1,t2}}{V_{c1,c2}}\right]\left|\frac{L_\lambda^b(T_1^c) - L_\lambda^b(T_2^c)}{L_\lambda^b(T_1^t) - L_\lambda^b(T_2^t)}\right|$$

$$= \varepsilon^c(\lambda)\,\frac{\Delta V(V_{c1,c2} + V_{t1,t2})}{V_{c1,c2}(V_{c1,c2} - \Delta V)}\left|\frac{L_\lambda^b(T_1^c) - L_\lambda^b(T_2^c)}{L_\lambda^b(T_1^t) - L_\lambda^b(T_2^t)}\right| \qquad (4.2)$$

Since both ΔL_λ^t and $\Delta\varepsilon^t(\lambda)$ represent (roughly) the two-sigma precision limit, about 95% of the true spectral radiance and emittance values lie between $L_\lambda^t \pm \Delta L_\lambda^t$ and $\varepsilon^t(\lambda) \pm \Delta\varepsilon^t(\lambda)$, respectively, where L_λ^t and $\varepsilon^t(\lambda)$ are calculated from recorded voltages.

4.4.2. ACCURACY. The accuracy of a radiance or emittance measurement is determined by the absolute accuracy with which each individual element necessary to the calculation is known and thus is determined by systematic as well as random errors. Hence, the accuracy, ΔT, of measuring the temperatures and the accuracy, $\Delta\varepsilon^c$, of knowing the reference cavity emittance must be considered in addition to the voltage errors. In practice, a total absolute error limit, not a probabilistic description, is determined.

The accuracy of a spectral radiance measurement, ΔL_λ^t, is determined in a manner analagous to the procedure for determining the precision: that is, by determining the value of ΔL_λ^t that could result if the individual errors of each input were combined in such a way that it was maximized.

ACCURACY: $\Delta L_\lambda^t = L_\lambda^b(T^c + \Delta T^c)$

$$+ [\varepsilon^c(\lambda) + \Delta\varepsilon^c]\left[\frac{V_{t,c} + \Delta V}{V_{c1,c2} - \Delta V}\right][L_\lambda^b(T_1^c + \Delta T_1^c) - L_\lambda^b(T_2^c - \Delta T_2^c)]$$

$$- \{L_\lambda^b(T^c) + \varepsilon^c(\lambda)\ \frac{V_{t,c}}{V_{c1,c2}}\ [L_\lambda^b(T_1^c) - L_\lambda^b(T_2^c)]\} \qquad (4.3)$$

where $\Delta\varepsilon^c = 0.002$ and ΔV is the same as used in the precision calculation. The ΔT's in equation 4.3 have three sources:

1) The initial calibration accuracy of the thermistors,
2) The accuracy with which the measurement circuitry can determine the thermistor resistances, and
3) The accuracy with which the heating effect of the finite measurement current flowing in the thermistors can be determined.

An expression for $\Delta\varepsilon^t(\lambda)$ based on the same premises as those used to obtain equation 4.3 can also be written employing equation 3.10. This expression and equation 4.3, together with the results of 1) - 3) above, are used in every FISR run data reduction computation to furnish spectral accuracy of the calculated results for L_λ^t and $\varepsilon^t(\lambda)$. These accuracy estimates can obviously be formulated to apply to spectral apparent temperature also. Every FISR run graphical presentation of any spectral quantity contains the appropriate spectral accuracy curve.

It should be noted that*

$$\text{ACCURACY } \Delta L_\lambda^t = \text{PRECISION } \Delta L_\lambda^t + \frac{\partial L_\lambda^t}{\partial T} \Delta T + \frac{\partial L_\lambda^t}{\partial \varepsilon^c} \Delta \varepsilon^c \qquad (4.4)$$

where the formal abbreviation

$$\frac{\partial L_\lambda^t}{\partial T} \Delta T = \frac{\partial L_\lambda^b(T^c)}{\partial T^c} \Delta T^c + \varepsilon^c \frac{V_{t,c}}{V_{c1,c2}} \left[\frac{\partial L_\lambda^b(T_1^c)}{\partial T_1^c} \Delta T_1^c + \frac{\partial L_\lambda^b(T_2^c)}{\partial T_2^c} \Delta T_2^c \right]$$

has been used. In equation 4.4, the spectral radiance in the rightmost two terms is evaluated from the measured voltage. These terms are essentially independent of wavelength (since ΔT and $\Delta \varepsilon$ are), so the only spectral dependence in the accuracy can be attributed to the spectral dependence in the precision. The important conclusion to be drawn from this fact is that any measured spectral-shape features are real if they exceed only the precision estimates. The magnitudes of such real features do not need to exceed the accuracy estimates. The quantitative implications are the following. If $A(\lambda_1)$ and $\langle A(\lambda_1) \rangle$ are, respectively, a measured value and the average of many measured values of the physical quantity "A" (e.g., spectral radiance, emittance, or apparent temperature) at the wavelength λ_1, then

$$-1 < \frac{A(\lambda_1) - \langle A(\lambda_1) \rangle}{\text{PRECISION } \Delta A_1} < 1 \qquad (4.5)$$

for about 95% of the measurements of $A(\lambda_1)$ where PRECISION ΔA_1 is the 2σ - precision estimate associated with the measurement of $A(\lambda_1)$. For FISR measurements, PRECISION ΔA_1 is known because many output values from the

*Equation 4.4 can be rigorously deduced from equations 4.1 and 4.3 if error terms are retained to first order only. The deduction is formally complicated, so it is not presented here.

instrument are recorded while the detector is viewing an opaque segment of the CVF. For convenience, the abbreviation $2\sigma_1$ = PRECISION ΔA_1 is made. Then, appropriate rearrangement of relation 4.5 gives

$$A(\lambda_1) - 2\sigma_1 < \langle A(\lambda_1)\rangle < A(\lambda_1) + 2\sigma_1 \qquad (4.6)$$

for about 95% of the $A(\lambda_1)$ measurements, or that only about 5% of the measurements fail to satisfy relation 4.6.* For example, suppose $\varepsilon(\lambda_1=9.2\mu m)= 0.89$ is measured with the approximate $2\sigma_1$ precision of 0.02. Then, from relation 4.6, it is about 95% certain that $0.87 < \langle\varepsilon(\lambda_1=9.2\mu m)\rangle < 0.91$. The precision estimate also gives a quantitative measure to the significance of measured differences in physical quantities at two different wavelengths, λ_1 and λ_2. Regarding this, the implication is

$$-1 < \frac{A(\lambda_1) - A(\lambda_2) - [\langle A(\lambda_1)\rangle - \langle A(\lambda_2)\rangle]}{2\sqrt{\sigma_1^2 + \sigma_2^2}} < 1 \qquad (4.7)$$

for about 95% of the measured values of $A(\lambda_1)$ and $A(\lambda_2)$. A most important conclusion follows from this since

$$\langle A(\lambda_1)\rangle - \langle A(\lambda_2)\rangle = [A(\lambda_1) - A(\lambda_2)]_{true} \qquad (4.8)$$

where the right-hand side of equation 4.8 represents the true difference. The equality holds because <u>both</u> random <u>and</u> systematic errors cancel in the <u>difference</u> of the <u>averages</u>. For example, if $\varepsilon(\lambda_1=9.2\mu m)= 0.89$ and $\varepsilon(\lambda_2=9.8\mu m)= 0.81$ with $2\sigma_1 = 2\sigma_2 = 0.02$ represent some measured values and 2σ-precision estimates of emittance, then it is about 95% certain that

$$-1 < \frac{0.89 - 0.81 - [\varepsilon(\lambda_1=9.2\mu m) - \varepsilon(\lambda_2=9.8\mu m)]_{true}}{2\sqrt{(0.01)^2 + (0.01)^2}} < 1$$

* Exact 2σ-precision limits correspond to the values of 95.45% and 4.55%, respectively.

or that

$$0.052 < [\varepsilon(\lambda_1=9.2\mu m) - \varepsilon(\lambda_2=9.8\mu m)]_{true} < 0.108$$

The accuracy estimate has different implications. This estimate includes both random and systematic errors (i.e., total maximum errors) and, hence, represents the maximum error associated with any spectral measurement. Since the systematic errors are essentially independent of wavelength, they only produce a translation of a true spectral curve parallel to itself; they do not affect spectral shape.

The precision and/or accuracy estimates given with the FISR measurements which are presented in this Report pertain to single spectral scans. If n spectral scans were averaged, the precision estimate should be divided by $\sqrt{n}$; the accuracy estimate is independent of n.

The precision and accuracy estimates will be seen to increase in the opaque regions of the atmosphere. This is because the signal to noise ratios are seriously degraded when the radiation signals from the sample and reference blackbody are attenuated by the intervening atmosphere.

In the graphical presentation of the field measurements of spectral apparent temperatures, only the accuracy curves are given. The precision curves necessarily lie below the accuracy curves, and there just is not enough room on the charts to present all of the curves. The precision estimates are available, however. It should be noted that spectral variations from some of the materials (especially under clear sky conditions) are repeatable well within even the accuracy estimates. The implication is that the spectral variations are real and that the actual target temperatures do not change during the scan. Since measurements have been made only under clear-sky

or uniformly-overcast sky conditions, the thermal driving functions remain constant and the actual target temperature do likewise. Regarding the sky spectral apparent temperature spectra, the accuracies are poorer because of the poor S/N ratio associated with these measurements.

4.5 ADDENDUM ON A METHOD TO DETERMINE THE TOTAL SPECTRAL RADIANCE OF THE SKY

The total target spectral radiance is generally the sum of an emitted and a reflected component. The environmental irradiance producing the reflected component may be considered as the irradiance from a hypothetical hemispherical surface which surrounds the target, the diametric plane of this imaginary hemisphere being an extension of the plane target surface. For targets composed of more than a single plane element, a distinct hemisphere must be considered for each such element. A knowledge of the angular distribution of radiance over each imaginary hemispherical surface is required before reflected target spectral radiance calculations can be made. In some situations, the angular distribution of spectral radiance can be exceedingly complex, as, for example, the case of a military vehicle hidden in trees. The horizontal sections of the vehicle will have an environmental hemisphere for which the angular distribution of spectral radiance is composed of the radiance (reflected and emitted) from nearby foliage, tree branches, and sky radiance not blocked by the tree canopy. A vertical section of the vehicle will have an environmental hemisphere in which the angular distribution of spectral radiance is determined by the nearby ground, tree trunks, overhead foliage and tree branches, and some sky radiance through openings in the tree canopy. However, in many practical instances, it will be the sky hemisphere which provides the major portion of the environmental radiance. Thus, a knowledge of this is significant

and necessary for making calculations of target spectral radiance in such situations.

It is well known (and may be readily substantiated with the aid of a relatively unsophisticated radiometer) that for a clear sky, in those spectral regions where the atmosphere is transparent, the radiance is minimal at the zenith and increases towards the horizon where the radiance is nearly that of a blackbody at ambient air temperature. Cloud cover results in greatly increased radiance at the zenith with a somewhat smaller increase near the horizon. Some limited sky radiance data have been available, but more comprehensive data are necessary if modeling of targets in the field using laboratory emittance data is to be realized.

The FISR as already described can be used to measure apparent sky spectral radiance in a chosen azimuthal plane with the polar angle as a parameter. To this end, the FISR instrumentation would be mounted horizontally and operated in the radiance measurement mode. For these measurements, following the calibration spectral scan, the heated reference cavity would be removed and the field of view of this instrument channel would then be directed at the sky by means of the rotatable 45° mirror. However, data of the nature so obtained, while of theoretical interest, are of limited use. For this reason, an adjunct to the FISR was developed for determination of total sky spectral radiance.

This adjunct consists of a 2 ft. x 2 ft. square panel of flame-sprayed aluminum. This panel is quite Lambertian and spectrally flat in the 3.3 - 14.0μm spectral region. It thus serves as a good "integrating" plate for the sky hemisphere (or any other, if the panel is appropriately oriented). The use of this panel in conjunction with the FISR allows determination of

the total apparent sky spectral radiance. A correction for the self-emission from the panel is (necessarily) routinely made by monitoring its temperature and using its known spectral directional emittance at the used polar viewing angle of 60°. Total apparent sky spectral radiance is presented with all FISR apparent target spectral radiance curves. A spectral accuracy curve for the sky data is also included. The sky-data accuracy is poorer than the target-data accuracy because of the required self-emission correction and lower S/N ratio in the former.

5

PROGRAMS

In this brief section, the measurement and data-reduction programs are described. Although the term "program" has two completely different contextual meanings here, it is convenient to discuss the two together.

5.1. BASIC MEASUREMENT PROGRAMS

5.1.1. FIELD SPECTRAL RADIANCE MEASUREMENT PROGRAM. It is necessary to have data on many target and background materials, data from each of these being taken under a variety of environmental conditions. Data are desirable from

1) Soils: bare and variously vegetated
2) Typical exposed rocks
3) Water of various types and agitation states
4) Vegetation other than grasses (trees, bushes, mosses)
5) Snow
6) Extensive range of manmade targets:
   a) Various transportation surfaces (roadtops, airstrips)
   b) Various rooftops and buildings
   c) Various tactical targets (painted surfaces)

Under the contractual requirements consistent with available time and funds, rather extensive FISR unpolarized data have already been gathered for items 1), 6.a), and 6.c). In addition, spectrally broadband (about 8.0-14.0μm) polarized data* have been gathered on items 1), 2), 3), and 6.c).

*See reference 12.

5.1.2. LABORATORY EMITTANCE DATA. Polarization-dependent data can be taken under laboratory conditions. These are among the most significant "target-signature" data obtained in the last two years. These data allow calculation of extensive results to be expected under field conditions. For detailed and explicit definitions of the kinds of emittance data which have been collected, reference should be made to Section 7. Some calculations of expected field results are given in Section 8. The materials on which it is desirable to perform measurements do not require the kind or enumeration given in the previous paragraph; manmade materials are the candidates. The reason is that the significant information is contained in the polarization character of the emittance of manmade materials; natural materials in their native state do not have any polarization character (water being a notable exception). The materials on which unclassified measurements have already been made are listed in Table II. a.

5.2. THE COMPUTER PROGRAM

This account can be very brief. The existing computer code furnishes all the relevant results corresponding to equations 3.6 (spectral radiance), 3.7 (spectral apparent temperature), 3.8 (spectral apparent emittance), 4.1 and 4.2 (precision), 4.3 (accuracy, emittance also), 7.4 (spectral normal emittance), and 7.6 or 7.7 (relative spectral directional emittance). The CALCOMP code can call for any combination of these as spectral plots. The actual temperature of the flame-sprayed aluminum panel is recorded when field measurements are made. From this, the known panel emittance, and the measured apparent spectral radiance from the panel, the spectral irradiance from the environment can be calculated.

FIELD SPECTRAL RADIANCE MEASUREMENT: TECHNIQUES AND RESULTS

For field measurements, the FISR was mounted in a small motor van. This allowed the instrumentation to be easily transported to and from the measurement site and the measurements could be made through the open side of the van without removing the instrument from it. The reference cavities were mounted on the instrument, and rotatable mirrors inclined at 45° to the optic axes of the two telescopes allowed viewing the interiors of the two reference cavities for calibration purposes. Then one of the mirrors was rotated until the target area was in the field-of-view and further spectral scans were made.

The 'look' angle from the FISR to the targets was 60°. In all cases, the targets were approximately horizontal, so the polar observation angle was also about 60°. The distance from the FISR to the targets was about 10 feet. Measurements were made on clear days with little or no cloud cover and on totally-overcast days. At each measurement site, five 3-14μm (unpolarized) spectral scans were made on spatially separated areas of a larger homogeneous target area. Immediately prior to the measurements on the target surface, a calibration spectral scan of the reference cavities was made followed by a spectral scan on the diffuse flame-sprayed aluminum panel. At the completion of the measurements on the target material, the spectral scans on the flame-sprayed aluminum and the reference cavities were repeated. During each measurement session, ground-truth data were also recorded. These data consisted of the solar irradiance, air temperature,

relative humidity, and wind speed and direction. They are available on request from the Target Signature Analysis Center. Photographs of the sky were also taken at regular intervals with a camera fitted with a wide-angle (fish eye) lens.

Shortly before the end of the field measurements portion of the program, the 3-6μm InSb detector failed and only the 6-14μm spectral radiance data were obtained for a few targets (FISR runs 0089 - 0091).

No polarized spectral radiance measurements have been made with the FISR in the field. The results of such measurements would be of great interest, but the FISR does not have sufficient sensitivity to overcome the signal-to-noise restrictions which would be imposed by the addition of a polarizer.*

The field data are presented graphically as apparent spectral temperature vs. wavelength (see Section 3.2.1). Plotting the actual spectral radiance data would require a logarithmic scale for this quantity and subtle but significant spectral "fine structure" would be lost in the resultant scale compression.

The field spectral radiance measurements made to date are listed in Table I. Those which are presented graphically (a representative sample of the total) are indicated by figure number. The figures are arranged so that the spectral apparent temperature of similar targets under extreme sky states can be easily compared. An artificiality is introduced in some

*Extensive broadband (about 8.0-14.0μm) polarization field data have been collected by the Infrared and Optics Laboratory. These are reported in detail in reference 12.

TABLE I. A DESCRIPTIVE LIST OF FIELD SPECTRAL RADIANCE RUNS MADE WITH THE FISR

FISR RUN NO.	TARGET	FRACTIONAL CLOUD COVER	FIGURE
0019, 0021	M-48 Tank and Grass	0.0	19
0069	Used Gravel Road	0.0	11
0070	O.D.-Painted Concrete	0.1	13
0071	Short Grass (6")	0.1	18
0072	Concrete	0.0	10
0073	Mown Grass (2")	0.1	15
0074	Tall Grass (16")	0.0	17
0075	Unused Gravel Road	0.2	12
0076	Bare Soil	0.1	9
0077	Medium Grass (12")	0.1	16
0078	Bare Soil	1.0	9
0079	Medium Grass (12")	1.0	16
0080	Unused Gravel Road	1.0	12
0081	Tall Grass (16")	0.9	17
0082	Mown Grass (2")	1.0	15
0083	O.D.-Painted Concrete	0.9	13
0084	Used Gravel Road	1.0	11
0085	Asphalt	1.0	14
0086	Asphalt	0.3	14
0087	Concrete	0.1	
0089	Concrete	Van and hangar obstructed most of sky	
0090	Concrete	0.7	
0091	Concrete	1.0	10
0128	Cloudy Sky	1.0	
0129	Clear Sky	0.0	
0130	Night Sky	Uncertain	
0131	Clear Night Sky	0.0	
0132	O.D. Panels and Sky	0.1	

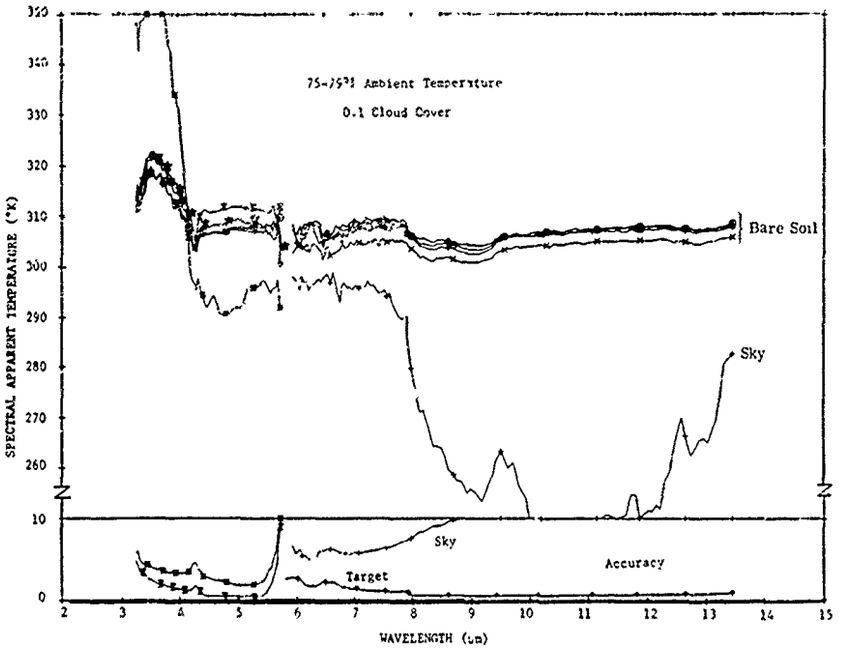

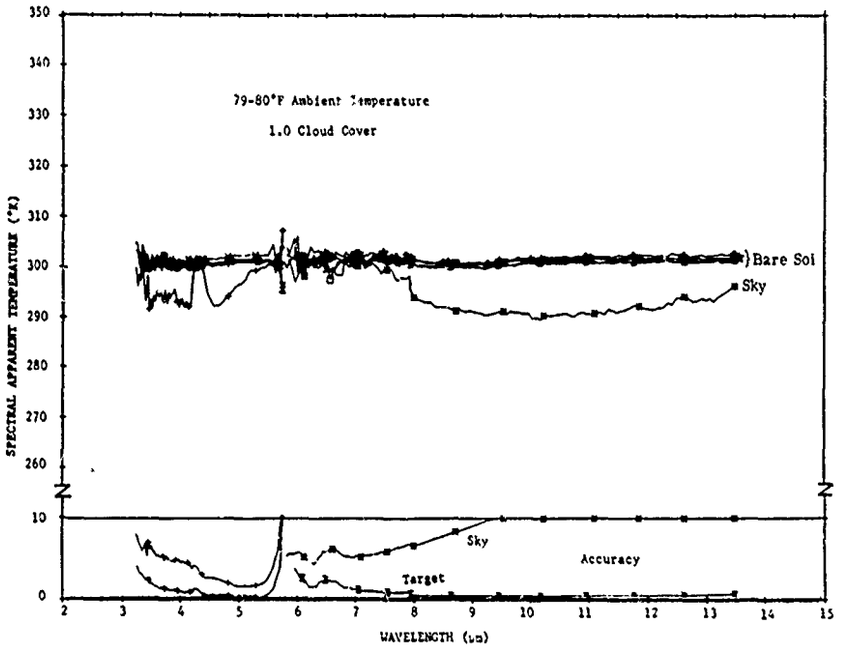

FIGURE 9. BARE SOIL AND SKY SPECTRAL APPARENT TEMPERATURE

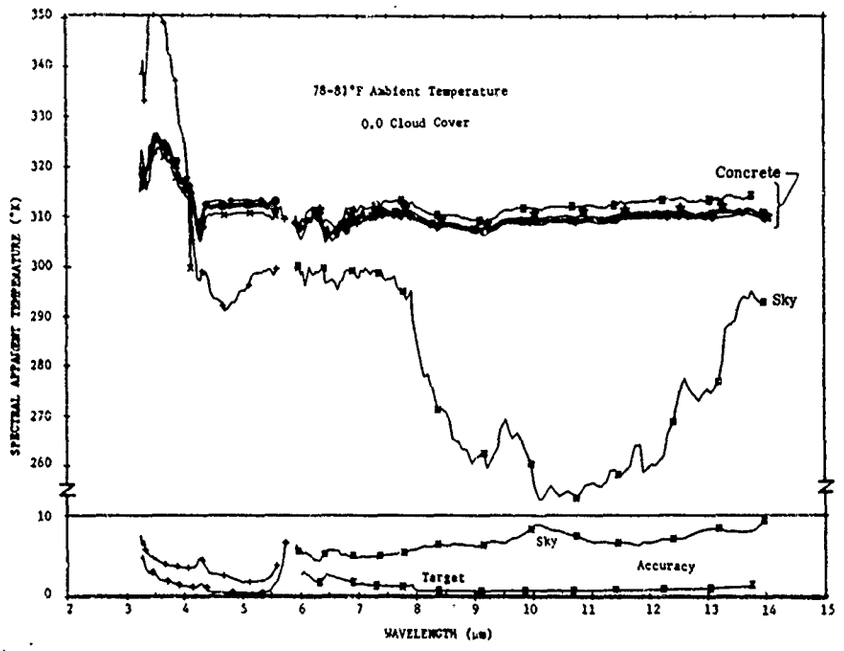

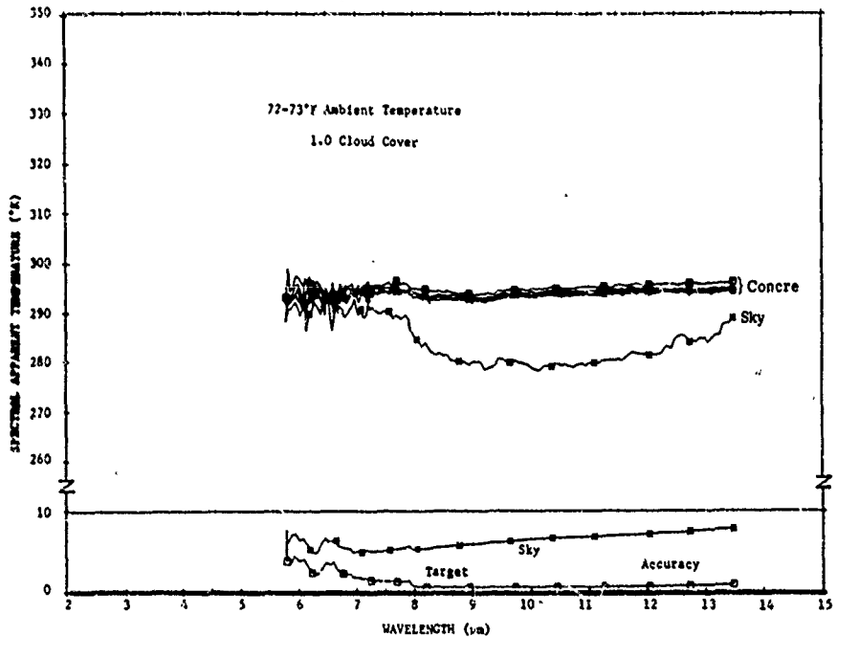

FIGURE 10. CONCRETE RUNWAY AND SKY SPECTRAL APPARENT TEMPERATURE

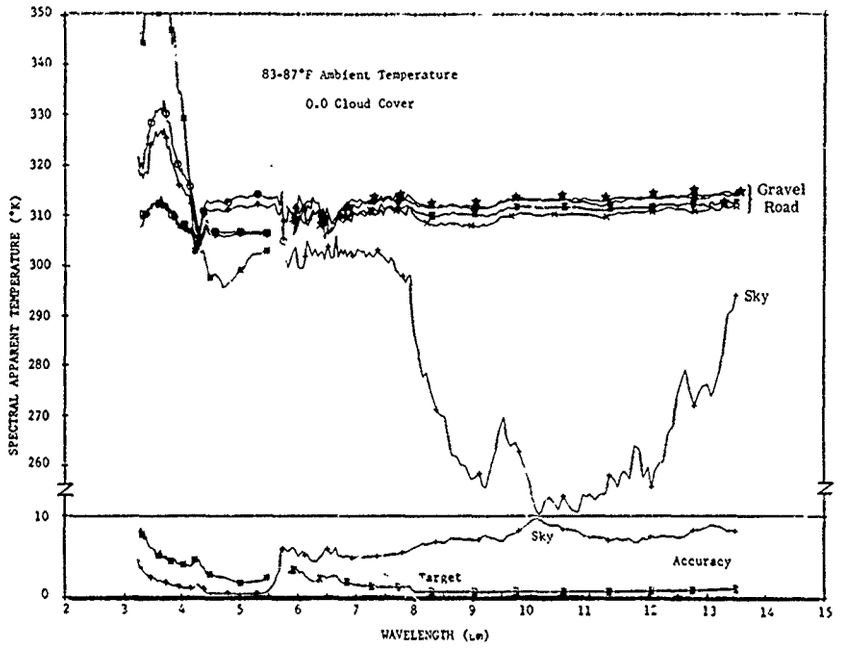

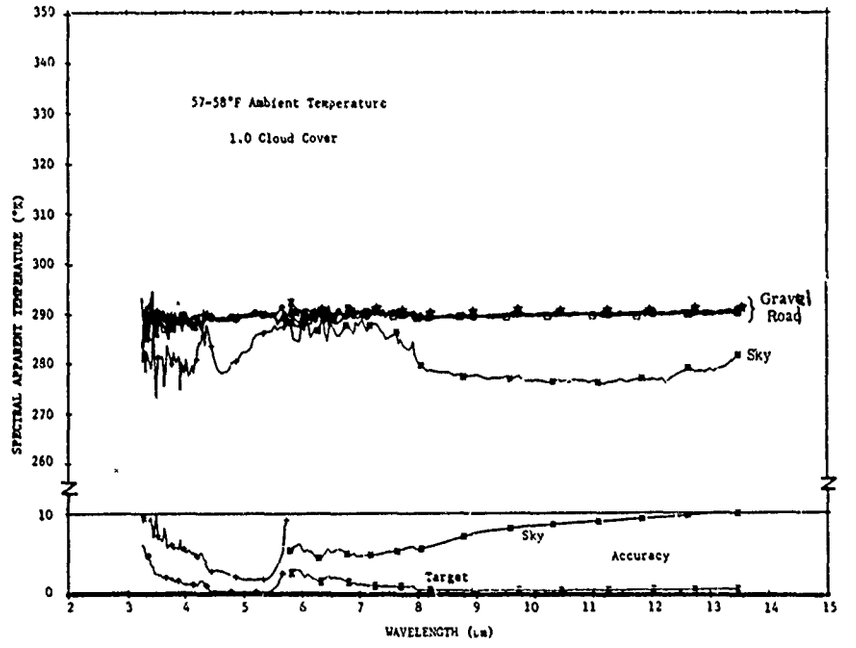

FIGURE 11. HEAVILY USED GRAVEL ROAD AND SKY SPECTRAL APPARENT TEMPERATURE

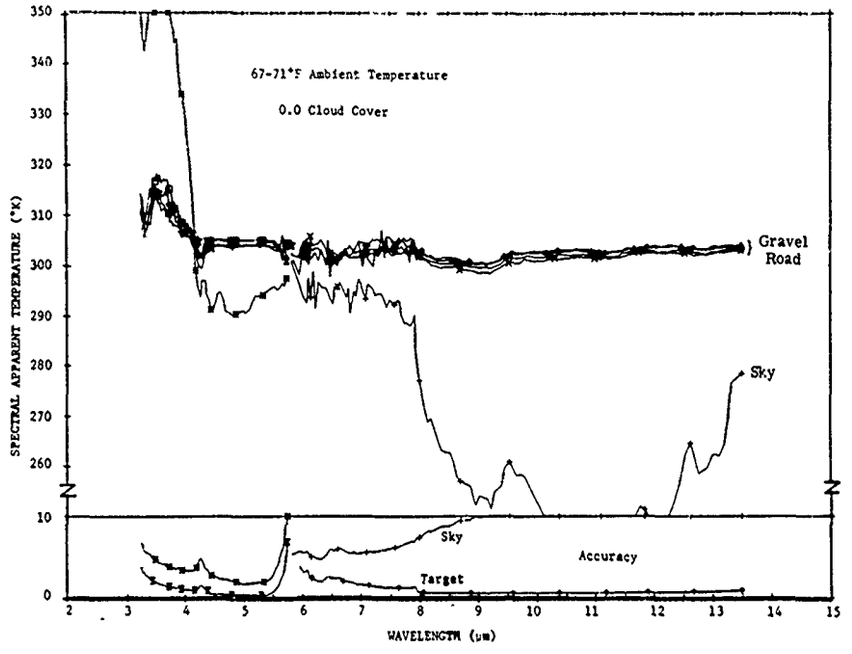

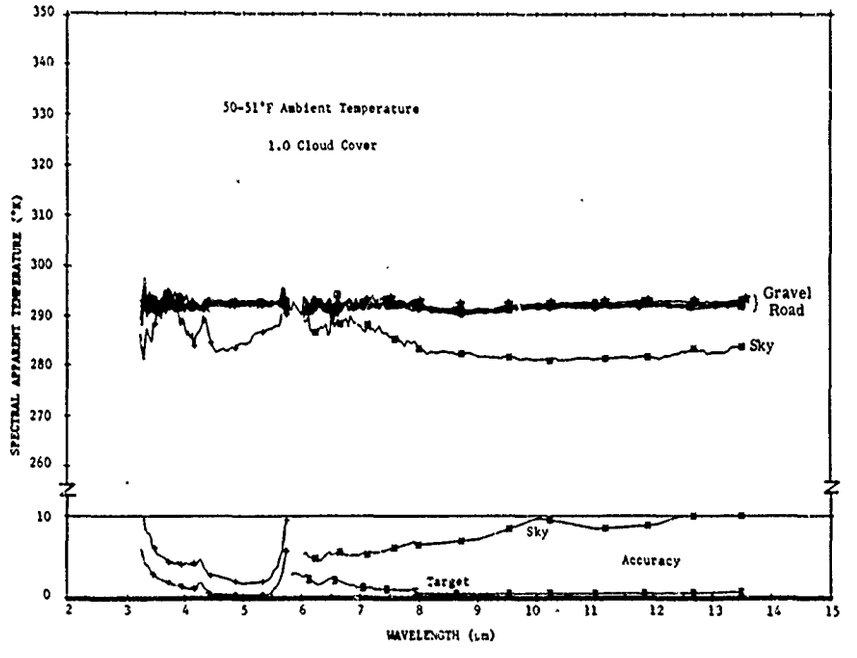

FIGURE 12. LIGHTLY USED GRAVEL ROAD AND SKY SPECTRAL APPARENT TEMPERATURE

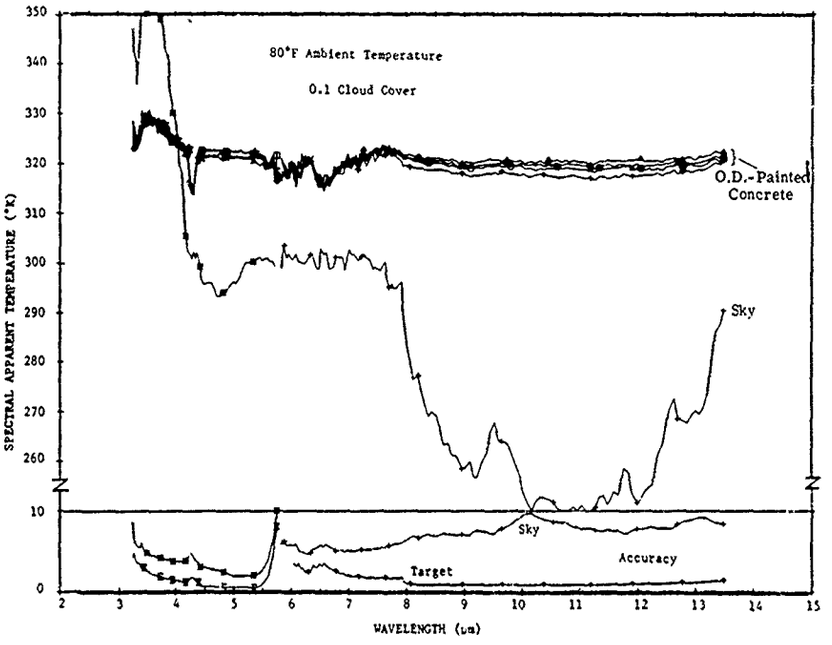

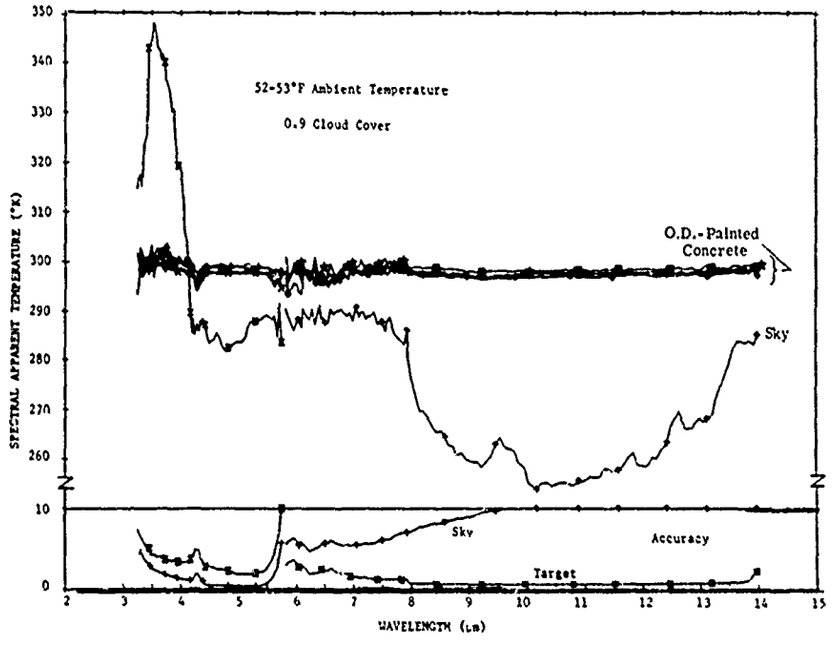

FIGURE 13. O.D.-PAINTED CONCRETE AND SKY SPECTRAL APPARENT TEMPERATURE

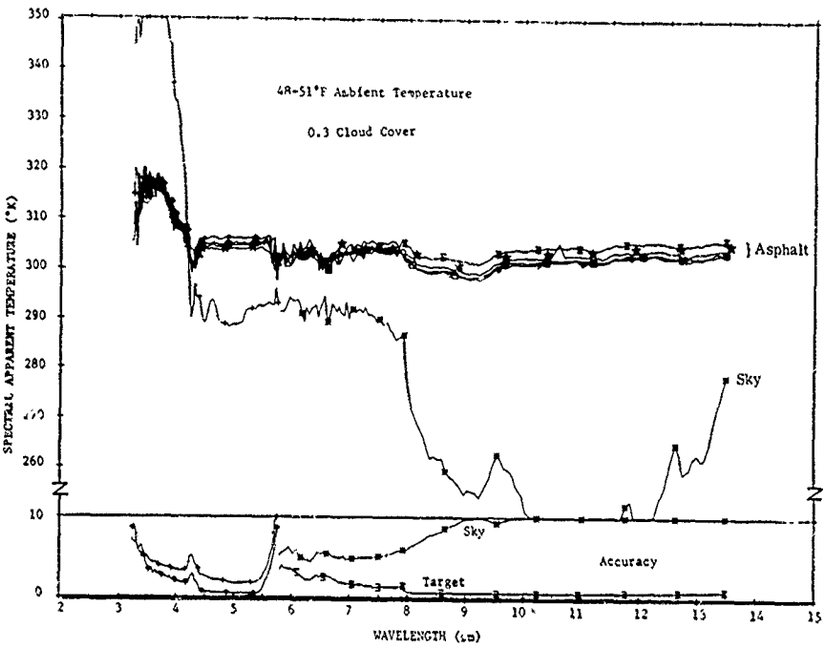

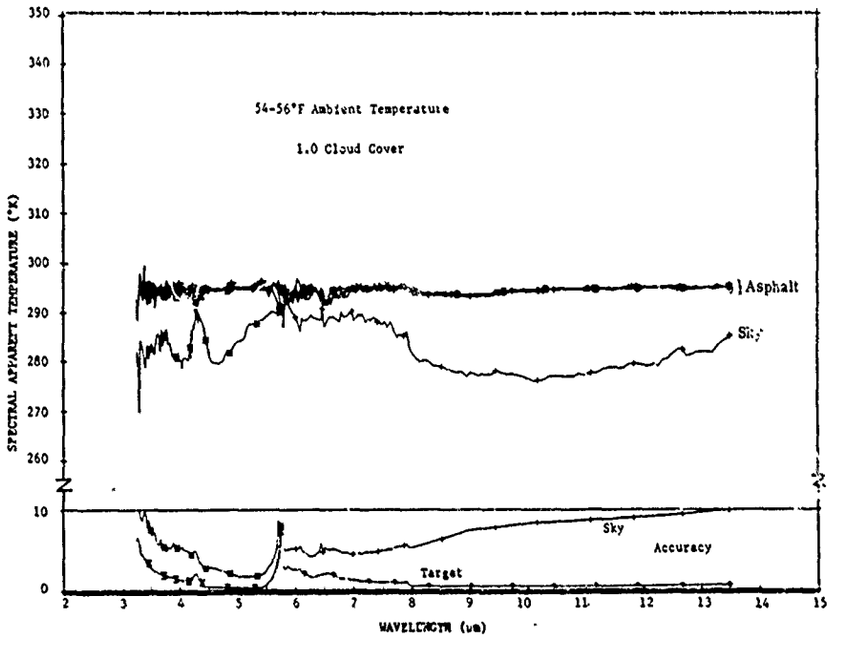

FIGURE 14. ASPHALT AND SKY SPECTRAL APPARENT TEMPERATURE

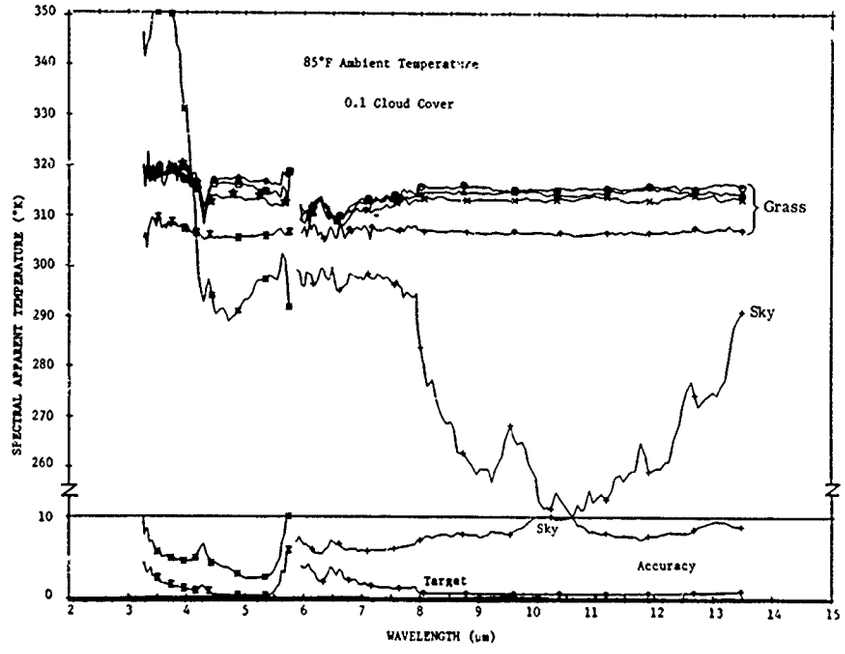

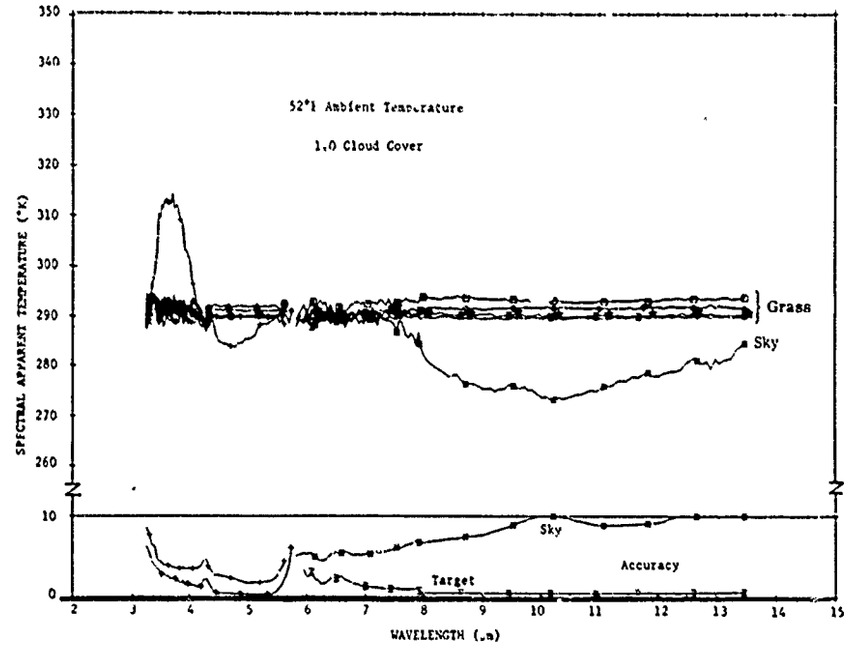

FIGURE 15. MOWN GRASS AND SKY SPECTRA APPARENT TEMPERATURE

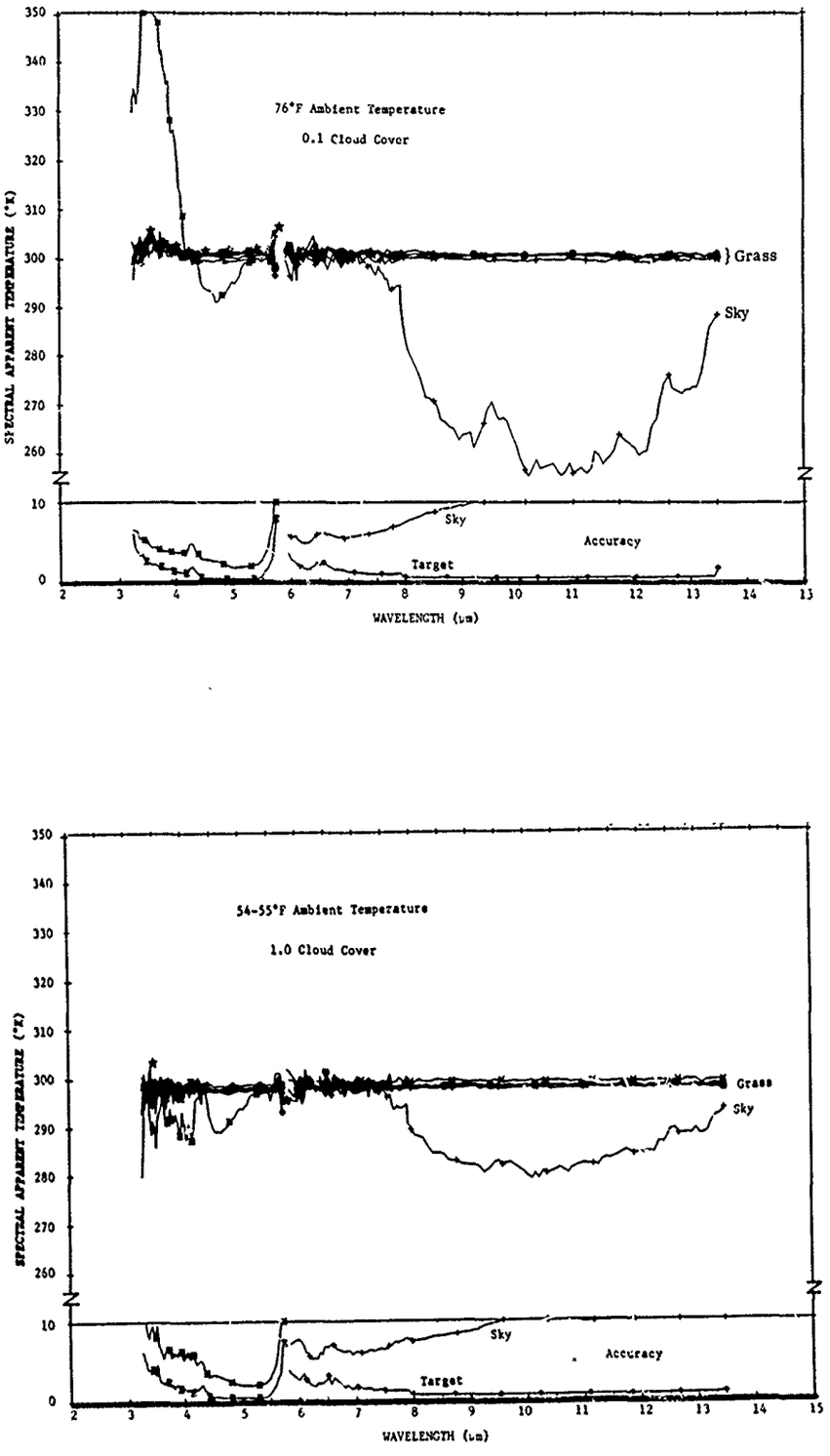

FIGURE 16. MEDIUM GRASS AND SKY SPECTRAL APPARENT TEMPERATURE

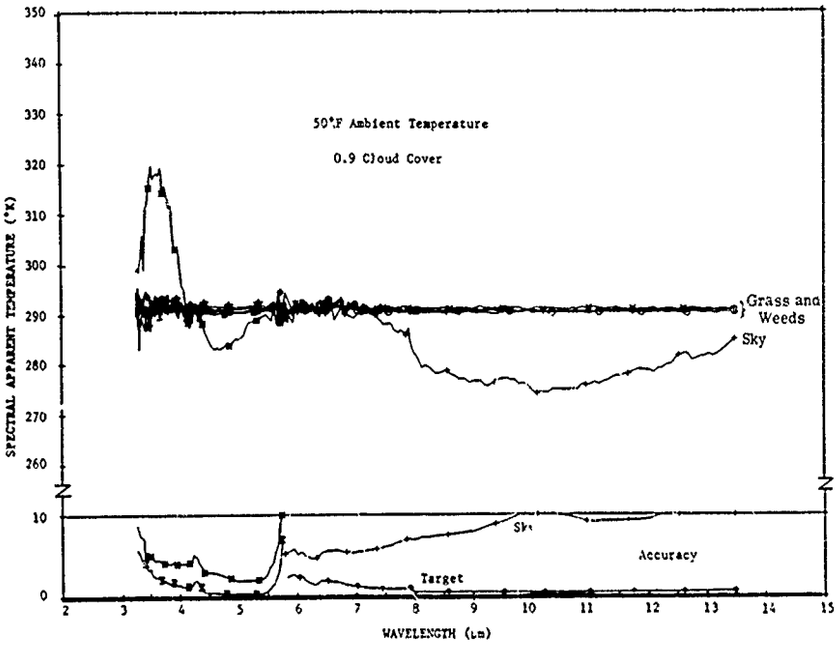

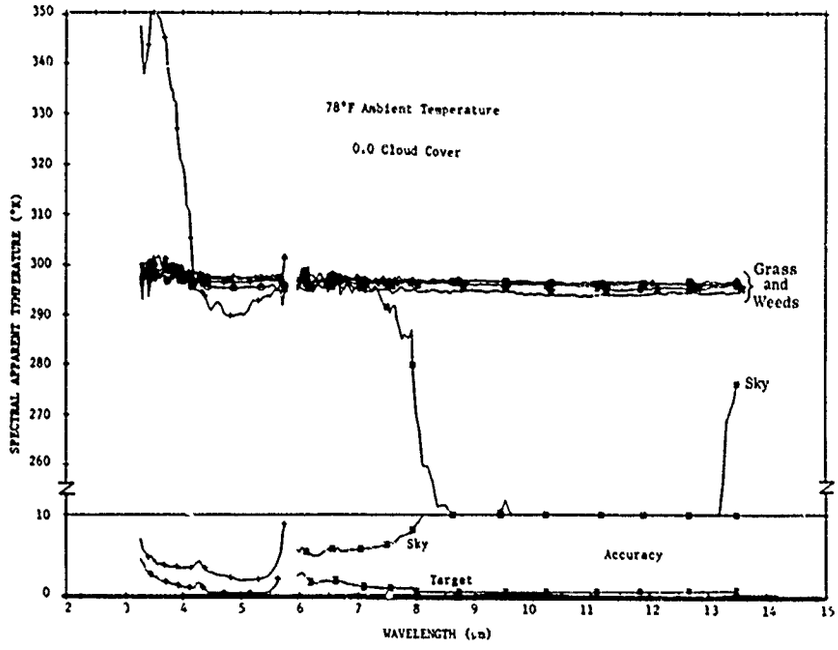

FIGURE 17. TALL GRASS AND SKY SPECTRAL APPARENT TEMPERATURE

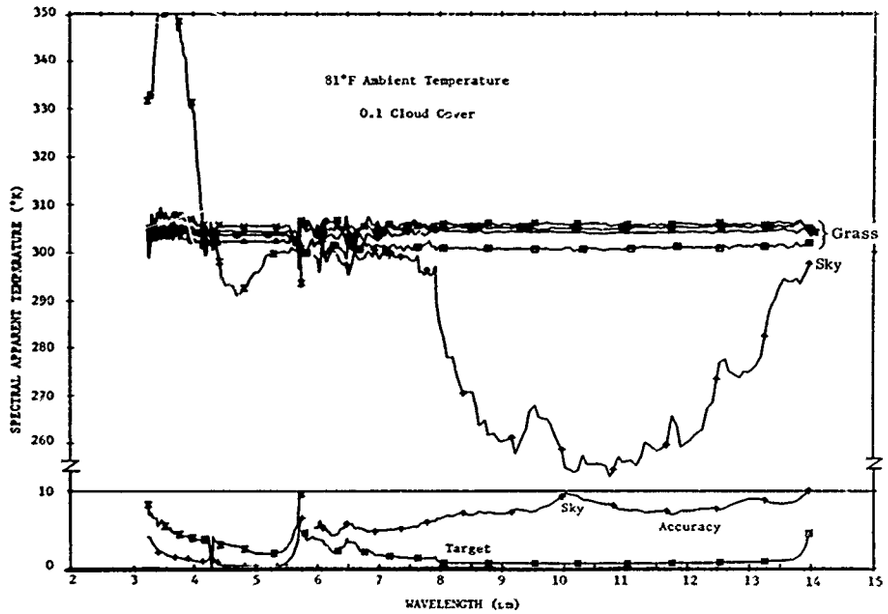

FIGURE 18. SHORT GRASS AND SKY SPECTRAL APPARENT TEMPERATURE (ONLY CLEAR-SKY DATA ARE AVAILABLE)

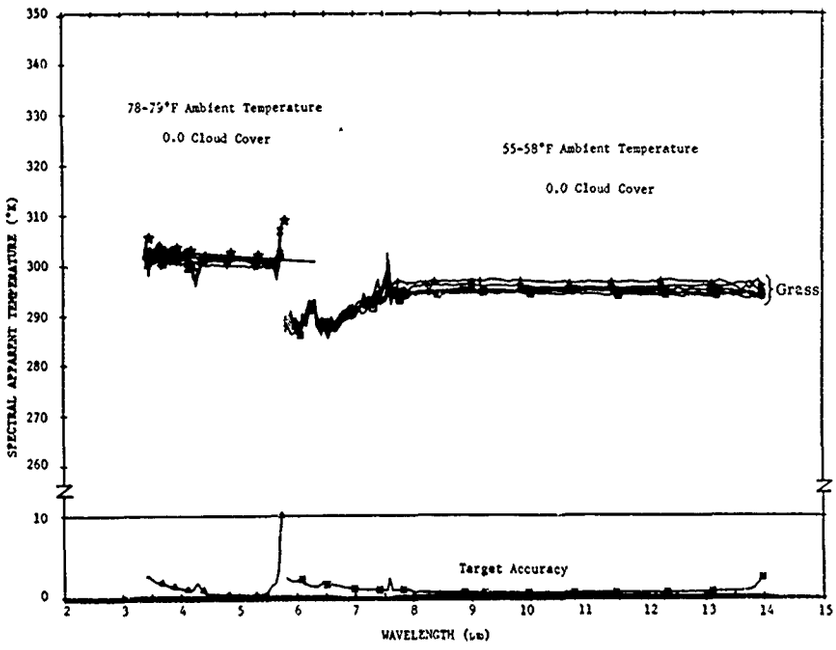

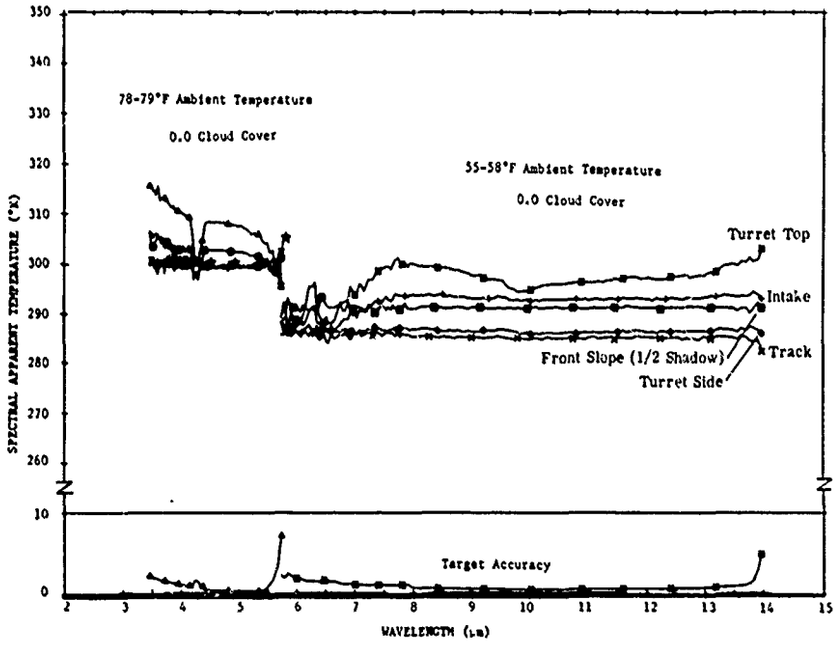

FIGURE 19. GRASS AND PORTIONS OF AN M-48 TANK SPECTRAL APPARENT TEMPERATURE

of the figures by the plotting. No apparent temperature below 250°K and no apparent temperature accuracy worse than 10°K can be plotted. The reduced data exceed these limits in some cases. Thus, any plotted apparent spectral temperature of 250°K is actually only at most 250°K, and any plotted apparent spectral temperature accuracy of 10°K is only at best 10°K. The actual computed values are available in such cases, though.

7

EMITTANCE MEASUREMENT: TECHNIQUES AND RESULTS

Laboratory emittance measurements were made on a number of materials, primarily materials in military use, using the FISR. A list of these materials is given in Table II. The operating characteristics of the FISR system require that spectral and polarization variables be investigated separately. Consequently, the data are presented in terms of the unpolarized spectral normal emittance, $\varepsilon(\lambda,T;0,-)$*, and the normalized polarized directional emittance, $\varepsilon_p(\lambda_o,T;\theta_e,\phi_{eo})/\varepsilon(\lambda,T;0,-)$, at some specific wavelength λ_o and specific azimuth angle ϕ_{eo}.

7.1. MEASUREMENT TECHNIQUES

Emittance measurements made with the FISR system depend upon the fact that this system measures the difference in spectral radiance from whatever two objects occupy the two matched optical channels. Thus, the voltage output, $V(\lambda,T_1^t,T_2^t;\theta_e,\phi_e)$, produced by the system when identical targets at different temperatures T_1^t and T_2^t are being viewed is characterized by the proportionality

$$V(\lambda,T_1^t,T_2^t;\theta_e,\phi_e) \sim [L_\lambda(T_1^t,\theta_e,\phi_e) - L_\lambda(T_2^t,\theta_e,\phi_e)] \tag{7.1}$$

The constant of proportionality, which will not be explictly displayed in this Section, has been given a brief discussion in Section 3.1. It is generally a function of both wavelength and polarization, but not the radiances in the two optical beams. For clarity, the FISR output voltage

---

*The - in the ϕ_e argument location indicates that ϕ_e is undefined for observations normal to the sample surface.

TABLE II.

a) SPECTRAL NORMAL EMITTANCE, $\varepsilon^{t}(\lambda,T;0,-)$, FISR RUNS

FISR RUN NO.	TARGET MATERIAL	FIGURE
0047-0053	Various Rough XN Laminated Phenolics	
0054	Flame-Sprayed Aluminum	
0055	3M Black Painted Microgrooved Copper Cavity	
0056		
0057	Flame-Sprayed Aluminum	
0058-0066	Liquid Hydrocarbons	
0067	Lake Erie Water	
0068	Carbon Black Coated Microgrooved Copper Cavity	
0093	Diesel Fuel	
0094	O.D. Panels	22
0097		23
0099		24
0100	Flame-Sprayed Aluminum	20
0101	O.D. Canvas	25
0104	Flame-Sprayed Aluminum	
0105	Black Krylon Paint	
0106	3M Black Paint	21
0111	Sterling Paint	
0112		
0118		
0119		
0120	Green Paint	
0121	Sterling Paint	
0122	Brown Paint	
0123	Gray Paint	
0124	Green Paint	26
0125	Blue/Black Paint	27

TABLE II. a) (Cont)

FISR RUN NO.	TARGET MATERIAL	FIGURE
0126	O.D. Paint	28
0127	Blackbody Calibration Check	
0137	O.D. Paint	29

TABLE II.

b) RELATIVE POLARIZED DIRECTIONAL EMITTANCE,
$\varepsilon_p^t(\lambda_o,T;\theta_e,\phi_{eo})/\varepsilon_p^t(\lambda_o,T;0,-)$, FISR RUNS

FISR RUN NO.	TARGET MATERIAL	FIGURE*
0047-0053	Various Rough XN Laminated Phenolics	
0054	Flame-Sprayed Aluminum	
0095	O.D. Panels	30
0096		31
0098		32
0102	O.D. Canvas	33
0103	Flame-Sprayed Aluminum	
0107	3M Black Paint	
0108	Black Krylon Paint	
0134	Green Paint and O.D. Paint	
0136	Blue/Black Paint	

*Finite sample size imposes a maximum value of 75° for θ_e.

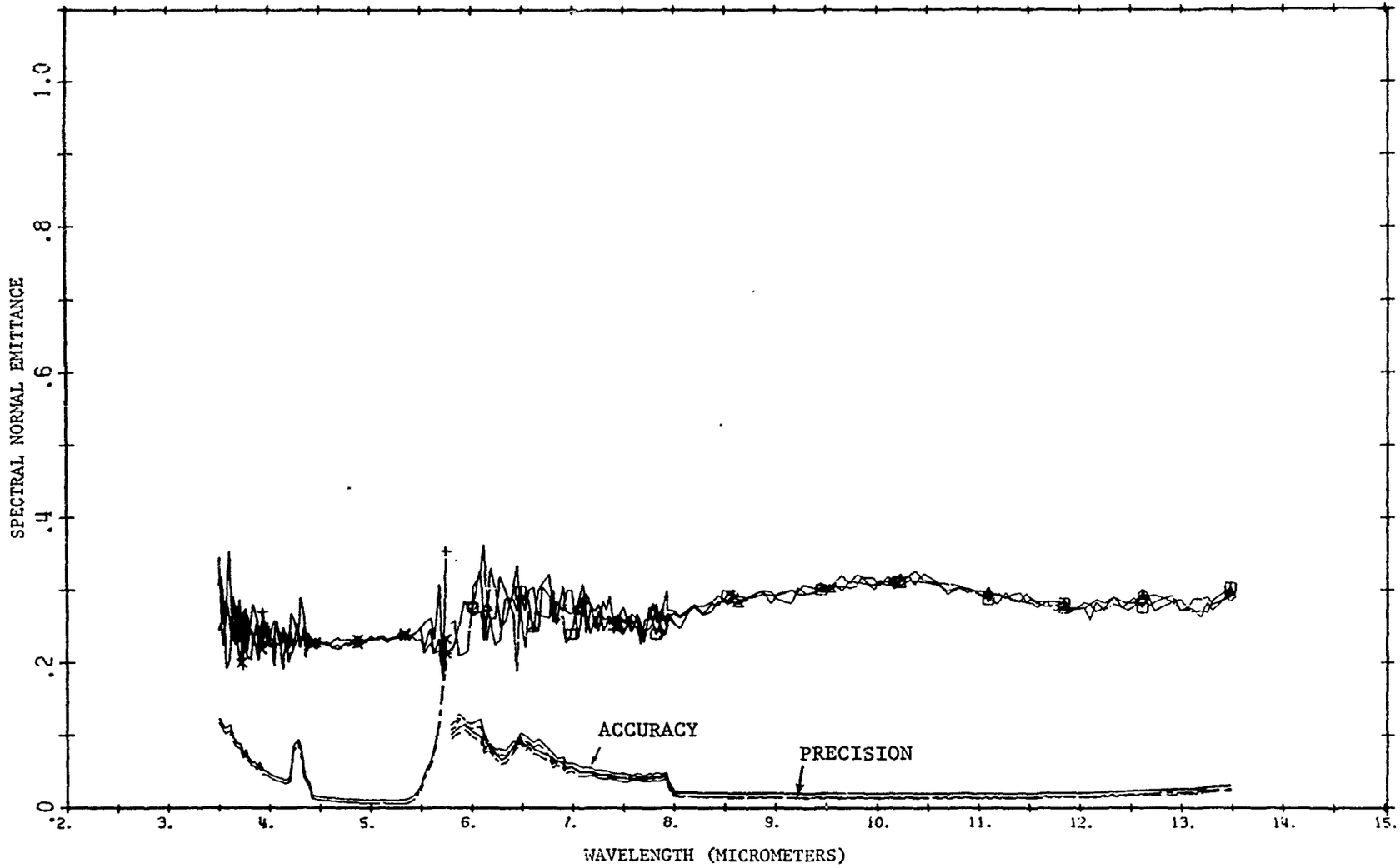

FIGURE 20. SPECTRAL NORMAL EMITTANCE OF FLAME-SPRAYED ALUMINUM

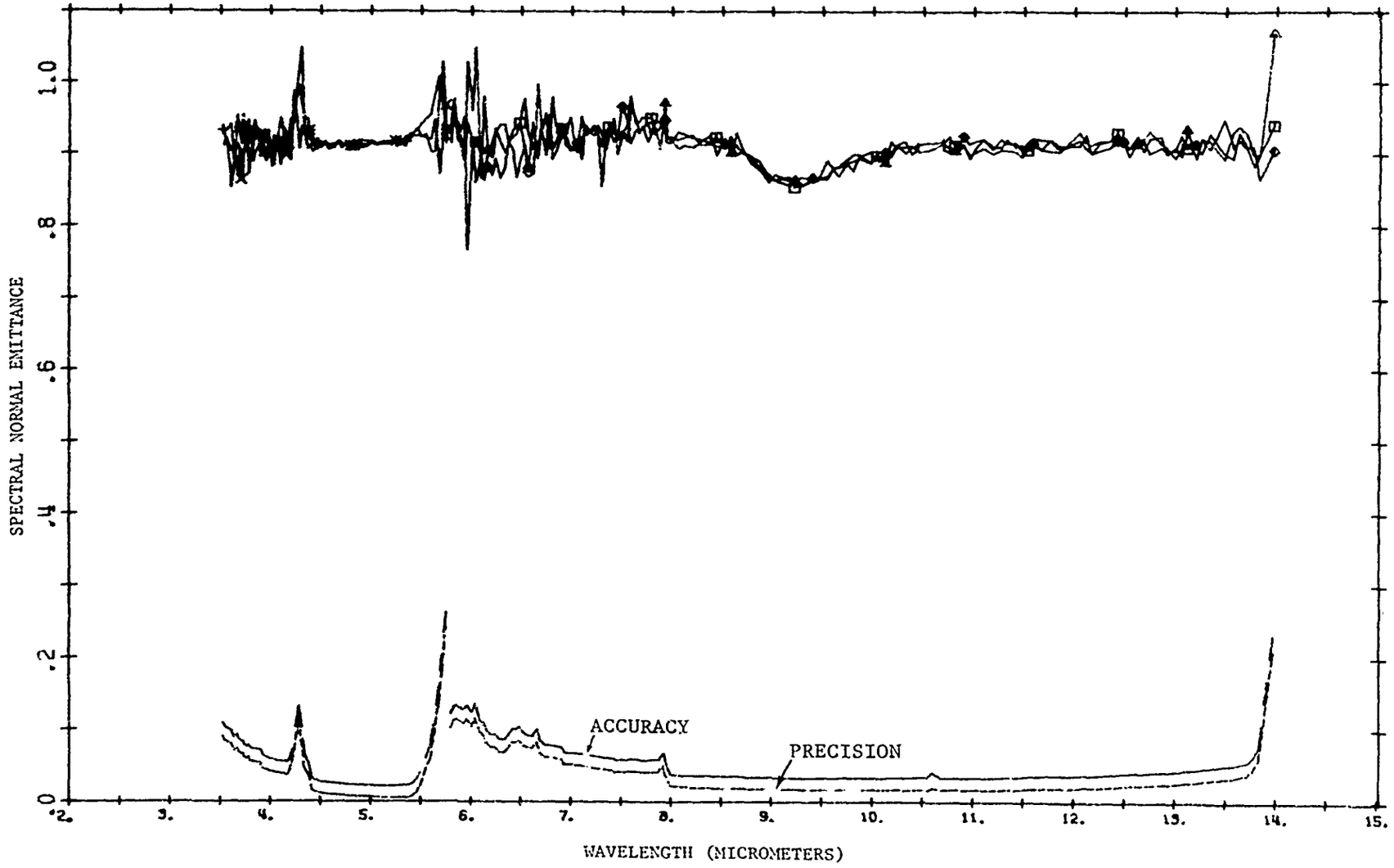

FIGURE 21. SPECTRAL NORMAL EMITTANCE OF 3M BLACK PAINT
(ALUMINUM SUBSTRATE, PAINT THICKNESS: 1.17×10^{-2} gm/cm^2)

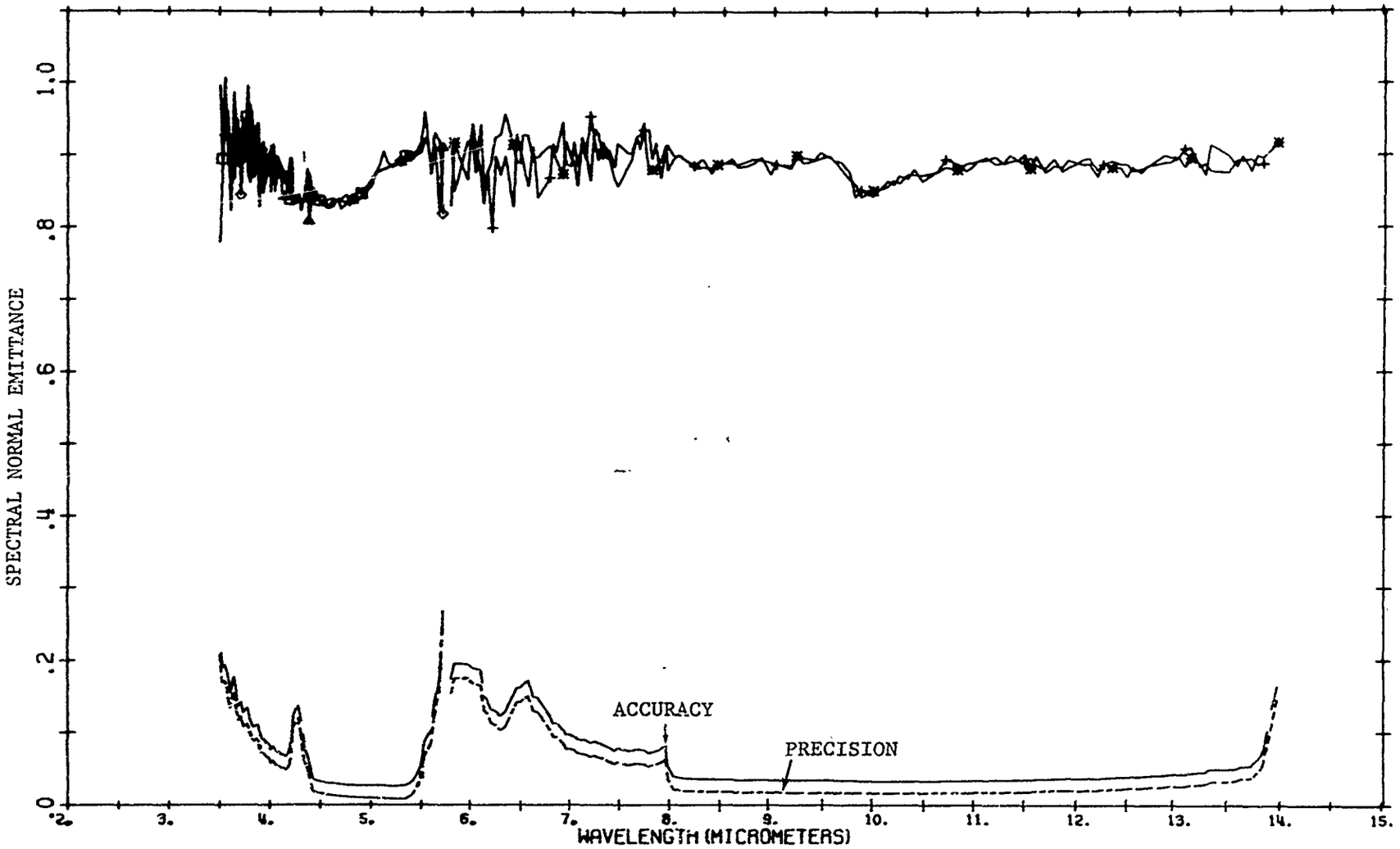

FIGURE 22. SPECTRAL NORMAL EMITTANCE OF MIL-E-46096 O.D. (x34087) LUSTERLESS ENAMEL (STEEL SUBSTRATE, MIL-P-15328C PRIMER/PRETREATMENT, MIL-P-8585 PRIMER)

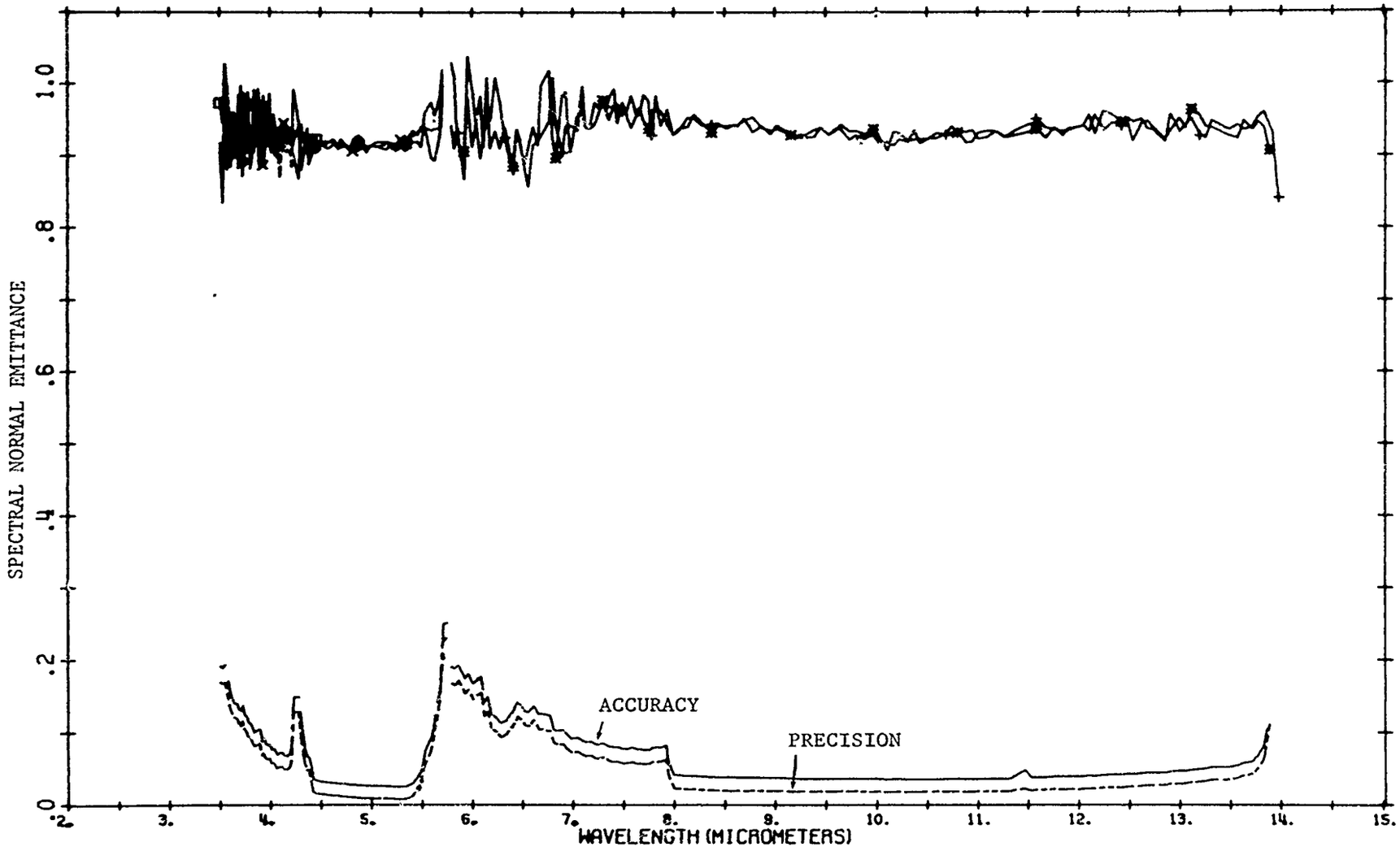

FIGURE 23. SPECTRAL NORMAL EMITTANCE OF TT-E-529 O.D. (x24087) SEMI-GLOSS
(STEEL SUBSTRATE, MIL-P-15328C PRIMER/PRETREATMENT, TT-P-636 PRIMER)

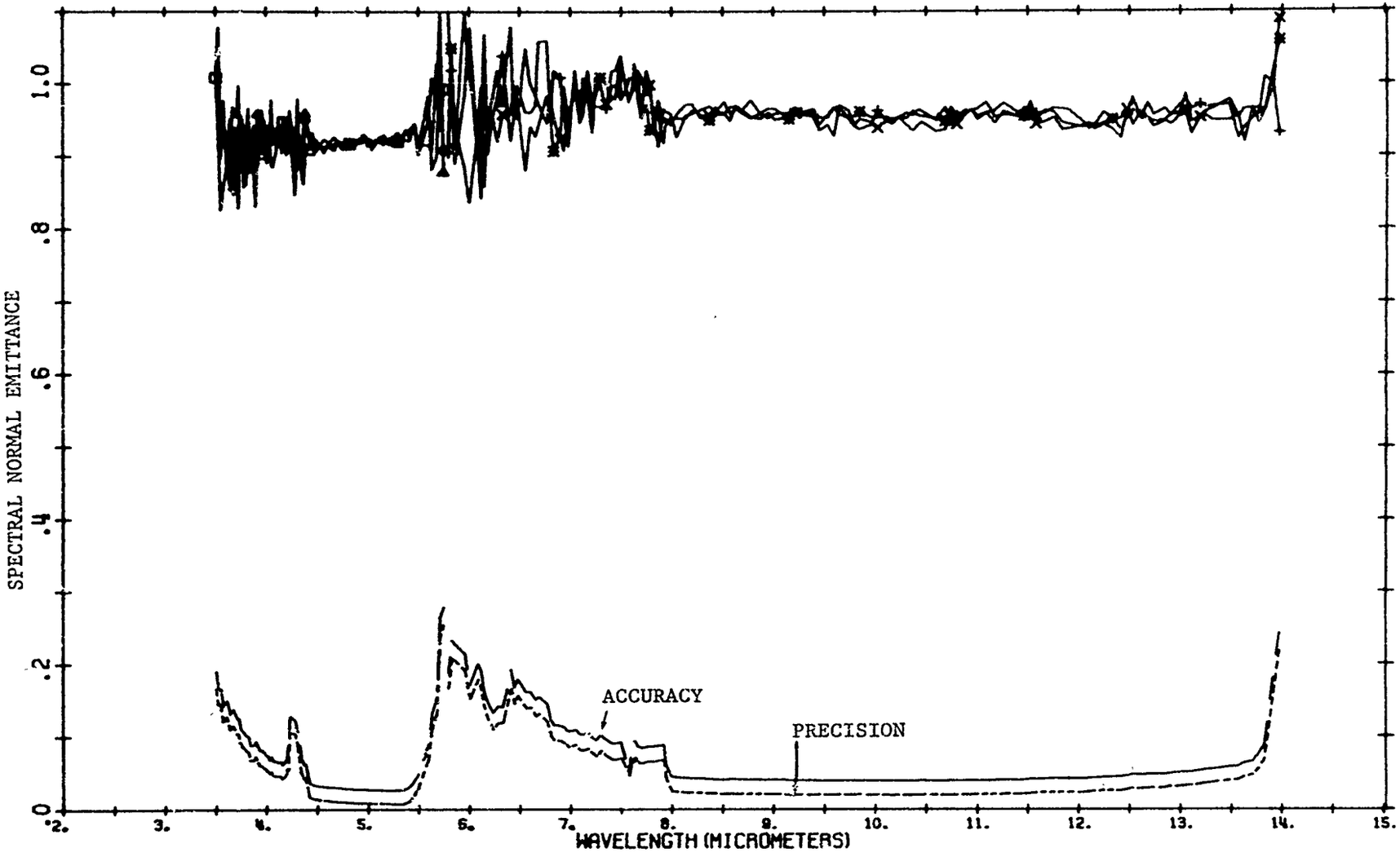

FIGURE 24. SPECTRAL NORMAL EMITTANCE OF MIL-L-52043 O.D. (x24087) SEMI-GLOSS LAQUER (STEEL SUBSTRATE, MIL-P-15328C PRIMER/PRETREATMENT, MIL-P-8585 PRIMER)

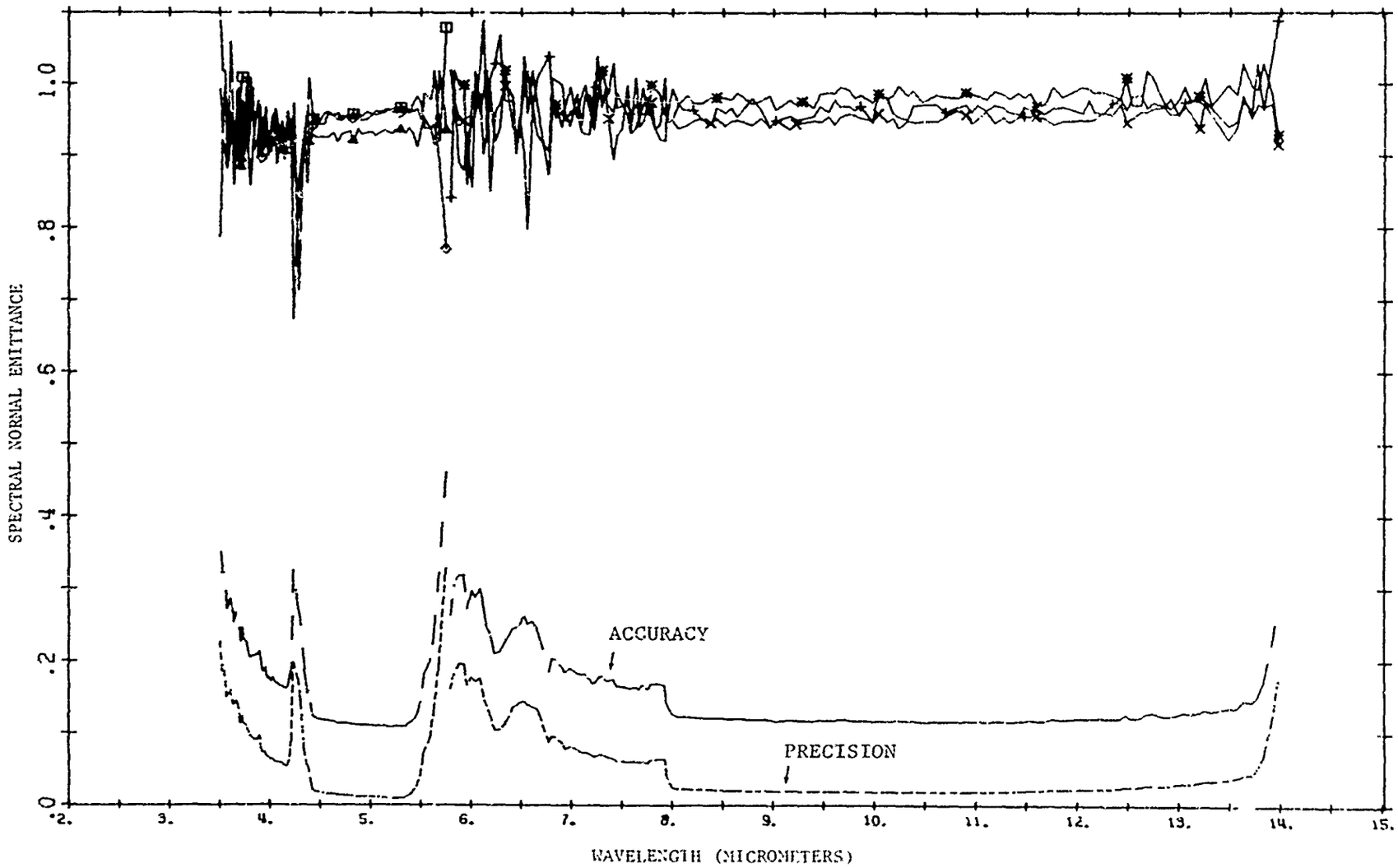

FIGURE 25. SPECTRAL NORMAL EMITTANCE OF O.D. CANVAS

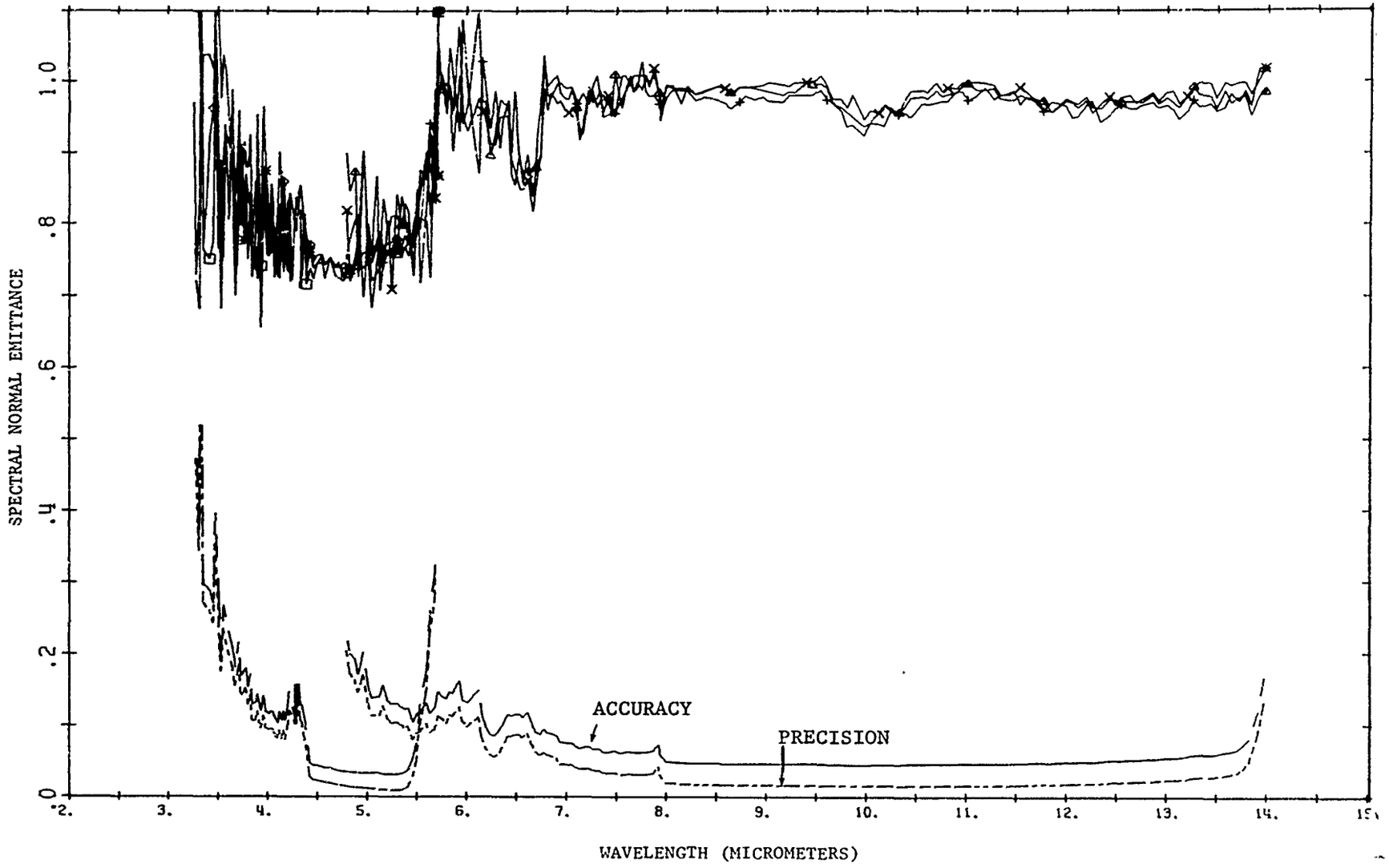

FIGURE 26. SPECTRAL NORMAL EMITTANCE OF MIL-L-19538B (FIELD GREEN ANA-627) PAINT
(ALUMINUM SUBSTRATE, MIL-C-5541 SURFACE PREPARATION, MIL-C-8514 WASH PRIMER, MIL-P-7962 PRIMER)

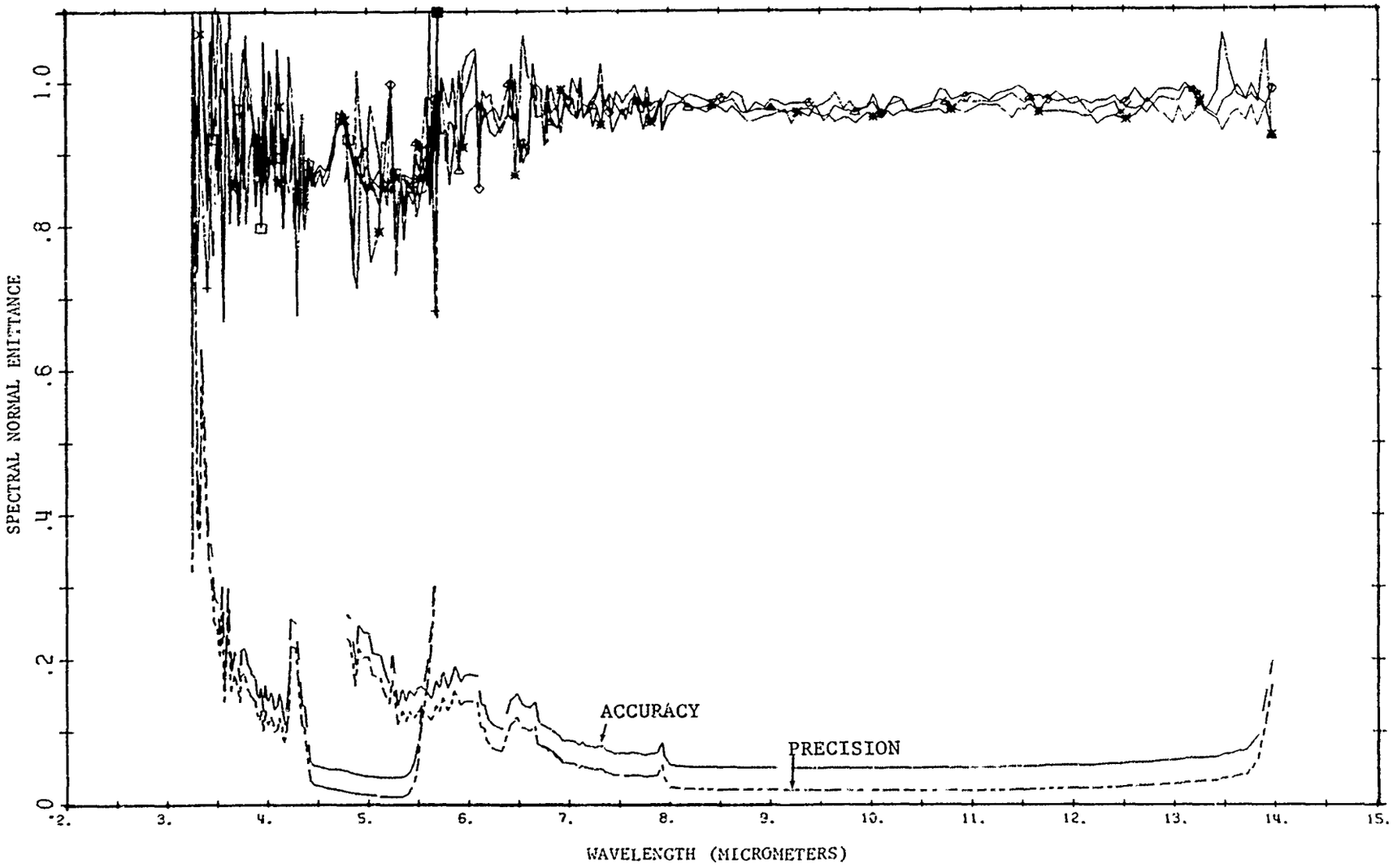

FIGURE 27. SPECTRAL NORMAL EMITTANCE OF MIL-L-19538B BLUE/BLACK (15042) GLOSSY ACRYLIC (ALUMINUM SUBSTRATE, MIL-C-5541 SURFACE PREPARATION, MIL-C-8514 WASH PRIMER, MIL-P-7692 PRIMER)

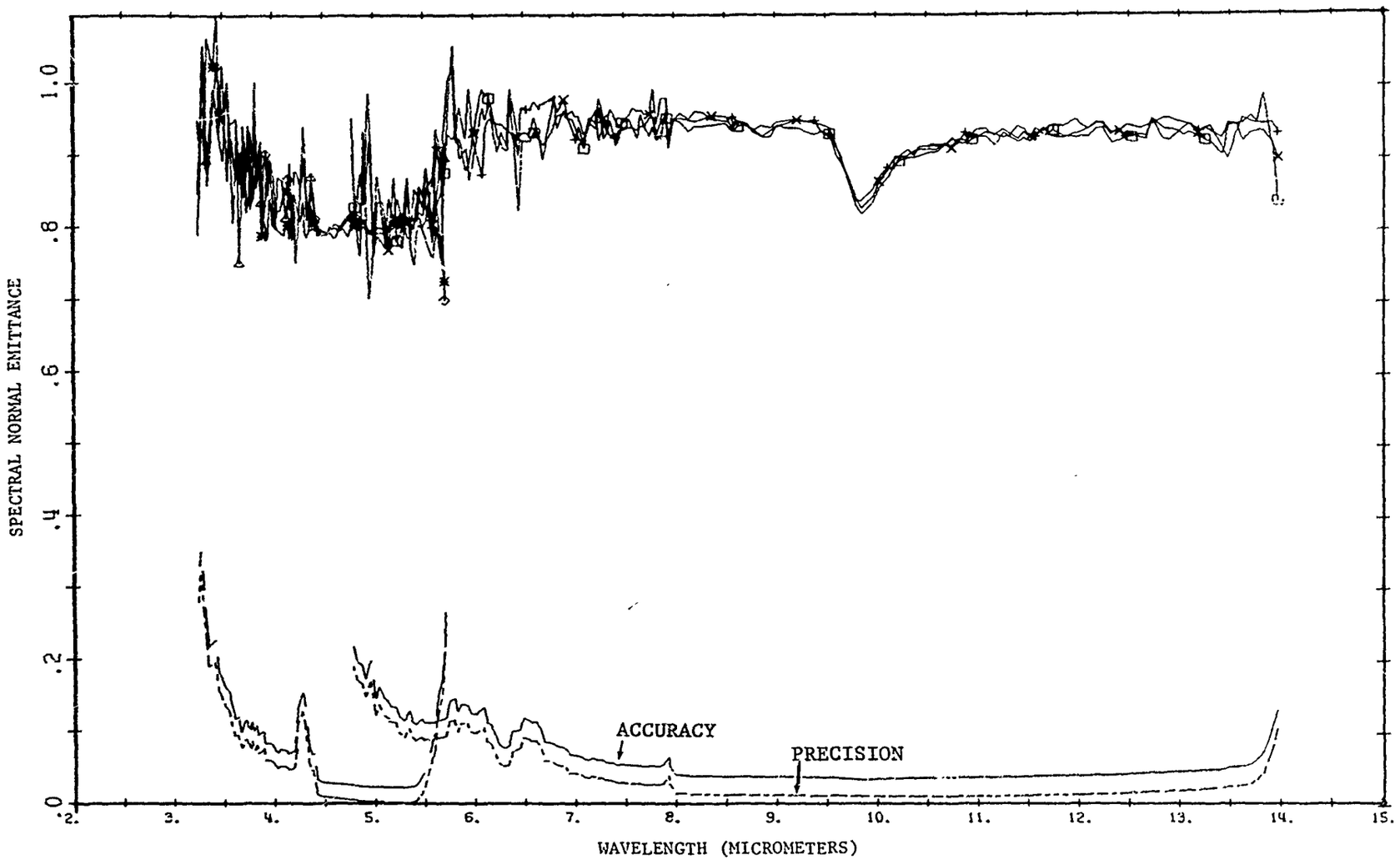

FIGURE 28. SPECTRAL NORMAL EMITTANCE OF O.D. (x34087) LUSTERLESS ACRYLIC
(ALUMINUM SUBSTRATE, MIL-C-5541 SURFACE PREPARATION, MIL-C-8514 WASH PRIMER, MIL-P-23377A PRIMER)

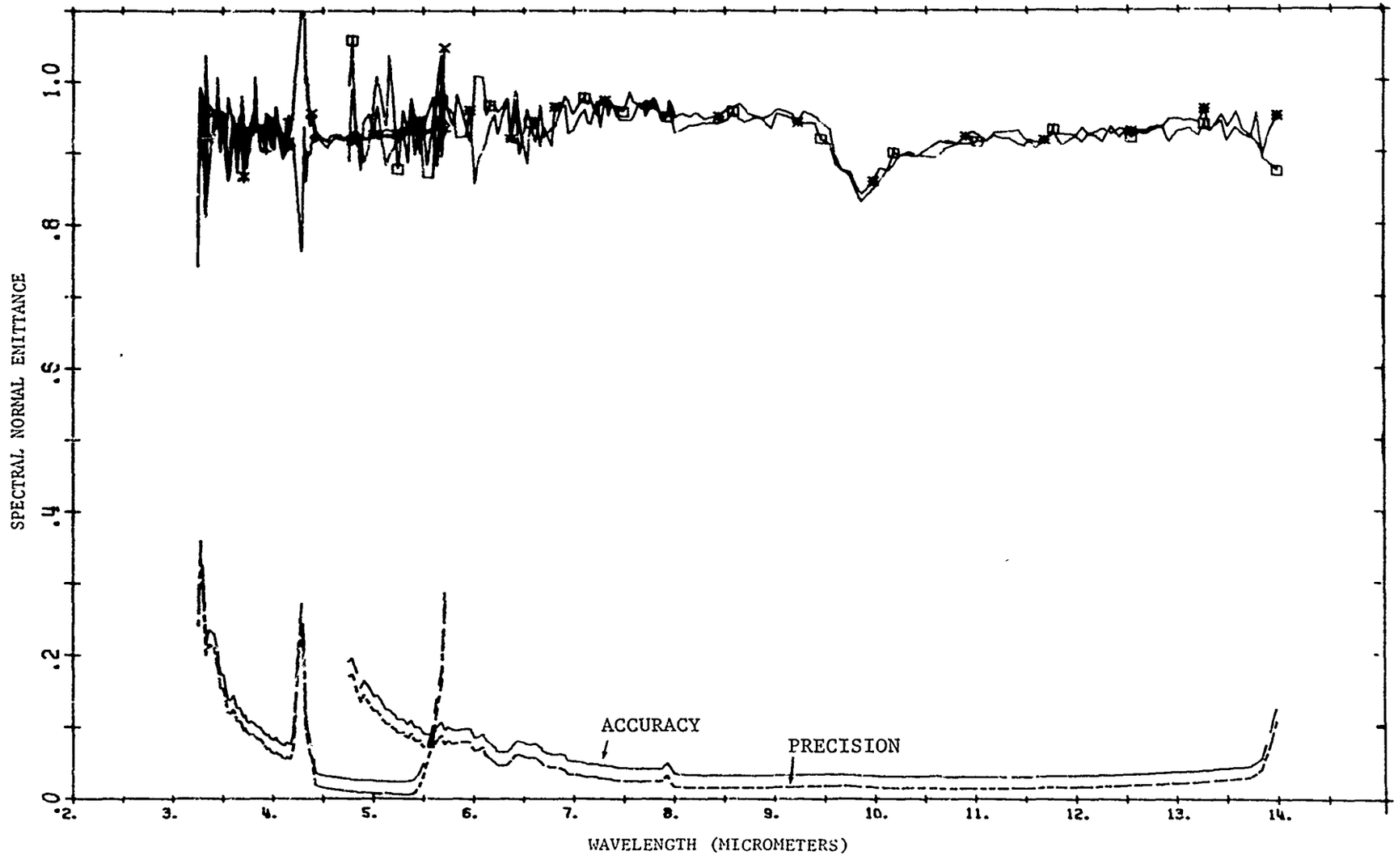

FIGURE 29. SPECTRAL NORMAL EMITTANCE OF TT-E-527A O.D. (x34087) LUSTERLESS ENAMEL (ALUMINUM SUBSTRATE, SURFACE PREPARATION AND PRIMER ARE NOT KNOWN)

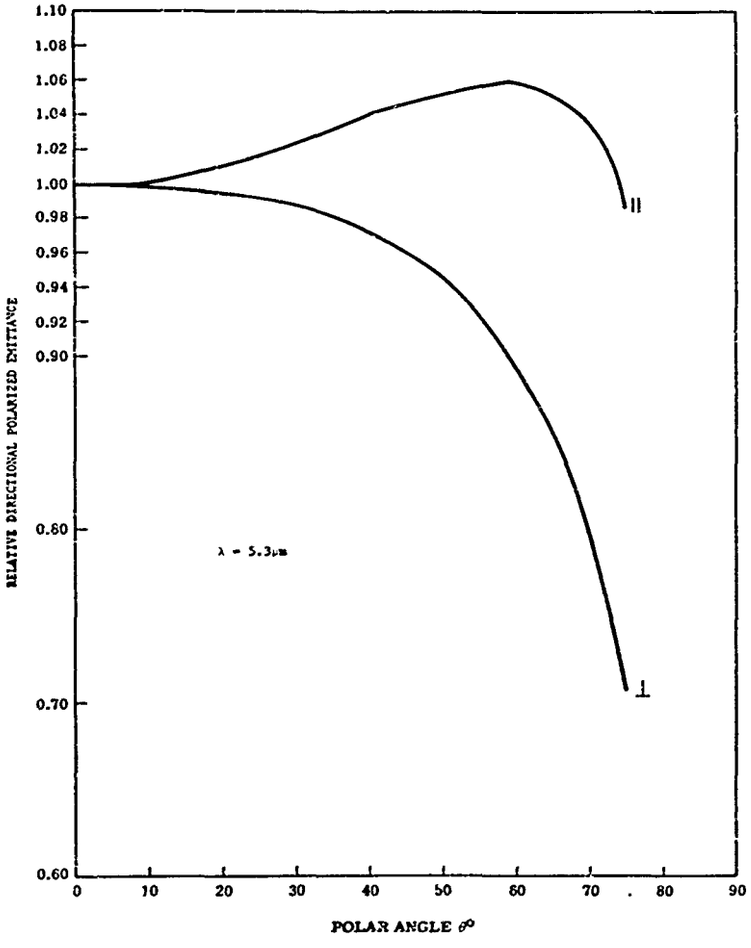

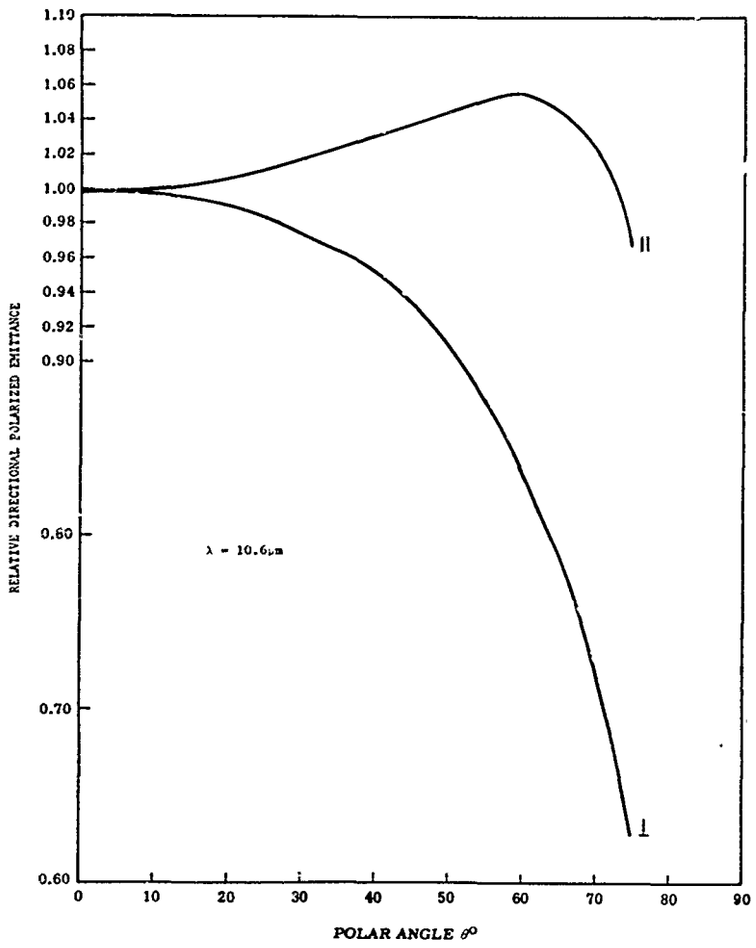

FIGURE 30. RELATIVE POLARIZED DIRECTIONAL EMITTANCE OF MIL-E-46096 O.D. (X34087) ENAMEL AT 5.3μm AND 10.6μm

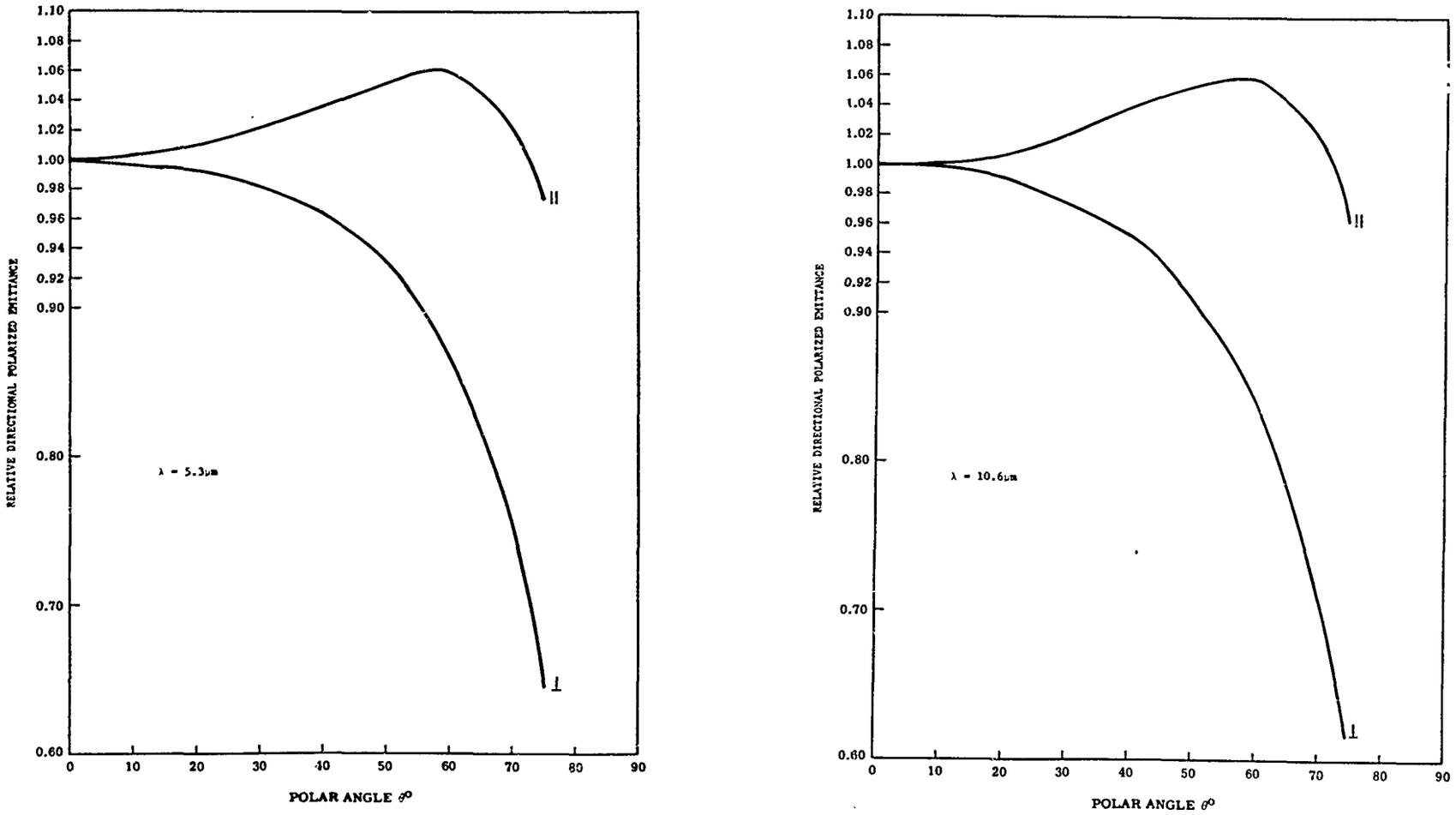

FIGURE 31. RELATIVE POLARIZED DIRECTIONAL EMITTANCE OF TT-E-529 O.D. (X24087) PAINT AT 5.3μm AND 10.6μm

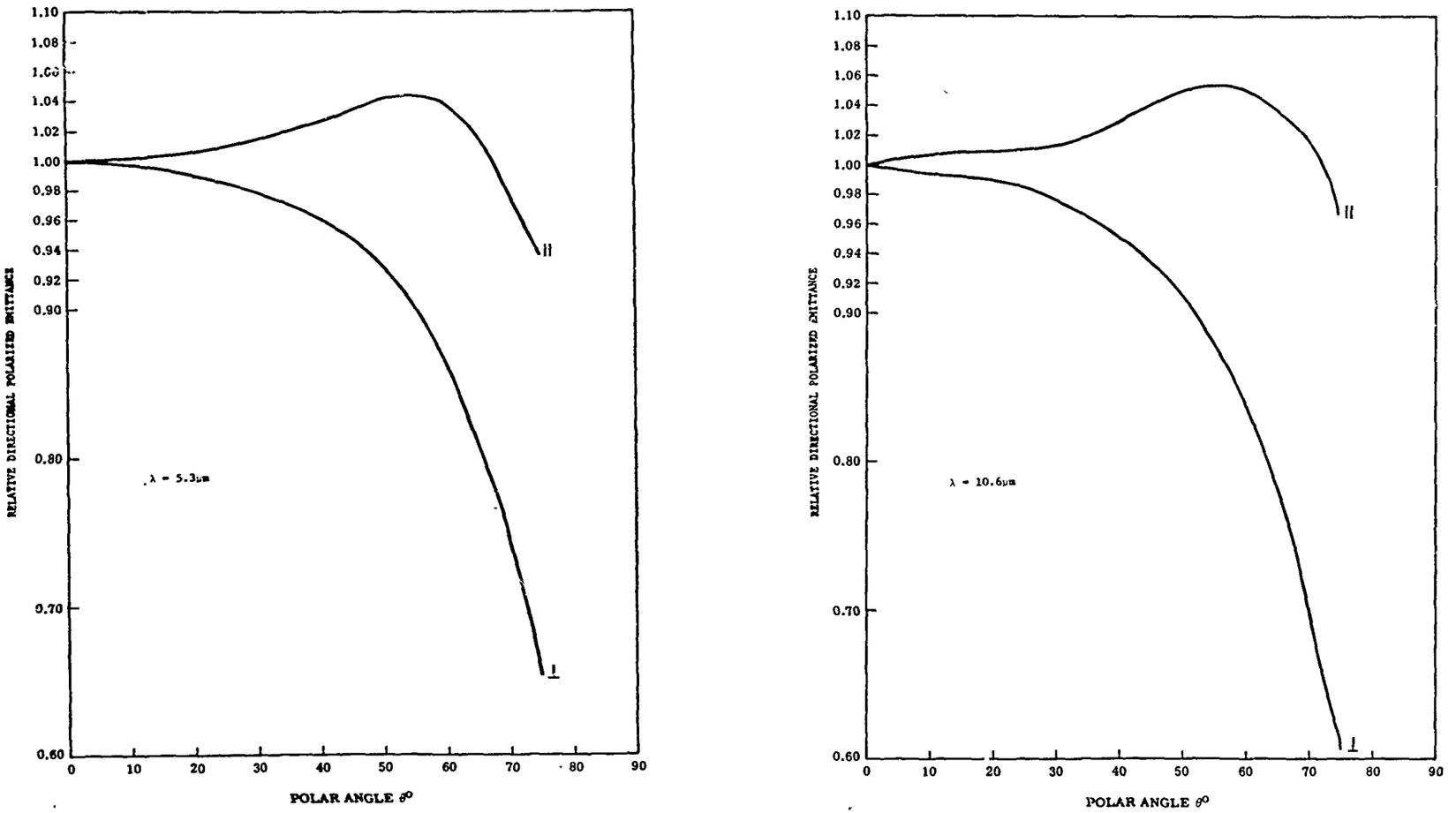

FIGURE 32. RELATIVE POLARIZED DIRECTIONAL EMITTANCE OF MIL-L-52043 O.D. (X24087) LAQUER AT 5.3μm AND 10.6μm

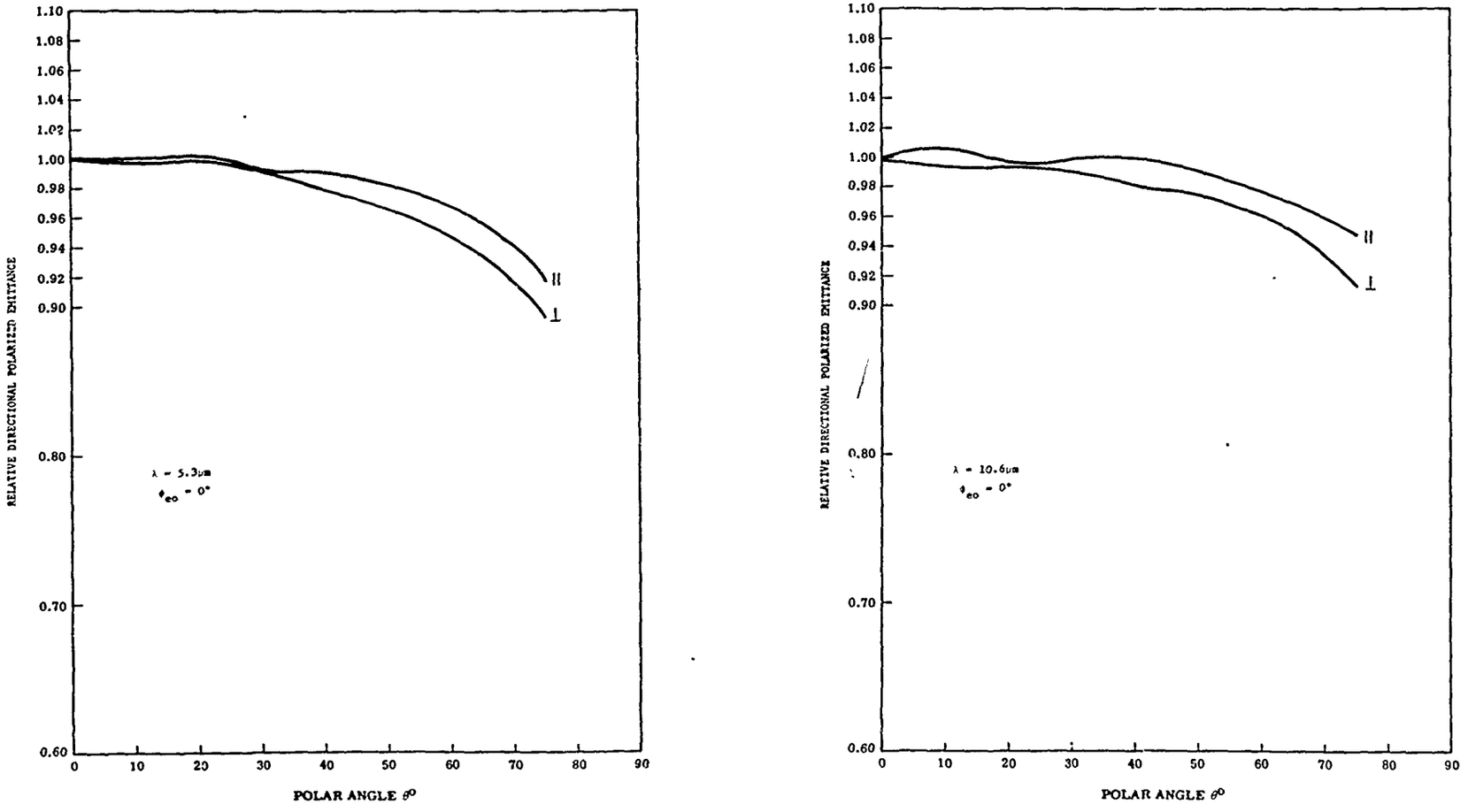

FIGURE 33. RELATIVE POLARIZED DIRECTIONAL EMITTANCE OF O.D. CANVAS AT 5.3μm AND 10.6μm. a) $\phi_{eo} = 0°$

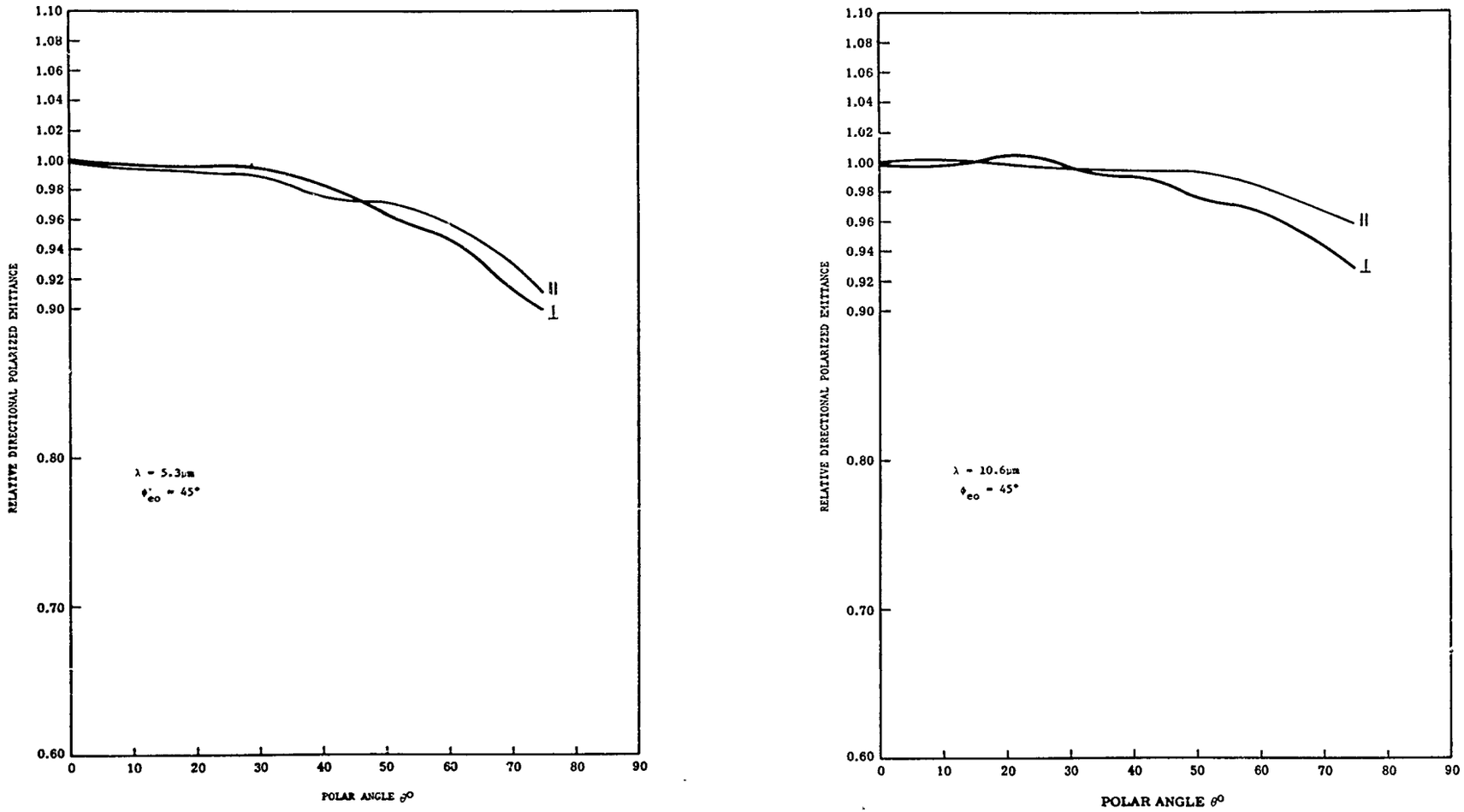

FIGURE 33. RELATIVE POLARIZED DIRECTIONAL EMITTANCE OF O.D. CANVAS AT 5.3μm AND 10.6μm. b) $\phi_{eo} = 45°$

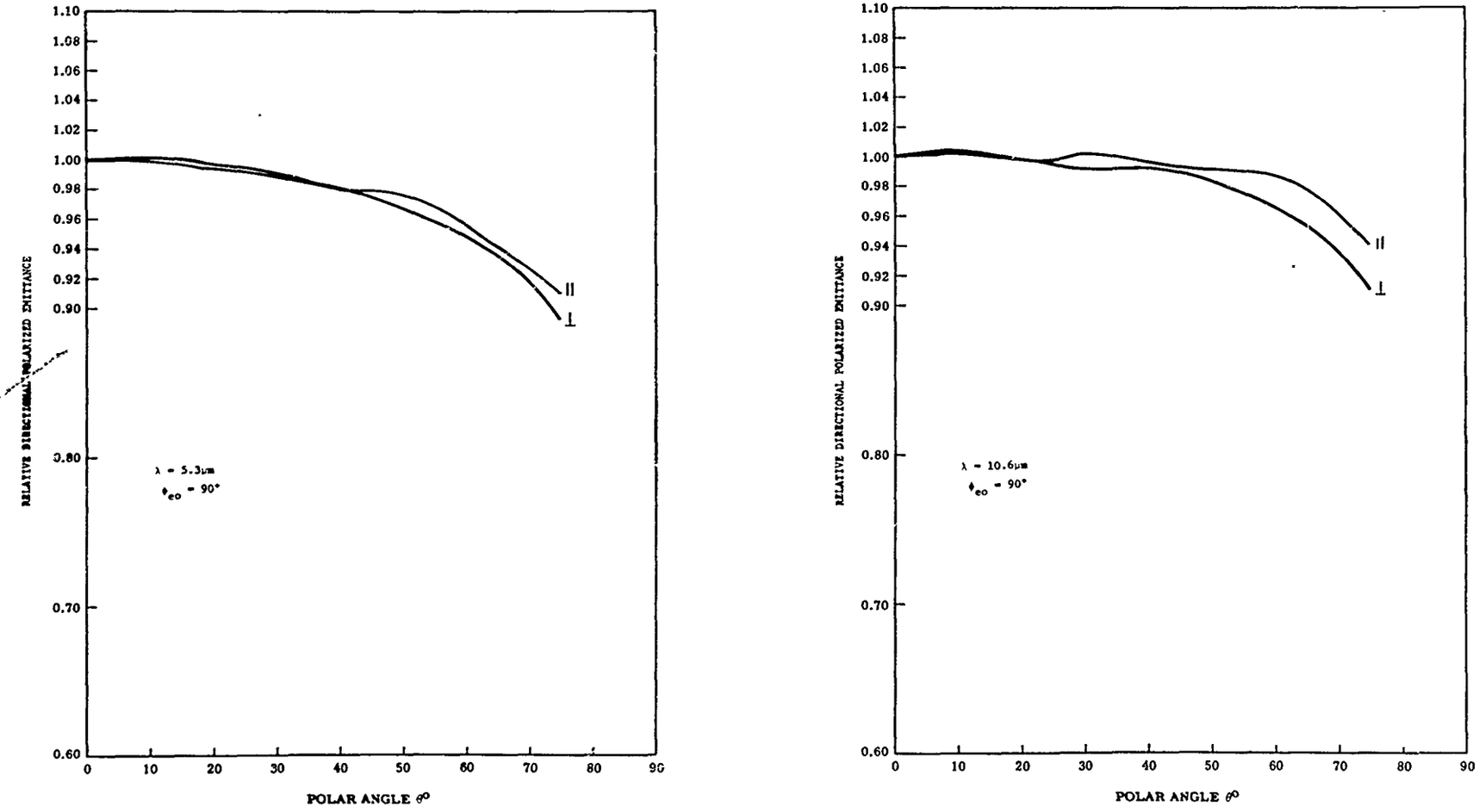

FIGURE 33. RELATIVE POLARIZED DIRECTIONAL EMITTANCE OF O.D. CANVAS AT 5.3μm AND 10.6μm. c) $\phi_{eo} = 90°$

has here been given arguments not necessary in the in the general discussion presented in Section 3.

As mentioned in Section 2, each of the total radiance terms in equation 7.1 is composed of both emitted and reflected terms. In this case, the reflected terms, which depend only upon the reflectance of the target* and the environmental radiance available for reflection, can be made to cancel in the above differences by placing both samples in the same radiation environment. Thus, the voltage proportionality reduces to the differences between the emitted radiance components,

$$V(\lambda,T_1^t,T_2^t;\theta_e,\phi_e) \propto \varepsilon^t(\lambda,T;\theta_e,\phi_e)[L_\lambda^b(T_1^t) - L_\lambda^b(T_2^t)] \qquad (7.2)$$

where T may be taken as T_1^t, T_2^t, or any intermediate temperature. Based on equation 7.2, many basically-different emittance measurements can be made. Two of the more useful are described below.

7.1.1. UNPOLARIZED SPECTRAL NORMAL EMITTANCE. Unpolarized spectral normal emittance measurements are made by spectrally scanning the targets from a normal viewing angle to produce the voltage, $V(\lambda,T_1^t, T_2^t;0,-)$. Calibration is achieved by subsequently spectrally scanning a matched pair of reference cavities at temperatures T_1^c and T_2^c producing a voltage $V(\lambda,T_1^c,T_2^c)$. In the ratio of these voltages, the proportionality constant cancels, giving

$$\frac{V(\lambda,T_1^t,T_2^t;0,-)}{V(\lambda,T_1^c,T_2^c)} = \frac{\varepsilon^t(\lambda,T;0,-)[L_\lambda^b(T_1^t) - L_\lambda^b(T_2^t)]}{\varepsilon^c(\lambda,T)[L_\lambda^b(T_1^c) - L_\lambda^b(T_2^c)]} \qquad (7.3)$$

*This is assumed to be sufficiently insensitive to temperature that it is essentially the same at T_1^t and T_2^t.

Rearrangement of this result produces

$$\varepsilon^t(\lambda,T;0,-) = \varepsilon^c(\lambda,T)\ \frac{V(\lambda,T_1^t,T_2^t;0,-)}{V(\lambda,T_1^c,T_2^c)}\ \left[\frac{L_\lambda^b(T_1^c) - L_\lambda^b(T_2^c)}{L_\lambda^b(T_1^t) - L_\lambda^b(T_2^t)}\right] \qquad (7.4)$$

Thus, the measured voltages together with the reference cavity emittance and temperatures of the matched targets and the matched cavities allow calculation of the unpolarized spectral normal emittance of the target material. Obviously, $\varepsilon^t(\lambda,T,\theta_{eo},\phi_{eo})$ could equally well be made where (θ_{eo},ϕ_{eo}) is any fixed set of angles.

7.1.2. POLARIZED EMITTANCE VS. ANGLE. Polarization and angular dependences are determined by inserting a linear polarizer into the FISR system and rotating the matched targets to vary the viewed polar emission angle θ_e while holding the wavelength and azimuth angle at some fixed values, λ_o and ϕ_{eo}, respectively. For arbitrary linear polarization state p, this produces a voltage

$$V_p(\lambda_o,T_1^t,T_2^t;\theta_e,\phi_{eo}) \propto \varepsilon_p(\lambda_o,T;\theta_e,\phi_{eo})[L_\lambda^b(T_1^t) - L_\lambda^b(T_2^t)] \qquad (7.5)$$

The voltage obtained at any angle θ_e can be divided by that obtained at $\theta_e = 0$ to produce

$$\frac{V_p(\lambda_o,T_1^t,T_2^t;\theta_e,\phi_{eo})}{V_p(\lambda_o,T_1^t,T_2^t,0,-)} = \frac{\varepsilon_p^t(\lambda_o,T;\theta_e,\phi_{eo})}{\varepsilon_p^t(\lambda_o,T;0,-)} \qquad (7.6)$$

where the radiance terms have cancelled since the temperatures T_1^t and T_2^t are the same for all θ_e. Thus the θ_e-dependence of the relative polarized

directional emittance at wavelength λ_o and azimuth angle ϕ_{eo} is given by this voltage ratio. If the discussion is limited to materials which do not exhibit anisotropy in polarization (i.e., neglecting materials with preferred crystalline optical axes or with grating-like surfaces*), the normal emittance is necessarily unpolarized and the absolute polarized directional emittance at wavelength λ_o and azimuth angle ϕ_{eo} becomes

$$\varepsilon_p^t(\lambda_o,T;\theta_e,\phi_{eo}) = \frac{V_p(\lambda_o,T_1^t,T_2^t;\theta_e,\phi_{eo})}{V_p(\lambda_o,T_1^t,T_2^t;0,-)}\,\varepsilon^t(\lambda_o,T;0,-) \quad \text{for all } \phi_{eo} \qquad (7.7)$$

since, as implied by equation 2.9, $\varepsilon^t(\lambda_o,T;0,-)$ must equal $\varepsilon_p^t(\lambda_o,T;0,-)$ when there is no polarization preference. For data presentation purposes, equation 7.6 is used because the accuracy of the emittance ratio is superior to that of the pure emittance represented by equation 7.7. Generally, only the relative angular dependence is of interest anyway. The technique of measuring emittance when only one material sample is available has already been discussed in Section 3.3.

*Actually, under these circumstances, there is no dependence on ϕ_{eo}. However, something must be written in the ϕ_e-variable-function-dependence position since ϕ_{eo} is defined in this case.

8

INTERPRETATION AND USE OF THE DATA

8.1. THE FIELD SPECTRAL RADIANCE DATA

The following general observations are indicated by Figures 9 - 19:

1. The spectral apparent temperature of materials in the field under clear-sky conditions varies from scan to scan although the spectral shape persists. Under heavy-overcast conditions this scan-to-scan variation is much reduced. This effect occurs because of actual target temperature variations from scan to scan. Under clear-sky conditions, this variation is larger than under overcast conditions.

2. For those materials which exhibit some structure in spectral apparent temperature, this structure is much more evident under clear-sky conditions than it is under overcast conditions. This is to be expected since heavy-overcast conditions correspond closely to the situation where the target is in a Hohlraum. That is, the target and the "walls" of its enclosure (the clouds) are very nearly in thermal radiative steady state. Under such conditions, any target should look gray.

3. For the targets examined, the structure in spectral apparent temperature under clear-sky conditions, if any, has two general characteristics:

   a) There is a "dip" in spectral apparent temperature between (roughly) 7.9 and 9.5 μm. This is due to a silicon dioxide reststrahlen band in this spectral region.

   b) Below about 4.3 μm, there is an increase in spectral apparent temperature. This is due to reflection of the marked increase in solar irradiance below 4.3 μm. That this effect is much weaker for

grass than it is for the other targets examined is due to the relatively low reflectance of grass in the 3.3 - 4.3 μm spectral region.

4. Some general observations concerning grass can be made. Medium-to-long grass shows no structure in its spectral apparent temperature under any sky state. In the 5.5 - 8.0 μm H_2O-emission band, the spectral apparent temperature of medium-to-long grass and the sky are the same. Some spectral structure exists for short grass (Figures 15 and 19) under clear skies in the 5.8 - 8.0 μm spectral region, but it strongly resembles that of soil (Figure 9). Since the soil is partially visible when it supports only short grass, that is the cause of the apparent spectral structure. That some of the scans in Figure 15 are so different from the others referring to grass in that figure is due to a cloud shadow falling on the target for those scans. The grass is still apparently warmer than the sky in the 5.5 - 8.0 μm spectral region because the sky is largely clear.

5. The sky spectral apparent temperature data consistently exhibit the following features:

a) Clear sky. Peaks in the spectral apparent temperature due to molecular emission bands occur. The main ones are

i) 4.3 μm (CO_2)

ii) 5.5 - 8.0 μm (H_2O)

iii) 9.6 μm (O_3)

iv) 11.8 μm (H_2O)

v) 12.6 μm (CO_2) and (H_2O).

b) Overcast sky

i) 4.3 μm (CO_2)

ii) 5.5 - 8.0 μm (H_2O)

The O_3 band for overcast skies is obscurred because this molecular specie exists only at high altitudes. Actually, the 11.8-μm H_2O and the 12.6-μm CO_2 and H_2O peaks are still present but they are so swamped by the greatly-increased thermal radiation that they are difficult to locate.

It is emphasized that thermal radiations from the FISR and its transporting van are always part of the environmental irradiance and that some of this radiation is scattered back to and collected by the FISR.

Figure 19 requires separate discussion. The discontinuity at roughly 5.6 μm is due to the fact that the data above and below this wavelength were taken on different days. The ambient temperatures on these two days were also different, thus accounting for the discontinuity. Further, the data in Figure 19 were taken very early in the FISR program and sky data from the flame-sprayed aluminum panel were not taken then. The substantial differences in the structure of the spectral apparent temperature of various parts of the tank are largely due to the irradiance environments of these parts. The runs labeled "track" and "turret side" were taken on shadowed areas of the tank. The "front slope" was about half-shadowed and half-sunlit. The (air) "intake" and "turret top" were completely sunlit. The "intake" is virtually black because of the many openings in it. Only the "turret top" displays the real structure in apparent spectral temperature to be expected from solid OD-painted steel. The structure below about 8.0 μm is probably due to partial spectral transparency of the paint. The dip around 9.8 μm is probably due to a corresponding dip in the emittance of the paint; such a dip occurs in some OD paints. See, for example, Figure 22.

8.2. THE LABORATORY EMITTANCE DATA

8.2.1. CHARACTERISTICS OF THE DATA. Two basic emittances of interest have been defined in equations 7.4 and 7.6. One very interesting characteristic of these two emittances for many paints is that although the normal spectral emittances (equation 7.4) may differ significantly for various paints, the relative polarized directional emittances (equation 7.6) are essentially identical for a given polarization. See Figures 22-24 and 30-32. A further important characteristic is that the "parallel" and "perpendicular" relative directional polarized emittances for paints are different from each other. The importance of this characteristic lies in the fact that most background materials do not exhibit it, water being a strong exception.* This is really to be expected since water and painted surfaces are essentially locally-smooth, lossless dielectrics in the 3.3 - 14.0 μm spectral region. Aside from water and ice, most natural backgrounds (grasses, soils, trees, rocks) are not. In fact, OD canvas, which is a militarily-interesting target, is expected not to be dielectric-like. Figure 33 supports that expectation (as yet, the normal spectral emittance data for OD canvas are not plotted).

8.2.2. PREDICTIVE EXERCISING OF THE LABORATORY DATA.** It is necessary to introduce some additional notation at this point. The importance of the results more than justifies the inconvenience. Data of the kind shown in Figures 30 - 32 indicate that each material represented in those figures would have different

---

*See reference 12 where extensive broadband field data are reported.

**Reference 13 has been borrowed from liberally in order to develop the material in this Section. The work was performed under Air Force sponsorship at the Infrared and Optics Laboratory, Willow Run Laboratories, Institute of Science and Technology, The University of Michigan, Ann Arbor.

spectral apparent temperatures if its radiance was sampled first as the parallel-polarized component and then as the perpendicular-polarized component. In fact, a target composed of any of the materials represented would appear to scintillate or blink if a linear polarizer were rotated in the input beam of the sensing device. Some analysis based on the FISR sky spectral apparent temperature data and emittance polarization data to quantitatively assess this effect is presented below.

Let $L_{\lambda,p}(T^t,T^{sky};\ \theta_e^t,\phi_e^t)$ represent the total spectral radiance from a target of actual temperature T^t being viewed at the angle (θ_e^t,ϕ_e^t) and exposed to a sky spectral radiance corresponding to the spectral apparent temperature denoted by T^{sky}. This latter is generally spectrally dependent, but it is not notationally so indicated. Now, $L_{\lambda,p}(T^t,T^{sky};\ \theta_e^t,\phi_e^t)$ can be represented as $L^b_{\lambda,p}(T^{app}_{t,p};\ \theta_e^t,\phi_e^t)$ where $T^{app}_{t,p}$ is the spectral apparent temperature of the target when its radiance is sampled with polarization state p and the target is exposed to spectral radiance having spectral apparent temperature T^{sky}. The real quantity of interest is $T^{app}_{t,p1,p2} = T^{app}_{t,p1} - T^{app}_{t,p2}$ which is the target spectral apparent temperature <u>difference</u> for the two polarizations p1 and p2. It is called a <u>polarization temperature difference</u>, and it generally depends on (θ_e^t,ϕ_e^t), p1, p2, λ, and T^{sky}.

The relationship between the polarization temperature difference and the spectral apparent radiance difference is now developed. A limiting case of the Planck law for radiance (see equation 2.1 and the equation preceeding 2.3) is a help here. This is known as the Wien law:

$$L^b_\lambda(T) = \frac{c_1}{\pi\lambda^5}\exp(-c_2/\lambda T) \qquad (8.1)$$

It is a very good approximation to the Planck law for $\lambda T < 5 \times 10^3$ μm - ^oK, a condition satisfied below 15 μm at field temperatures. From equation (8.1),

$$dL^b_{\lambda(T)} = \frac{c_2}{\lambda T^2} L^b_\lambda(T)\, dT \tag{8.2}$$

so the temperature difference, ΔT, associated with a radiance difference ΔL, is about

$$\Delta T \cong \frac{\lambda T^2}{c_2} \quad \frac{\Delta L^b_\lambda(T)}{L^b_\lambda(T)} \tag{8.3}$$

This leads to

$$T^{app}_{t,p1,p2} = T^{app}_{t,p1} - T^{app}_{t,p2}$$

$$\cong \frac{\lambda}{c_2}\left[\frac{T^{app}_{t,p1} + T^{app}_{t,p2}}{2}\right]^2 \left[\frac{L^b_{\lambda,p1}(T^{app}_{t,p1};\ \theta_e,\phi_e) - L^b_{\lambda,p2}(T^{app}_{t,p2};\ \theta_e,\phi_e)}{L^b_\lambda\,[(T^{app}_{t,p1} + T^{app}_{t,p2})/2;\ \theta_e,\phi_e]}\right] \tag{8.4}$$

This is a very general result which relates the polarization temperature difference at any two polarizations to the mean spectral apparent temperature and the apparent spectral radiance difference. The last term in brackets in equation 8.4 is commonly referred to as radiance contrast.

In order to illustrate some actual use of equation (8.4), the following assumptions are made:

1) The environmental spectral irradiance is unpolarized and the "sky" spectral apparent temperature data in Figures 9 - 18 are representative and typical.

2) The targets are horizontal plates* coated with the paints depicted

*Geometrically more-general target shapes are considered in reference 13. For simplicity, only the horizontal plate is considered here.

in Figures 22, 23, 30, and 31. The polarization states to be considered are the ones identified as // and ⊥ in the latter two figures. Under these assumptions (the validity of which is well established), equations 2.26 can be used. Then, all quantities appearing in the right-hand side of equation 8.4 are known and the polarization temperature differences for various paints under various sky states and viewing angles can be calculated. The results of the calculations are presented in Figures 34 - 37. In Figure 34,the effects of sky state and target polar viewing angle on spectral apparent temperature can be seen for paint MIL-E-46096 (X34087). An actual target temperature of 315°K was assumed. A constant spectral apparent temperature of 283°K was chosen to represent the overcast sky. Figure 35 illustrates the polarization temperature difference for the same target at a polar viewing angle of 70° under clear and overcast skies. The effects of variations in normal spectral emittance under clear sky illumination at two different polar viewing anlges are shown in Figure 36. Finally, the polarization temperature difference resulting from variations in normal spectral emittance under clear sky illumination at a polar viewing angle of 70° is shown in Figure 37. The conclusions to be drawn from the figures is that polarization temperature difference spectral signatures exist for OD paints, that overcast skies reduce the differences, and, indirectly, that OD paints can be identified in field situations because background (excluding water) polarization temperature differences are essentially zero.

---

*These figures apply to the condition of zero range; that is, the figures do not contain the effect of atmospheric attenuation and path radiance. Reference 13 addresses these problems.

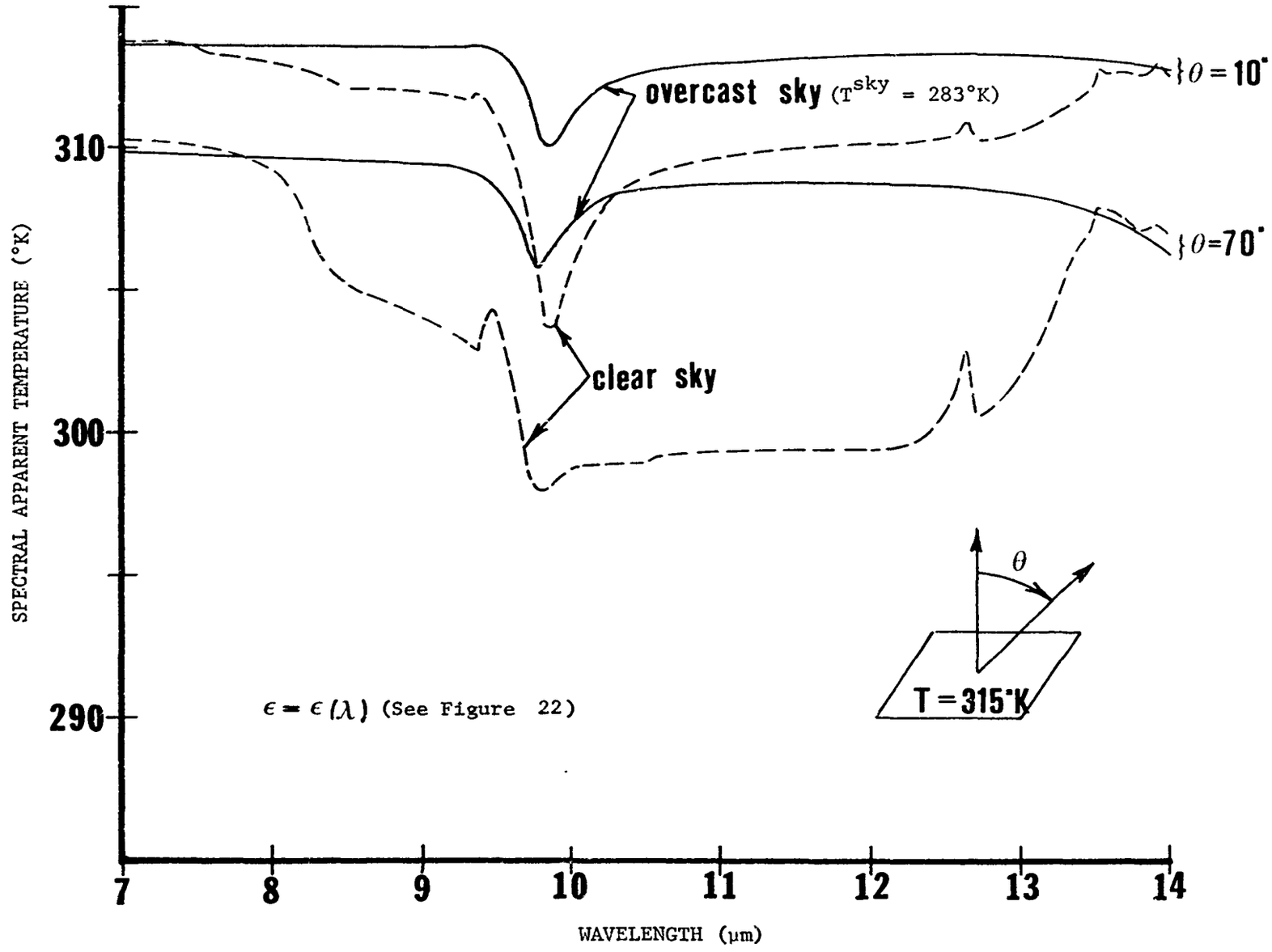

FIGURE 34. SPECTRAL APPARENT TEMPERATURE

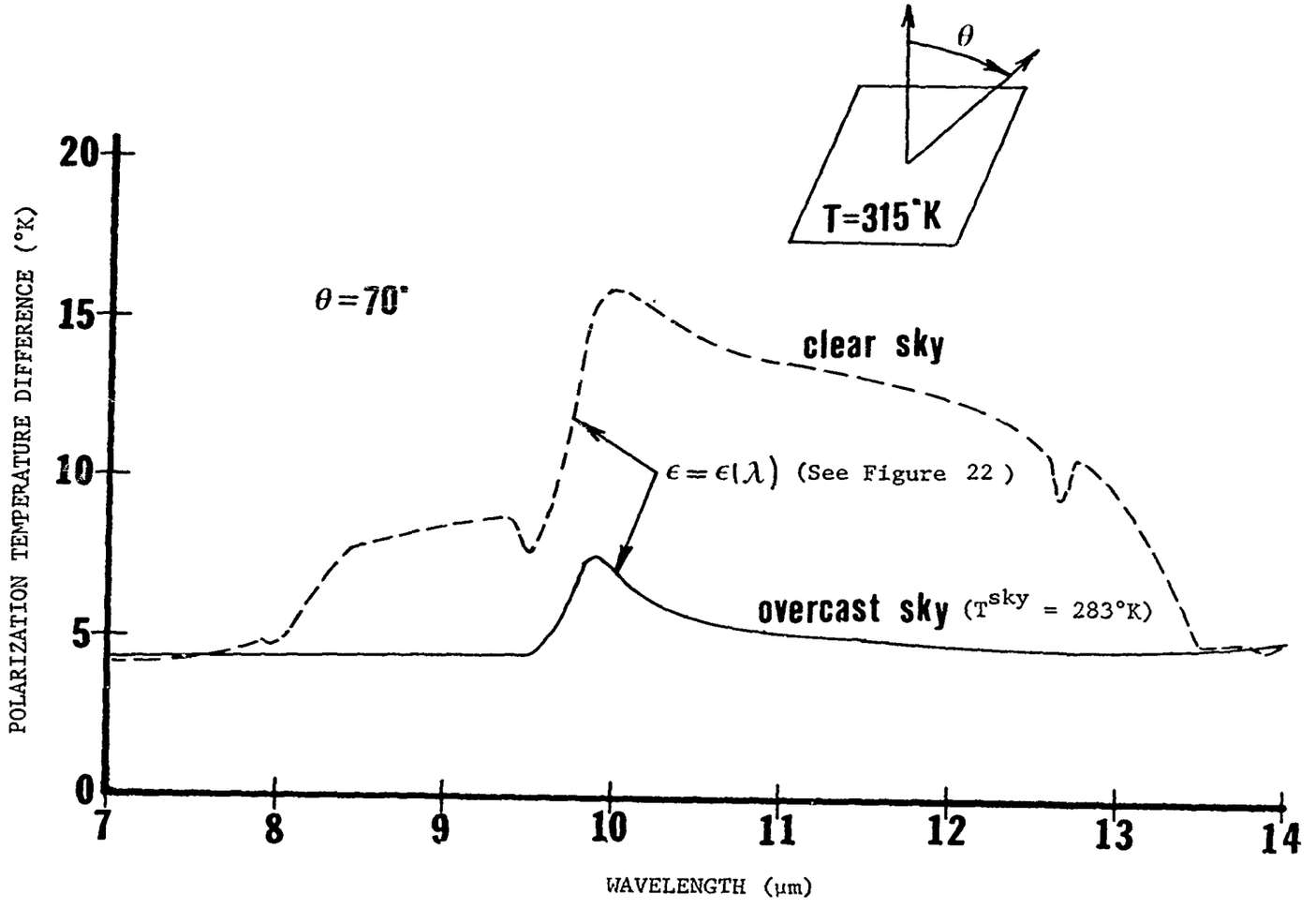

FIGURE 35. POLARIZATION TEMPERATURE DIFFERENCE

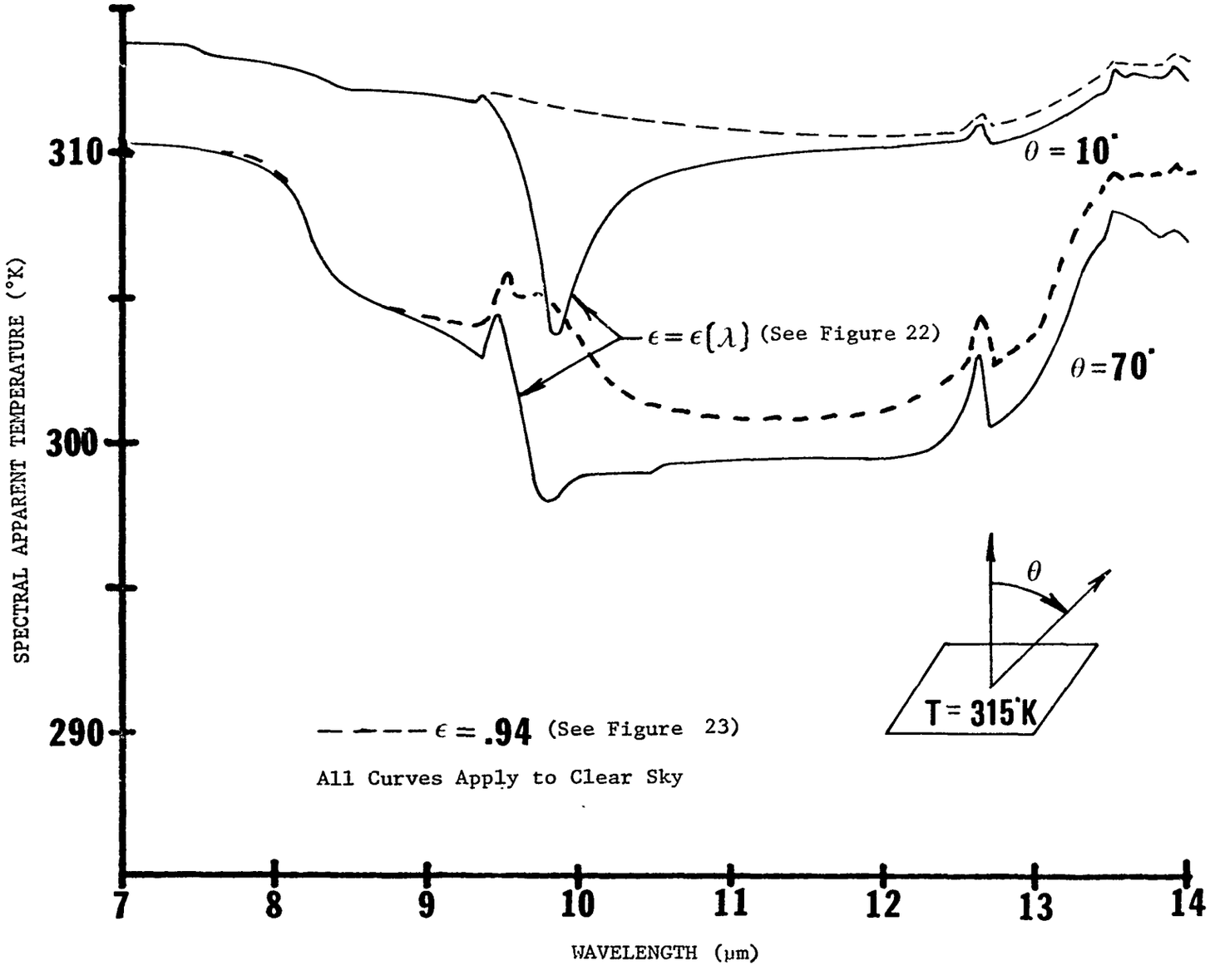

FIGURE 36. SPECTRAL APPARENT TEMPERATURE

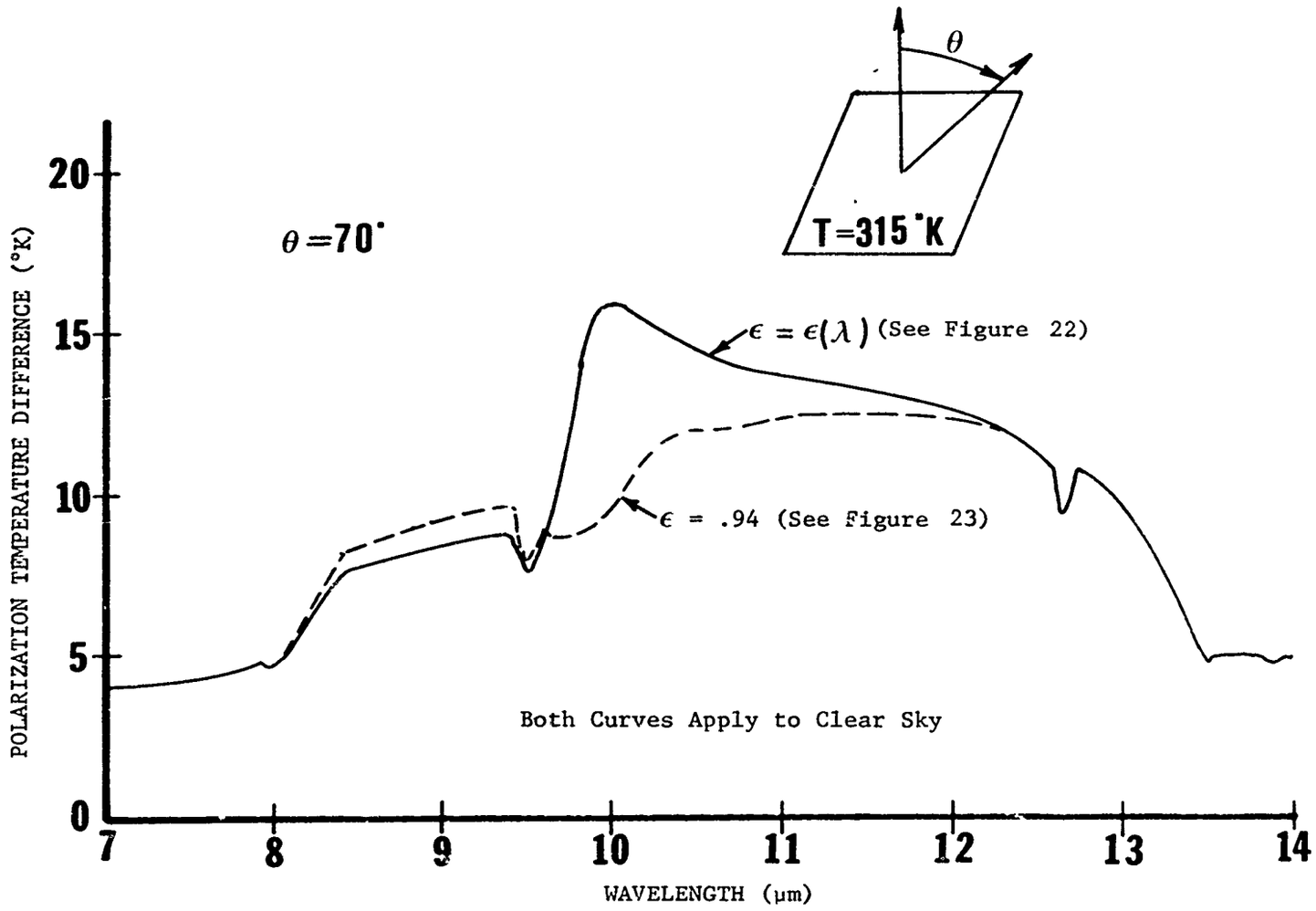

FIGURE 37. POLARIZATION TEMPERATURE DIFFERENCE

REFERENCES

1. International Commission on Illumination, International Lighting Vocabulary, (Bureau Central de la CIE, Paris, 1970), Paragraph 45-05-215.

2. Ibid. Paragraph 45-05-235.

3. M. E. Bair, D. C. Carmer, and S. R. Stewart, "A Gonioreflectometer Facility Using Coherent and Incoherent Sources," Institute of Science and Technology, The University of Michigan, Ann Arbor, August 1970. Available as Air Force Avionics Laboratory Report AFAL-TR-70-161.

4. F. E. Nicodemus, "Reflectance Nomenclature and Directional Reflectance and Emissivity," Appl. Opt. 9 (1970) p. 1474.

5. ———, "Target-Signature Measurements Final Report," Infrared and Optics Laboratory, Willow Run Laboratories, Institute of Science and Technology, The University of Michigan, Ann Arbor. Report No. 8047-28-F, September, 1968. Reference is made to Section 2 by T. Limperis and I. Ginsberg.

6. F. E. Nicodemus, "Directional Reflectance and Emissivity of an Opaque Surface," Appl. Opt. 4 (1965) p. 767.

7. F. A. Jenkins and H. E. White, Fundamentals of Optics (McGraw-Hill Book Co., Inc., N. Y. 1957), p. 510.

8. Handbook of Military Infrared Technology, (Office of Naval Research, Dept. of the Navy, Washington, D. C., 1965. Ed. W. L. Wolfe), p. 32.

9. A. Gouffé, "Corrections d'ouverture des corps-noir artificiels compte tenu des diffusions multiple internes," Rev. Optique 24 (1945)p. 1.

10. D. L. Stierwalt, "Infrared Spectral Emittance Measurements of Optical Materials," Appl. Opt. 5 (1966), p. 1911.

11. North American Aviation, Inc., unpublished data.

12. ———, "Analysis of Polarization and Thermal Properties of Targets and Backgrounds," Report No. 3221-11-P, Infrared and Optics Laboratory, Willow Run Laboratories, Institute of Science and Technology, The University of Michigan, Ann Arbor, August, 1970.

13. J. L. Beard and J. R. Maxwell, "Multispectral and Polarization Signatures in the Thermal Infrared," Presented at the 19th National Infrared-Information Symposium. To be published in Proc. IRIS 16.